UNIVERSITÀ DEGLI STUDI DI PAVIA
DOTTORATO DI RICERCA IN FISICA – XXI CICLO

X-ray Observations of Galactic Isolated Neutron Stars

Paolo Esposito

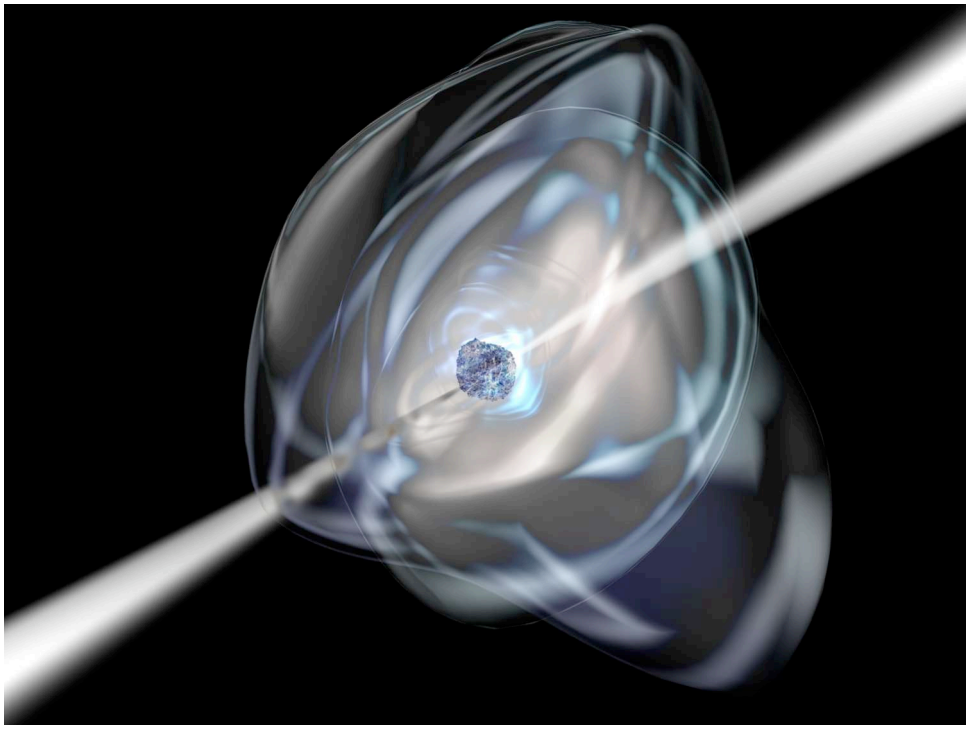

Supervisors: Dott. Marco Roncadelli
Dott. Sandro Mereghetti

Tesi per il conseguimento del titolo

Università degli Studi di Pavia

Dipartimento di Fisica Nucleare e Teorica

Istituto Nazionale di Astrofisica

Istituto di Astrofisica Spaziale e Fisica Cosmica - Milano

Istituto Nazionale di Fisica Nucleare

Sezione di Pavia

DOTTORATO DI RICERCA IN FISICA – XXI CICLO

X-ray Observations of Galactic Isolated Neutron Stars

dissertation submitted by

Paolo Esposito

to obtain the degree of

DOTTORE DI RICERCA IN FISICA

Supervisors: **Dr.** ***Marco Roncadelli***
Istituto Nazionale di Fisica Nucleare, Sezione di Pavia
Dr. ***Sandro Mereghetti***
INAF/Istituto di Astrofisica Spaziale e Fisica Cosmica – Milano
Referee: **Prof.** ***Roberto Turolla***
Università degli Studi di Padova
Mullard Space Science Laboratory, University College London

Cover
Artist's view of a magnetar. Credit: ESA-European Space Agency

X-ray Observations of Galactic Isolated Neutron Stars
Paolo Esposito
PhD thesis – University of Pavia
Printed in Pavia, Italy, November 2008
ISBN 978-88-95767-19-2

Contents

Plan of the thesis

During the course of my PhD Thesis, I have been involved in the study of neutron stars, mostly on the observational side. Neutron stars represent the final evolutionary stages of those stars which undergo a massive explosion and they hold the most peculiar physical conditions that may be observed in the present-day universe.

Chapter 1 is devoted to the presentation of the underlying scientific framework my research belongs to. Given the contents of this thesis, here I focused on isolated neutron stars. Recent multi-wavelength observations radically changed the classic idea that all isolated neutron stars are fast-spinning radio pulsars. A rich phenomenology emerged, which led to the classification of neutron stars into different species. However, a clear picture, connecting different species in a coherent physical scenario, is still lacking.

Chapter 2 reports on the discovery of X-ray emission from the very young radio pulsar PSR J1357–6429 using archival data. Most pulsars are detectable only at radio wavelengths, however only a small fraction of the emitted energy emerges as radio pulsations while the X-ray emission is much more energetically important. For this reason X-ray observations of radio pulsars provide a powerful diagnostic of the energetics and emission mechanisms of rotation-powered neutron stars. The X-ray spectrum of PSR J1357–6429 includes a non-thermal component and possibly also a thermal one. This thermal radiation could result by cooling of the surface of the neutron star or arise from polar-cap reheating, due to return currents from magnetospheric gaps.

Chapter 3 is the first of three chapters in which I concentrate on a magnetar, that is, an isolated neutron star believed to have an extremely strong magnetic field powering its bright X-ray emission and peculiar bursting activity. Here we present the systematic analysis of the whole *BeppoSAX* data-set of the soft gamma-ray repeater SGR 1900+14. The most surprising result in this work is the discovery of hard X-rays from the source. I also studied in detail the long-term spectral variability of the source and its spectral evolution

during the afterglow of a very bright flare.

Chapter 4 deals with SGR 1806-20. SGR 1806-20 was the first soft gamma-ray repeater to be discovered (in 1979), and it is currently the most burst-active and the best studied of the known sources of its kind. In particular SGR 1806-20 has attracted great attention in the last years since in 2004 it emitted the most powerful flare ever observed from a neutron star. This probably involved a large-scale rearrangement of the magnetosphere leading to observable variations in the properties of its X-ray emission. In this Chapter I present the results of the first *Suzaku* observation of SGR 1806–20, performed about two year after the flare, together with almost simultaneous observations with *XMM-Newton* and *INTEGRAL*. The broad-band spectral properties of SGR 1806–20, covering both persistent and bursting emission, are discussed in the context of recent theoretical developments of the magnetar model.

Chapter 5 is centered on the soft gamma-ray repeater SGR 1627–41 and its recent spectacular re-activation following a quiescent stretch of nearly a decade. Thanks to the rapid response of the *Swift* satellite, SGR 1627–41 was repeatedly observed immediately after the first bursts, leading to the earliest post-burst observations ever obtained for this source. In this Chapter I discuss the pre- and post-burst properties of the source, as well as the spectral characteristics of the bursts. One of the main results is the observation of two distinct phases in the flux decay after the onset of the active interval, possibly reflecting two different cooling mechanisms.

Chapter 6 pertains to RX J0002+6246. This X-ray source was discovered close to a supernova remnant in a *ROSAT* observation performed in 1992. The source phenomenology (soft spectrum, apparent lack of counterparts, possible pulsations at 242 ms, hints for surrounding diffuse emission) led to interpret it as an isolated neutron star in a new supernova remnant. In this Chapter I report on the re-analysis of an archival *XMM-Newton* observation performed in 2001. Our surprising conclusion is that RXJ0002+6246 is not an isolated neutron star, but the X-ray counterpart of a bright optical/infrared source, most likely a main sequence or supergiant star, located at a smaller distance than previously thought.

Chapter 1

Introduction

Note: Besides the cited papers this introduction is based on Becker & Pavlov (2001), den Hartog (2008), Kaspi et al. (2006), and Mereghetti (2008).

1.1 A historical introduction

In a paper discussing the possible origin of cosmic rays Walter Baade and Fritz Zwicky proposed the idea that stars composed entirely of neutron could be formed in supernovae: "With all reserve we advance the view that a supernova represents the transition of an ordinary star into a neutron star, consisting mainly of neutrons" (Baade & Zwicky 1934). They were aware that neutron stars could have peculiar properties, in particular very small radii and extremely high densities (mean density $\gtrsim 10^{14}$ g cm^{-3}). In fact, shortly after the discovery of the neutron by James Chadwick in 1932 (Chadwick 1932), Lev D. Landau speculated on the possible existence of neutron stars (Landau 1932). Using the newly-established Fermi-Dirac statistics he was able to estimate that such a star, consisting of $\sim 10^{57}$ neutrons, would form a giant nucleus with a radius of the order of $R \sim (\hbar/m_n c)(\hbar c/G m_n^2)^{1/2} \simeq 3 \times 10^5$ cm, where $\hbar$, c, G and m_n are the Planck constant, the speed of light, the gravitation constant, and the mass of the neutron.

First models for the structure of neutron stars were worked out in 1939 by Robert Oppenheimer and George Volkoff, who calculated an upper limit for the neutron-star mass. Using general relativistic equilibrium equations and assuming that the star is entirely described by an ideal Fermi gas of neutrons, they found that any star more massive than 3 times the solar mass (the solar mass is $M_\odot = 1.988\,92 \times 10^{33}$ g) will collapse and eventually form a black hole ('Oppenheimer-Volkoff limit'; Oppenheimer & Volkoff 1939).

Baade (1942) and Minkowski (1942) studied the Crab Nebula - the remnant associated with a supernova explosion observed in 1054 A.D. (e.g. Stephenson & Green 2002) - and observed that most of the optical emission in the inner

part of the diffuse nebulosity showed a continuous spectrum. They argued that this spectrum is likely produced by free-free and free-bound transitions of electrons in a highly ionized gas. One of two visible stars in the centre of the supernova remnant could be the candidate responsible for exciting the nebula. It was remarkable as it did not show any spectral lines. Minkowski (1942) discussed that the mass of the central star should be around $1 M_{\odot}$ and that it should have a small radius. Therefore, its density should be very high. However, he did not realize that a neutron star was a possible explanation: at the time it was generally expected that neutron stars would not be observable because of their small size and low optical luminosity.

After the detection of the Crab Nebula at radio wavelengths (Bolton et al. 1949) it was argued that the continuous spectrum from the nebula was caused by synchrotron radiation from relativistic electrons moving through a magnetic field (Alfvén & Herlofson 1950; Shklovsky 1954). This theory suggested that also the highly polarized optical continuous radiation (Dombrovsky 1954; Oort & Walraven 1956) could be better explained by synchrotron origin rather than by the emission mechanism suggested by Minkowski (1942). Oort & Walraven (1956) calculated that the relativistic electrons loose their energy within ∼200 years, which meant a source must exist which continuously supplies the nebula with new electrons. They suggested as source for the electrons the same continuous-spectrum star investigated by Minkowski (1942).

After the discovery of the Crab Nebula in X-rays (Bowyer et al. 1964b), Chiu (1964) and Chiu & Salpeter (1964) suggested that the X-rays could be the thermal radiation from the surface of a hot neutron star. However, the X-ray emission from the Crab supernova remnant was found to be of a finite angular size (∼1 arcmin) whereas a neutron star was expected to appear as a point source. Thus, the early X-ray observations were not sensitive enough to prove the existence of neutron stars. However, Woltjer (1964) and Hoyle et al. (1964) noted that a neutron star with a high magnetic field ($\sim 10^{10}$ G) might somehow be able to produce relativistic electrons.

In 1967, Jocelyn Bell and Anthony Hewish came across a series of pulsating radio signals while using a radio telescope specially constructed to look for rapid variations in the radio emission of quasars. These radio pulses, 1.32 seconds apart, with remarkable regularity, were emitted from an unknown source in the sky at right ascension $19^{\mathrm{h}}20^{\mathrm{m}}$ and declination $+23^{\circ}$.[1] Further observations refined the pulsating period to 1.337 301 13 s. The extreme precision of the period suggested at first that these signals might be generated by extraterrestrial intelligence. They were subsequently dubbed as LGM-1, an acronym for 'Little Green Man 1'. However, as a few more similar sources had been detected, it became clear that a new kind of celestial objects was discovered (Hewish et al. 1968).

[1] CP 1919+21, where the 'CP' stands for 'Cambridge Pulsar'; the source is now known as PSR B1919+21.

The link between these pulsating radio sources, which were called 'pulsars', and fast spinning neutron stars was provided by Franco Pacini and Thomas Gold (Pacini 1967, 1968; Gold 1968, 1969). Pacini had published a paper a few months before the discovery by Bell and Hewish in which he discussed a possible emission mechanism which could feed the Crab Nebula continuously. He proposed a rapidly rotating neutron star with a strong magnetic field emitting dipole radiation. Right after the publication of the discovery by Bell and Hewish, Gold and Pacini suggested that the pulsars could be rotating neutron stars. In particular Gold (1968) and Gold (1969) introduced the concept of the rotation-powered pulsar which radiates at the expense of its rotational energy (pulsars spin down as rotational energy is radiated away) and recognized that the rotational energy is lost via electromagnetic radiation of the rotating magnetic dipole and emission of relativistic particles. The particles are accelerated in the pulsar magnetosphere along the curved magnetic field lines and emit the observed intense curvature and synchrotron radiation. The alternative interpretation of pulsars as white dwarfs was dismissed with the discovery of the Crab pulsar with a pulse period of 33 ms by Staelin & Reifenstein (1968): these pulsations were in fact difficult to explain in the white-dwarf framework and were interpreted as the rotation period of a neutron star. The identification between pulsars and rotating neutron stars was further straightened when also the spin down of the Crab pulsar, predicted by Pacini (1968) and Gold (1968) was measured (Richards & Comella 1969).

While the evidence for the existence of neutron stars came, as seen, from radio astronomy with the discovery of the first radio pulsars, X-ray photons from a neutron star had already been detected from Scorpio X–1, which is an accreting neutron star in a binary system.

X- and gamma-rays can only be observed from above the Earth's atmosphere (X-rays are absorbed at altitudes of 20–100 km), and this requires detectors to operate from high flying balloons, rockets or satellites. One of the first X-ray detectors brought to space was launched by Herbert Friedman and his team at the Naval Research Laboratory in order to investigate the influence of solar activity on the propagation of radio signals in the Earth's atmosphere. Using simple proportional counters put on old V-2 (captured in Germany after the World War II) and Aerobee rockets, they were the first who detected X-rays from the very hot gas in the solar corona (Friedman 1981). However, the intensity of this radiation was found to be a factor 10^6 lower than that measured at optical wavelengths. It was therefore widely believed that all other stars, much more distant than the Sun, should be so faint in X-rays that further observations at that energy range would be hopeless. On the other hand, results from high-energy cosmic ray experiments suggested that there exist celestial objects which produce high-energy cosmic rays in processes which, in turn, may also produce X-rays and gamma-rays (Morrison et al. 1954).

These predictions were confirmed in 1962, when the team led by Bruno Rossi and Riccardo Giacconi accidentally detected X-rays from Scorpio X–1.

With the aim to search for fluorescent X-ray photons from the Moon, they launched an Aerobee rocket on 1962 June 12 from White Sands (New Mexico) with three Geiger counters as payload, each having a $\sim 100^\circ$ field of view and an effective collecting area of about 10 cm^2 (Giacconi 1974). The experiment detected X-rays not from the Moon but from a source located in the constellation Scorpio. Sco X–1, as it was dubbed, is the brightest extra-solar X-ray source in the sky. The X-ray emission from this source was confirmed by independent measurements by Bowyer et al. (1964a). Evidence for a weaker source in the Cygnus region and the first evidence for the existence of a diffuse isotropic X-ray background was also reported from that experiment (Giacconi et al. 1962). Subsequent flights launched to confirm these first results detected Tau X–1, a source in the constellation Taurus which coincided with the Crab supernova remnant (Bowyer et al. 1964b).

By the end of the 60's about 20 X-ray sources were located and it was noticed that most of these objects were concentrated along the Galactic plane (Morrison 1967) and therefore likely of Galactic origin. Shklovsky (1967) proposed that the X-rays from Sco X–1 originated from a hot gas flowing onto a neutron star from a close binary companion. It was also noticed that the orbital parameters of such a system could indicate the nature of the compact object, which could also be a black hole (Zeldovich & Guseynov 1966). Great advances in understanding compact X-ray sources where achieved after the launch of *Uhuru*,[2] the first astronomical satellite, at the end of 1970. Within just over two years of observing, *Uhuru* detected and localized 339 X-ray sources (Giacconi et al. 1972; Forman et al. 1978). Moreover pulsations were detected from Cen X–3 which was therefore the first pulsar discovered in X-rays (Giacconi et al. 1971a). Binaries with black holes, neutron stars, or white dwarfs were all found, as well as isolated neutron stars.

1.2 Neutron-star basics

A neutron star can be formed inside a heavy star at the end of its life while the rest of the star explodes in the form of a supernova. The mass of the progenitor determines whether the compact object will be a neutron star, or a black hole (neutron stars are thought to originate from stars with masses from about $9M_\odot$ to $25M_\odot$; Heger et al. 2003). At the final stages of the star's life silicon burning will start. Within days a massive iron core is produced. Then, the iron will be dissociated by photo-disintegration because of the extreme core temperatures. Important processes are ${}^{56}_{26}\mathrm{Fe} + \gamma \rightarrow 13\,{}^{4}_{2}\mathrm{He} + 4\,n$ and ${}^{4}_{2}\mathrm{He} + \gamma \rightarrow 2\,p^+ + 2\,n$. Degenerate electrons - which are responsible for the pressure inside the core (Pauli exclusion principle) - are captured by protons ($p^+ + e^- \rightarrow n + \nu_e$) and therefore the electron-degeneracy pressure in the core is lifted and the core will collapse. The hot core cools rapidly by neutrino

[2] *Uhuru* means 'freedom' in Swahili.

emission. The core will divide in an inner core and an outer core. Where the infall speed equals the local sound speed the outer core cannot keep up with the inner core. The inner core is formed until the neutron-degeneracy pressure prevents further collapse. At that point the core will bounce and an outward shock will be the onset to the supernova explosion. The result is that most of the original iron core is photo-disintegrated and a small core which is dominated by neutrons remains. Depending on whether the neutron-degeneracy pressure can withstand the extreme gravity or not, either a neutron star will stabilize or the core will collapse into a black hole. This phase corresponds to a type-II, -Ib, or -Ic supernova explosion (see, e.g., Heger et al. 2003) that for a short period of time can be as bright as the whole galaxy in which it appears.

For binary systems it is also possible to form neutron stars from white dwarfs. There are two formation possibilities. One way is by accretion-induced collapse, the other way by collapse after merging two white dwarfs. Both cases will result in an electron-capture type-Ia supernova if the mass of the white dwarf exceeds the Chandrasekhar critical mass ($\sim 1.4 M_{\odot}$; Chandrasekhar 1931).

The neutron star is formed at very high temperatures ($\sim 10^{11}$ K) and quickly ($\sim$1 day) cools down to $\sim 10^9$–10^{10} K through neutrino emission. The dominating processes in this phase are 'direct Urca processes'[3] ($n \rightarrow p^+ + e^- + \nu_e$ and $p^+ + e^- \rightarrow n + e^-$) and neutrino bremsstrahlung ($e + e \rightarrow e + e + \nu + \bar{\nu}$). At temperatures below 10^9 K, the direct Urca processes for nucleons are suppressed, because protons and neutrons become degenerate and energy and momentum can be conserved only if an additional particle is involved in the reaction ('modified' Urca processes: $N + n \rightarrow N + p^+ + e^- + \bar{\nu_e}$ and $N + p^+ + e^- \rightarrow N + n + \nu_e$). Since the modified Urca processes are less efficient than the direct ones, the neutron star cooling proceeds more slowly than before. However, if exotic particles, such as pions or kaons, are present in the core, as expected for very massive neutron stars, the direct Urca processes involving these particles would still be possible and the cooling would become more efficient (see Figure 1.1).[4]

[3]Urca is the name of a long-since-closed casino in Rio de Janeiro, and was adopted as a name for these reactions by Gamow & Schoenberg (1941) who saw a parallel between how quickly money disappears from gamblers' pockets and how quickly energy is lost in these processes.

[4]Other ingredients that can affect the neutron star cooling are the presence of superfluidity, magnetic field, and mass accretion. The possible presence of superfluidity (only for protons or for both protons and neutrons) affects the neutrino emissivity and the heat transport from the interior to the neutron star crust. The main effect of the magnetic field is the breaking of the spherical symmetry in the heat transport, but a super-strong field can even affect the superfluidity properties of the neutron star interior and the field decay can be a substantial heating process. The presence of an accreted envelope of light elements in the neutron star crust can instead enhance the thermal conductivity of the outer layers. Thus, when the cooling is dominated by neutrino processes from the star interior, the high conductivity increases the surface temperature, but it causes an acceleration of the neutron star cooling when it is dominated by emission processes in the external layers. Therefore, the neutron star temperature critically depends on its structure and composition and so the observations of its cooling evolution can give important information on the neutron star

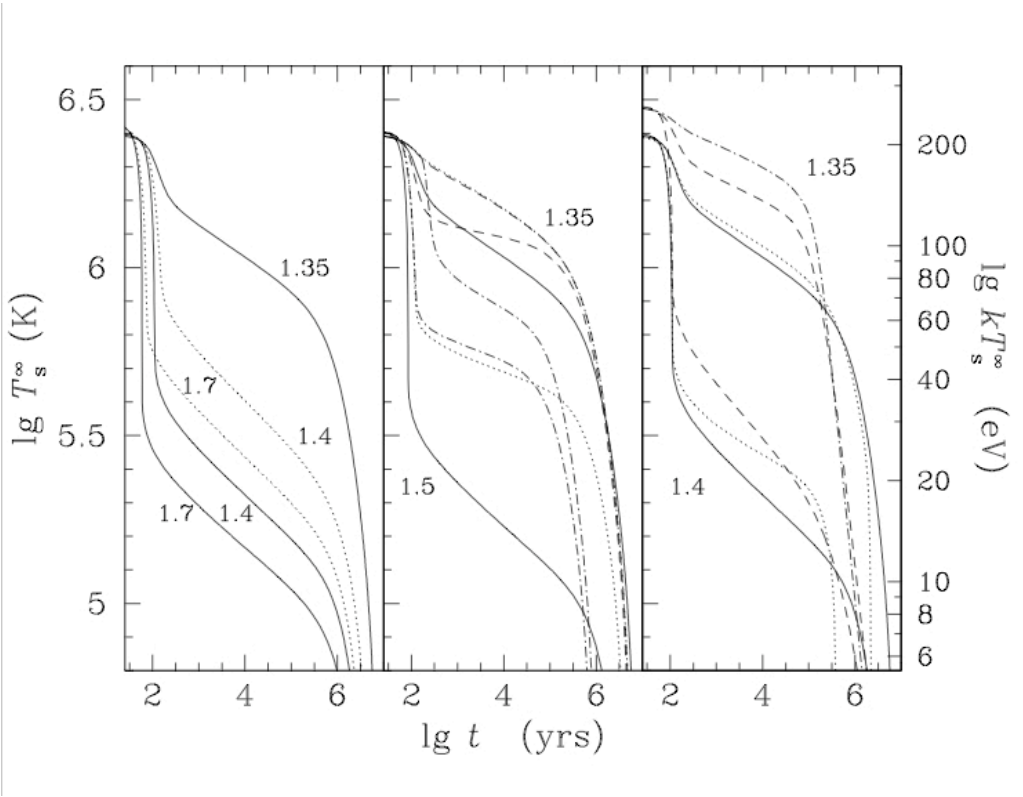

Figure 1.1 Cooling evolution for neutron stars of different masses (labeled in solar mass units) when different ingredients are added to the non-superfluid model (solid lines in all panels). *Left panel*: pion condensate in the core (dotted lines). *Middle panel*: different types of superfluidity for protons (dotted and dashed lines) and both protons and neutrons (dot-dashed lines). *Right panel*: a magnetic field of 10^{14} G at the pole (dotted lines) and accreted envelope mass of $10^{-7} M_\odot$ with (dot-dashed line) or without proton superfluidity (dashed lines). Image credit: Kaspi et al. (2006)/D. Yakovlev.

According to any cooling models, neutrino emission from the interior will still dominate over photon emission from the neutron star surface for at least 10^5 years. However, this electromagnetic emission is very important because it can be observed as a thermal component in the X-ray spectra of young and nearby neutron stars.

This spectral component is not expected to be a perfect blackbody since the magnetic field and the composition of the neutron star's atmosphere can substantially modify the emission spectrum (e.g. Zavlin & Pavlov 2002; Zavlin 2007). The atmosphere of an isolated neutron star should contain a consistent presence of iron and other heavy elements and therefore its X-ray spectrum should be rich of edges corresponding to different ionization states of the heavy

equation of state and on the poorly known properties of super-dense matter.

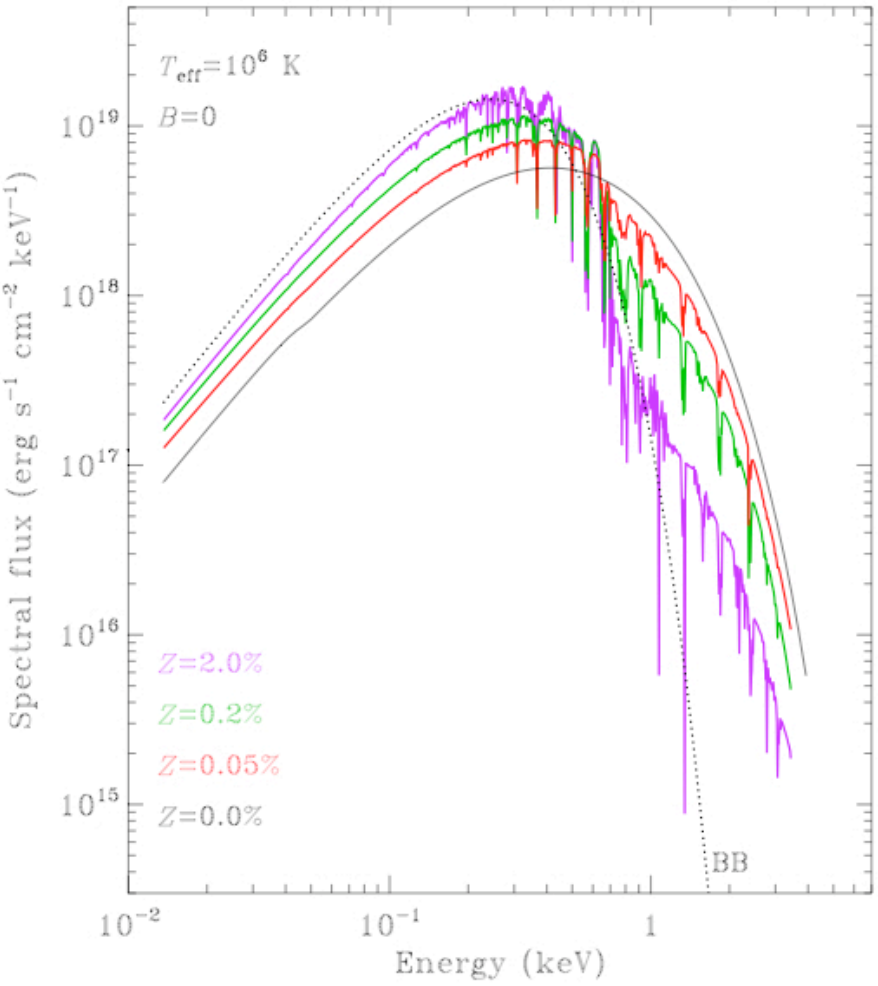

Figure 1.2 Spectra of emergent radiation in non-magnetic neutron star atmospheres having $T_{\rm eff} = 10^6$ K for different metallicities Z (Z = 2.0% corresponds to Solar metallicity.) The corresponding blackbody is shown with a dotted line. Image credit: Kaspi et al. (2006)/Zavlin & Pavlov (2002).

elements (see Figure 1.2). If the neutron star has instead experienced episodes of mass accretion, its atmosphere might be constituted mainly of light elements (H and He). The models developed to predict such a spectrum show no narrow features, but a continuum spectrum that results harder than a blackbody at the same temperature. This is due to the fact that the light elements opacity decreases with energy and so at higher temperatures deeper, and therefore hotter, layers of the neutron stars are seen. However, if observed at low energetic resolution, all these spectra are quite similar to a blackbody at the same temperature.

The inner structure of a neutron star, described by the equation of state

(EOS, i.e. the relationship between density and pressure), is still an open question in neutron-star astrophysics. See Lattimer & Prakash (2007) and Weber et al. (2007) for recent reviews and for an overview of the current status and difficulties in the quest for the EOS. A variety of neutron-star EOSs predict very different neutron-star mass-radius relations. Therefore, this relation is subject to many observational studies.

In this thesis a 'canonical' neutron star with mass $M = 1.4 M_{\odot}$ and radius $R = 10^6$ cm $= 10$ km. is used for first order estimates. The moment of inertia is $I = \frac{2}{5} M R^2 \simeq 10^{45}$ g cm^2, apart from an unknown factor of the order of the unit accounting for the mass distribution.

If a neutron star does not accrete, it generally slows down. The kinetic energy loss for a certain pulse period (P), period derivative ($\dot{P}$) and moment of inertia (I) yields the 'spin-down luminosity' of the pulsar:

$$\dot{E} = -I\omega\dot{\omega} = 4\pi^2 \frac{\dot{P}}{P^3}, \tag{1.1}$$

in which $\omega = 2\pi/P$ is the angular frequency. For radio pulsars the bulk of this energy is not emitted in the form of radio emission, but in the form of energetic particles ('pulsar wind') and high-energy radiation.

The simple 'magnetic-dipole braking model' (Pacini 1967, 1968; Gunn & Ostriker 1969) assumes that the neutron star rotates in vacuum at angular frequency ω and possesses a magnetic dipole moment $\mathbf{m}$ forming an angle α with the rotation axis. Independent of the internal field geometry, a pure magnetic dipole field at the magnetic pole of the star, B_p is related to $\mathbf{m}$ by $\mathrm{m} = |\mathbf{m}| = \frac{1}{2} B_p R^3$. While constant in module, the dipole's direction varies in time, thus radiating energy at a rate $\dot{E} = -\frac{2}{3c^3}|\ddot{\mathbf{m}}|^2$. By introducing a coordinate system with a unit vector parallel to the rotation axis ($\mathbf{e}_{\parallel}$) and two mutually orthogonal unit vectors perpendicular to the rotation axis ($\mathbf{e}_{\perp}$, $\mathbf{e'}_{\perp}$), one can explicitly write $\mathbf{m} = \mathrm{m}\,(\mathbf{e}_{\parallel}\cos\alpha + \mathbf{e}_{\perp}\sin\alpha\cos\omega t + \mathbf{e'}_{\perp}\sin\alpha\sin\omega t)$. Thus the radiate power is

$$\dot{E} = -\frac{2}{3c^3}\mathrm{m}^2\sin^2\alpha\omega^4 = -\frac{B_p^2\sin^2\alpha R^6\omega^4}{6c^3}. \tag{1.2}$$

If one assumes that the spin down of the neutron star is caused by the torque of the magnetic field with its surroundings and that the emission process is dipole radiation, one can infer a characteristic surface magnetic field (at the poles) by equating Equation 1.1 with Equation 1.2:

$$B_{\perp} = B_p \sin\alpha = \left(\frac{3c^3}{8\pi^2}\frac{IP\dot{P}}{R^6}\right)^{1/2} \simeq 3.2 \times 10^{19}(P\dot{P})^{1/2}\ \ [\mathrm{G}]. \tag{1.3}$$

$B_{\perp}$ generally ranges in neutron stars from $\sim 10^8$ to 10^{15} G and a typical value is 10^{12} G, an intensity which is dimensionally consistent with the enhancement

of the frozen-in magnetic field of a main sequence star induced by the gravitational collapse.

If one generalizes Equation 1.3 by assuming a spin-down formula $\dot{\nu} \propto \nu^{-n}$, where n is the 'braking index' and $\nu = 1/P$ the spin frequency, one can calculate the age of the pulsar (assuming no temporal distortions). By integrating the spin-down formula one finds the pulsar's age:

$$\tau = \frac{P}{(n-1)\dot{P}}\Big[1 - \Big(\frac{P_\circ}{P}\Big)^{n-1}\Big], \tag{1.4}$$

where $P_\circ$ is the pulse period at birth. If one assumes that the pulse period at birth is much smaller than the current pulse period ($P_\circ \ll P$) and pure magnetic dipole braking ($n = 3$), then the 'characteristic age', a first-order estimate of the pulsar's true age, is found:

$$\tau_c = \frac{P}{2\dot{P}}. \tag{1.5}$$

Different processes lead to different braking indices: a quadrupolar braking field (gravitational or magnetic) implies $n = 5$, while the ejection of a un-magnetized particle wind would result in $n = 1$. The braking index can be directly inferred from the measurement of the pulsar's frequency and its derivatives by:

$$n = -\frac{\nu\ddot{\nu}}{\dot{\nu}^2} \tag{1.6}$$

that can be considered an operational definition of n, as it is independent on the nature of the braking process. For the six pulsars for which a constant value of n has been measured the observed values are in the range 1.4–2.91 (Livingstone et al. 2007).

The situation is more complicated for the initial spin period. P can be determined from Equation 1.4 if the age is known and n measured: this is only the case for the Crab pulsar for which $P_\circ \simeq 19$ ms. Moreover, the initial spin period distribution of neutron stars is not well predicted by theory.

Although Equations 1.3 and 1.4 are based on a simple magnetic dipole braking in a vacuum - which is almost certainly not the case (see below) - and on assumption of a negligible initial spin period, they provide at least estimates of other important physical information. For this reason the P–$\dot{P}$ diagram (Figure 1.3) plays a role similar to the Hertzsprung-Russell diagram for ordinary stars.

At birth pulsars appear in the upper left corner of the P–$\dot{P}$ diagram. If B is conserved and they age as described above, they gradually move to the right and down, along lines of constant B and crossing lines of constant τ_c. Pulsars with $\tau_c < 10^5$ years are often found in or near recognizable supernova remnants. Older pulsars are not, either because their supernova remnants have faded to invisibility or because the supernova explosions expelled the pulsars

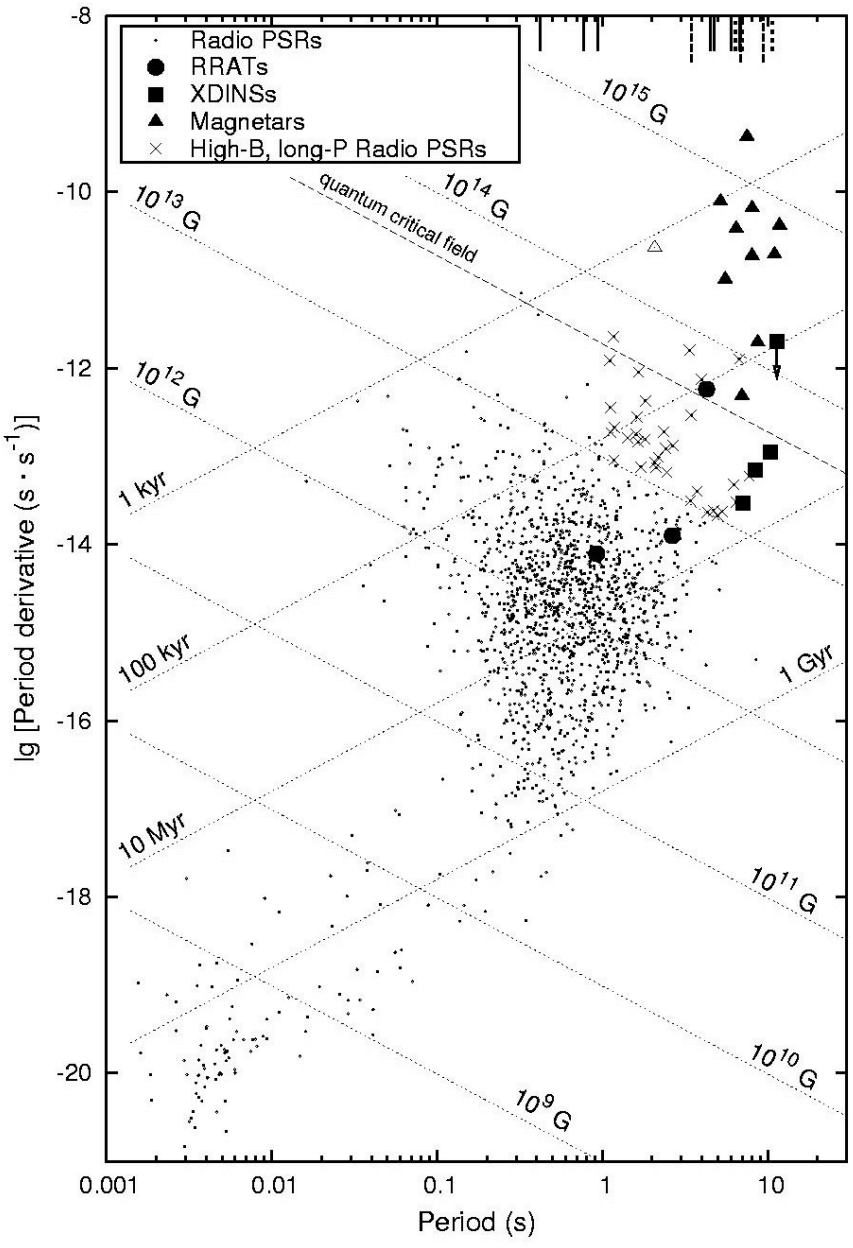

Figure 1.3 The P–$\dot{P}$ diagram encodes a great amount of information about the pulsar population and its properties, as determined and estimated from two of the primary observables, P and $\dot{P}$. Lines of constant B and τ_c are indicated. Image credit: courtesy of R. Turolla.

with enough speed that they have since escaped from their parent supernova remnants. The bulk of the pulsar population is older than 10^5 years but much younger than the Galaxy ($\sim 10^{10}$ years). The observed distribution of pulsars in the P–$\dot{P}$ diagram indicates that something changes as pulsars age. One controversial possibility is that the magnetic fields of old pulsars must decay

on time scales $\sim 10^7$ years, causing old pulsars to move almost straight down in the P–$\dot{P}$ diagram until they fall into the 'graveyard' below the 'death line' and cease radiating radio pulses.

Almost all short-period pulsars below the spin-up line[5] near $\log[\dot{P}/P] \approx -16$ are in binary systems, as evidenced by periodic (i.e. orbital) variations in their observed pulse periods. These 'Millisecond' pulsars (MSPs) are often referred to as 'recycled' since they have been spun up by accreting mass and angular momentum from their companions, to the point that they emit radio pulses despite their relatively low magnetic-field strengths ($B \sim 10^8$ G; the accretion causes a substantial reduction in the magnetic field strength, see e.g. Possenti et al. 1998 and references therein). The magnetic fields of neutron stars funnel ionized accreting material onto the magnetic polar caps, which become so hot that they emit X-rays. As the neutron stars rotate, the polar caps appear and disappear from view, causing periodic fluctuations in X-ray flux; many are detectable as X-ray pulsars. MSPs with low-mass ($M \sim 01$–$1 M_\odot$) white-dwarf companions typically have orbits with small eccentricities. Pulsars with extremely eccentric orbits usually have neutron-star companions, indicating that these companions also exploded as supernovae and nearly disrupted the binary system. Stellar interactions in globular clusters cause a much higher fraction of recycled pulsars per unit mass than in the Galactic disk. These interactions can result in very strange systems such as pulsar–main-sequence-star binaries and MSPs in highly eccentric orbits. In both cases, the original low-mass companion star that recycled the pulsar was ejected in an interaction and replaced by another star. A few MSPs are isolated: they were probably recycled via the standard scenario in binary systems, but the energetic MSPs eventually ablated their companions away.

Although the magnetic-dipole braking model is so useful in providing important physical information, it is almost certainly wrong in the assumption that pulsars rotate in vacuum. That a neutron star cannot be surrounded by a vacuum was first shown by Goldreich & Julian (1969). A rotating magnetic dipole surrounded by a vacuum will induce a Lorentz force parallel to the magnetic field. For pulsars this force will exceed the gravitational force by orders of magnitude. Charged particles will be lifted from the surface into the magnetosphere and the surface charge layer could not be in dynamical equilibrium. Moreover, the particles will co-rotate with the neutron star within the light cylinder magnetosphere.

Most current theories for magnetospheric emission can be grouped into polar cap, outer gap, and nebular models. These models, at least in some cases, need not be mutually exclusive; the Crab pulsar (among others), for example, shows clear evidence for pulsed emission from the magnetosphere and unpulsed emission from the surrounding nebula. The common thread between all magnetospheric models is that the energy is derived from the spin-down

[5]The minimum spin period attainable by accretion from a companion star.

of the neutron star. It is for this reason that the X-ray detected pulsars are generally those with the greatest spin-down luminosity and thus comparisons between the spin-down power and the X-ray luminosity provide crucial constraints. Clearly a simple interpretation with X-ray luminosity scaling as some

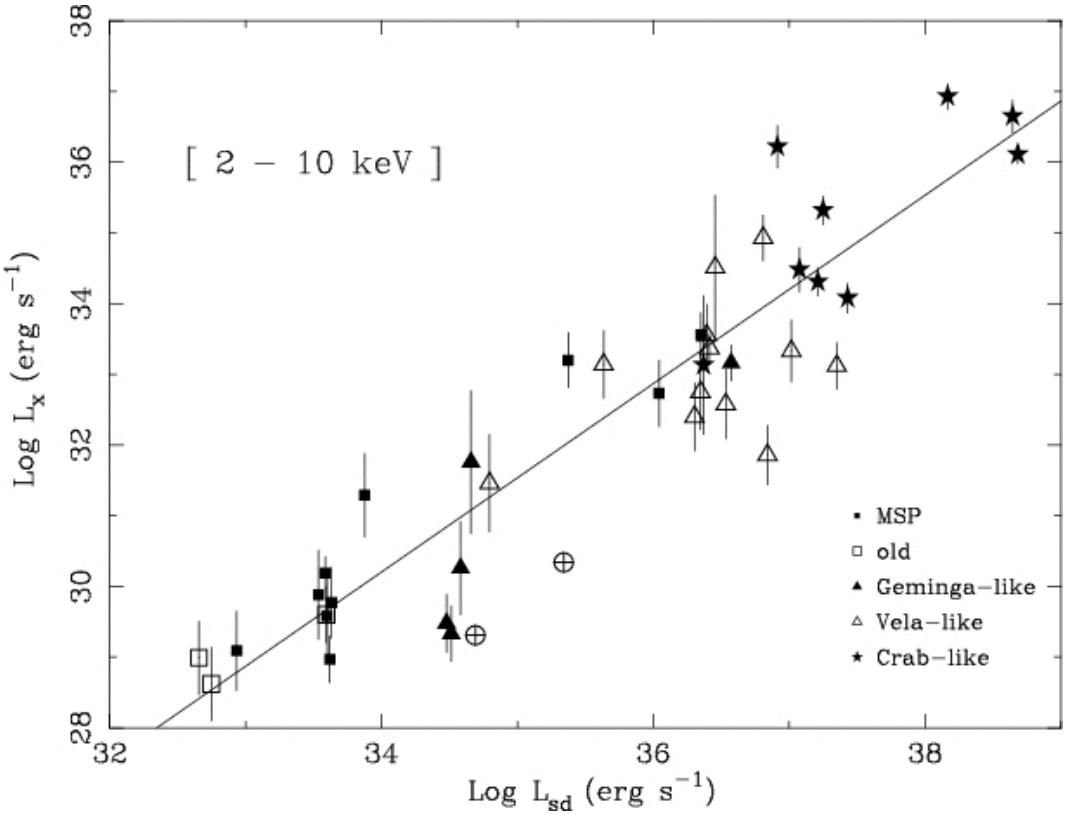

Figure 1.4 Plot of $L_{\rm X}$ (2–10 keV) versus $L_{\rm SD} \equiv \dot{E}$ (from Possenti et al. 2002). (Note that the luminosity for each pulsar is derived on the basis of a particular spectral model, and that this varies from point to point.) The line shown correspond to the empirical relationship $\log L_{\rm X} = 1.34 \log L_{\rm SD} - 15.34$ (similar relationships were derived by Seward & Wang 1988 and Becker & Truemper 1997). Image credit: Possenti et al. (2002).

power of the spindown energy loss does not hold for all pulsars, although the general correlation is clear (see Figure 1.4). In particular, there appears to be a number of pulsars for which the X-ray emission, relative to the available spin-down power, exceeds that characteristic of the majority. This is suggestive of a second emission component - perhaps associated with cooling emission from the neutron star's surface. This suggestion is strengthened by observation of a distinct soft emission component, consistent with the cooling scenario, from several of these pulsars. Other pulsars fall distinctly below the curve, perhaps indicating geometrical effects which limit the X-ray emission.

The general view of pulsar magnetospheres derives from the model of Goldreich & Julian (1969) who showed that within the star and magnetosphere,

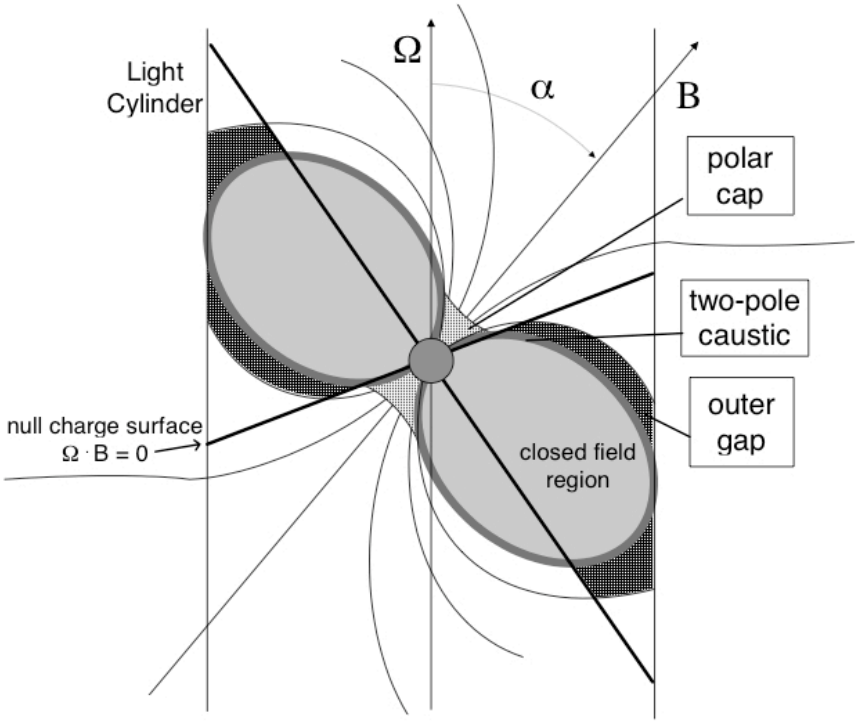

Figure 1.5 Schematic view of the high-energy emission geometry of several proposed models. Image credit: Kaspi et al. (2006).

the component of **E** along **B** must vanish because any nonzero component would result in charge flow which would rearrange the charge density until the field was canceled. The dynamics produce a charge-separated, corotating magnetosphere. In regions where the charge density is zero (the so-called 'gap regions', see Figure 1.5), however, no charge redistribution is possible, and regions with large $\mathbf{E} \cdot \mathbf{B}$ may be formed. For sufficiently large rotation rates and magnetic fields, these large fields can result in $e^{\pm}$ production generating a pair plasma which effectively 'shorts' the circuit; the charges are accelerated along the field lines, resulting in curvature radiation of gamma-rays, and ensuing photon-particle cascades. Models for such gap sites have concentrated on regions just above the magnetic polar caps (Sturrock 1971; Ruderman & Sutherland 1975), and on regions in the outer magnetosphere ('outer gaps' - e.g. Cheng et al. 1986a,b; Chiang & Romani 1994; Romani & Yadigaroglu 1995). The models are not mutually exclusive, and each invokes potential drops along the magnetic field associated with the rotational dynamo action of the pulsar magnetic field.

In outer gap models, the X- and gamma-ray emission from the more luminous pulsars are accommodated by an acceleration site where the magnetic field is low enough for pair-production via photon-photon interactions to dom-

inate the process. The gap is formed in the outer magnetosphere between the $\mathbf{\Omega} \cdot \mathbf{B} = 0$ surface (which defines the charge-separated regions) and the light cylinder, along the last closed field line (see Figure 1.5).

Three important regions contribute to the emission mechanism in a bootstrap manner. In region I, electrons and positrons are accelerated by the large potential difference across the gap, radiating curvature gamma-rays and/or boosting soft photons via inverse Compton scattering. These primary gamma-rays move away from the closed-field-line region and collide with ambient photons to produce secondary $e^{\pm}$ pairs in region II, just above region I. These energetic particles produce synchrotron radiation in the ambient magnetic field (and/or boost photons by inverse Compton scattering), covering energies from optical to gamma-rays. These photons limit the growth of region I above the last closed field line. The secondary photons move beyond region II to form tertiary pairs in region III. These pairs have insufficient energy for formation of X- or gamma-rays, but provide a sea of infrared and optical photons which illuminate the entire open magnetosphere. These photons refuel the gap so that the mechanism in region I can continue.

For young pulsars such as the Crab, a relativistic wind produced by the pulsar can be confined by the circumstellar material representing the ejected envelope of the progenitor. The result of this confinement is a synchrotron nebula which is X-ray luminous due to the interaction of the relativistic electrons with the ambient magnetic field (Pacini & Salvati 1973; Helfand & Becker 1987). For older pulsars, any such circumstellar envelope has long since dissipated; however, confinement of the electron wind can still result from the ram pressure associated with the pulsar proper velocity into the interstellar medium (Cheng 1983). The pulsar wind expands relativistically near the pulsar, but encounters a reverse shock at $R_{\rm s} \lesssim 0.1 R_{\rm N}$ where $R_{\rm N}$ is the radius of the confining volume. The synchrotron emission region lies beyond the reverse shock, and extends to $\sim R_{\rm N}$; between the reverse shock and the pulsar, the emission is underluminous. The size of the confinement volume relates wind parameters to the pulsar motion and the density of the interstellar medium.

1.3 Magnetars

About two thousand pulsars are known (ATNF Pulsar Catalogue;[6] Manchester et al. 2005). Almost all of these are located within the Milky Way Galaxy (nine pulsars are located in the Magellanic Clouds, none has been detected so far in more distant galaxies), most within the Galactic disk. About half of the ∼100 known MSPs are found in globular clusters: the high concentration of stars in the cores of these clusters facilitates the formation of binaries by star capture the spin up of old neutron stars to millisecond periods. Most pulsars are detectable only at radio wavelengths, but about 40 especially young

[6] See http://www.atnf.csiro.au/research/pulsar/psrcat .

and short-period pulsars are detectable at optical, X-ray, and even gamma-ray wavelengths. About half of these are detectable only at high energies. Among these are the 'magnetars', which have periods from 2 to 12 s and period derivatives as large as 10^{-10} s s^{-1}, implying magnetic fields of 10^{14} to 10^{15} G. The high-energy emission in these objects is believed to be powered by decay of the ultra-strong magnetic field rather than by the neutron star rotational kinetic energy, as it would be the case for normal pulsars and MSPs. Two classes of X-ray pulsars have been recognized in the last decade as magnetars: the Anomalous X-ray Pulsars (AXPs) and the Soft Gamma-ray Repeaters (SGRs).

1.3.1 Soft Gamma-ray Repeaters

The first burst from a soft gamma-ray repeater was detected on 1979 January 7 (Mazets et al. 1982; Laros et al. 1986). This event originated from SGR 1806–20 and was detected by the *Venera 11* probe which was looking for Gamma-Ray Bursts (GRBs; extremely luminous cosmic explosions). Soon after, on 1979 March 5 an extraordinary bright event was observed (Mazets et al. 1979). It had an initial extremely bright spike and a 3-minute decaying tail in which 8-s pulsations were visible (suggesting the neutron-star nature of the source). The energy released during this burst was enormous: $\sim 5 \times 10^{44}$ erg (assuming isotropic emission). It was the first of three 'giant flares' detected from SGRs so far. The source is currently known as SGR 0526–66 and is located in the Large Magellanic Cloud (e.g. Kulkarni et al. 2003). Within a day another burst, orders of magnitude less intense, was detected from SGR 0526–66 (Aptekar et al. 2001). Another recurrent burster was discovered when on 1979 March 24, 25, and 27 three soft short bursts were detected from the same location (SGR 1900+14). It is remarkable that the first three out of the currently four (plus a few candidates) known SGRs were discovered within three months from each other. These bursts were first classified as strange soft GRBs.[7] However, before the above-mentioned cases a GRB had never been observed from the same location more than once. All three bursters, SGR 0526–66, SGR 1900+14, and SGR 1806–20 showed recurrent bursting activity (Golenetskii et al. 1987; Atteia et al. 1987; Laros et al. 1987) and the name of Soft Gamma-ray Repeater was therefore chosen to distinguish them from the typical GRBs.

Persistent emission with $L \approx 10^{35}$ erg s^{-1} was also observed from SGRs in the soft X–ray range (<10 keV; Rothschild et al. 1994; Murakami et al. 1994; Vasisht et al. 1994). A *RossiXTE* observation of SGR 1806–20 led to the discovery of pulsations in the persistent emission with period $P \simeq 7.47$ s and period derivative $\dot{P} \simeq 8 \times 10^{-11}$ s s^{-1} (Kouveliotou et al. 1998a). It was noticed that the persistent X-ray flux from SGR 1806-20 is two orders of magnitude

[7] At that time GRB research was also still in its infancy, only a few years after the discovery of the first GRB (Klebesadel et al. 1973).

higher than the energy available from spin down (Equation 1.1). Moreover, under the assumption of pure magnetic dipole braking (Equation 1.3), these values imply a surface magnetic field strength of 8×10^{14} G.[8] This supports the idea that energy is produced by the decay of an extremely high magnetic field as it was already (independently) proposed by Duncan & Thompson (1992) and Paczynski (1992).

The bursting behaviour of SGRs is very irregular. SGRs tend to have episodes of bursting activity during which episodes hundreds of bursts can be seen within several weeks. It can also occur that an a SGR does not show any bursts for years. For example, no bursts have been detected from SGR 0526–66 since 1983, and SGR 1627-41 (discovered in 1998; Kouveliotou et al. 1998b) showed only one bursting episode of six weeks (Woods et al. 1999c) before its 2008 re-activation (Chapter 5). The most common bursts have durations of ∼0.04–1.0 s with the peak of the distribution around 0.1–0.2 s (Aptekar et al. 2001; Göğüş et al. 2001). Three giant flares with luminosity $\gtrsim 10^{43}$ erg s^{-1} have also been observed to date, each one from a different SGR: on 1979 March 5 from SGR 0526–66 in the Large Magellanic Cloud (Mazets et al. 1979), on 1998 August 27 from SGR 1900+14 (Hurley et al. 1999a), and on 2004 December 27 from SGR 1806–20 (Hurley et al. 2005).

The spectra of SGR-bursts are very different from spectra from other transient events like e.g. GRBs. The SGR-burst spectra can (usually) be described by optically-thin thermal bremsstrahlung and double blackbody models (e.g. Olive et al. 2004; Feroci et al. 2004; Israel et al. 2008, but see also Chapters 4 and 5). They are hard up to a spectral break after which they decay is steep. X-ray bursts from X-ray binary sources are much softer and do not reach energies as high as SGR bursts. GRBs do have high-energy photons but their spectra do not decay as steeply after their spectral breaks.

The persistent X-ray spectra (<10 keV) from SGRs are power-law like with in some cases a thermal blackbody component (e.g. Kulkarni et al. 2003; Kouveliotou et al. 2001; Chapters 3 and 4). Recently, persistent hard X-ray emission (>20 keV) has been detected from SGR 1806–20 and SGR 1900+14 with *INTEGRAL* (Mereghetti et al. 2005a; Molkov et al. 2005; Götz et al. 2006; Chapters 3 and 4). These spectra are also power-law like.

SGR 0526–66 is likely associated with the supernova remnant N49 whose estimated age is ∼5000 years (Shull 1983; Vancura et al. 1992). SGR 1806–20 and SGR 1900+14, and possibly also SGR 0526–66, are likely associated with young clusters of massive stars (Eikenberry et al. 2001; Figer et al. 2005; Vrba et al. 2000; Klose et al. 2004). Moreover, the sky distribution of the SGRs (Figure 1.6) confirms that they are young objects: three SGRs are in the Galactic Plane and one in the Large Magellanic Cloud. This means also that for the SGRs the detection of optical/infra-red counterparts is hampered

[8] Shortly after, periodic pulsations in the X-ray counterpart of SGR 1900+14 (period of ∼5.2 s) were discovered with the *ASCA* satellite (Hurley et al. 1999d). Subsequent observations with *RossiXTE* confirmed the pulsations and established that the source was spinning down rapidly, with a period derivative of $\sim 10^{-11}$ s s^{-1} (Kouveliotou et al. 1999).

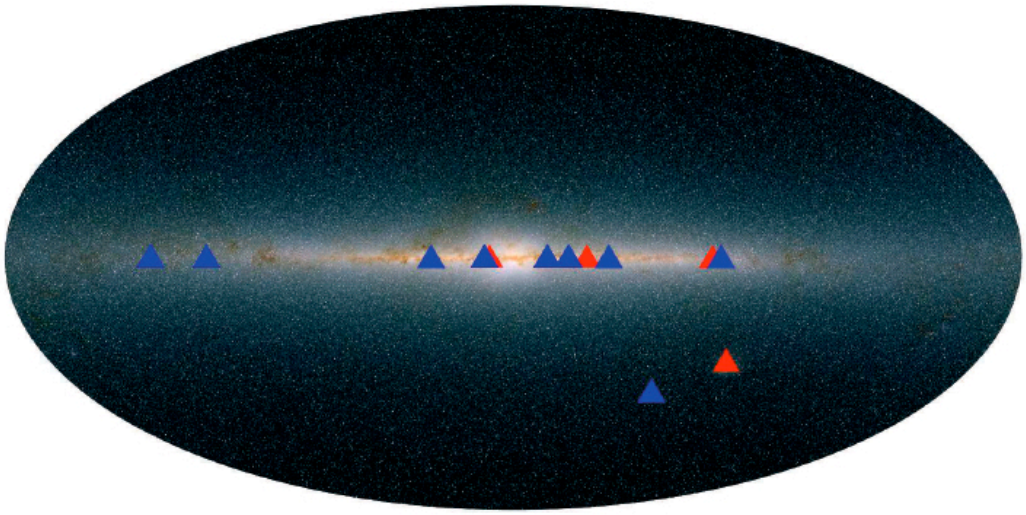

Figure 1.6 Two Micron All-Sky Survey image mosaic with the locations of the magnetars. AXPs are indicated in blue and SGRs are indicated in red. Except for the two sources in the Magellanic Clouds the magnetars are distributed close to the Galactic plane. Image credit: den Hartog (2008)/J. Carpenter, T. H. Jarrett, & R. Hurt; Image mosaic obtained as part of the Two Micron All Sky Survey (2MASS), a joint project of the University of Massachusetts and the Infrared Processing and Analysis Center/California Institute of Technology.

by the large number of field sources within their X-ray error circles and by dust extinction (for the Galactic ones). For this reason, it is not surprising that only one SGR has an identified infra-red counterpart: a variable infra-red source (Kosugi et al. 2005; Israel et al. 2005a) was seen in the very small error box obtained from the bright radio transient detected at a position consistent with SGR 1806–20 after its giant flare (Cameron et al. 2005). Apart from this case, only SGR 1900+14, soon after its giant flare, was detected at radio wavelengths (Frail et al. 1999), while no persistent or pulsed radio emission from any SGR has been detected yet.

1.3.2 The magnetar model

For SGRs the evidence for an ultra-strong magnetic field is supported by several independent requirements, some of which are based on the energetic and spectral properties of giant flares. The magnetic energy stored in the crust (the depth of the crust is $\Delta R \sim 1$ km) is $\frac{B^2}{8\pi} 4\pi R^2 \Delta R \approx 10^{45}$ erg for $B \sim 10^{15}$ G, and it is sufficient to power magnetars for several thousand years for the observed luminosities of $\sim 10^{35}$ erg s^{-1}.

The secular spin-down measured in magnetars allows to infer their magnetic field through the dipole braking relation (Equation 1.3). This yields values in the range $\sim 10^{14}$–10^{15} G. However, these estimates are subject to some uncertainties since other plausible processes, such as for example the ejection of a

relativistic particles wind (see Section 1.2), can contribute to the torques acting on these neutron stars.

The most compelling evidence for the presence of high magnetic fields comes from the extreme properties of the giant flares observed in SGRs. The first object to be interpreted as a magnetar was in fact SGR 0526–66, responsible for the exceptional flare observed on 1979 March 5 (Mazets et al. 1979). Several properties of this event could naturally be explained by invoking a super-strong magnetic field (Duncan & Thompson 1992; Paczynski 1992). The extremely challenging properties of this first observed giant flare were subsequently confirmed by the more detailed observations of similar events from two other SGRs. Two aspects of the March 1979 event were crucial for the magnetar interpretation: its spatial coincidence with the young supernova remnant N49 in the Large Magellanic Cloud, which immediately enabled to set the energetics through a secure distance determination, and the evidence for a periodicity of 8 s, strongly hinting to the presence of a rotating neutron star. Giant flares are characterized by an initial hard spike of emission up to the MeV range, lasting a fraction of a second, followed by a long tail (several minutes) with a softer spectrum and clearly showing the periodic modulation due to the neutron star rotation. Magnetic confinement of the hot plasma responsible for the pulsating tails is one of several evidences for the presence of a high field, and sets a lower limit of the order of a few 10^{14} G on its intensity. Other motivations for a high magnetic field include: (a) the reduction, due to the magnetic field, in the photon opacity required to exceed by at least a factor $\sim 10^3$ the Eddington limit[9] for a neutron star in the short gamma-ray bursts (an argument first applied to SGR 0526–66 by Paczynski 1992); (b) the necessity of providing enough free energy to power the giant flares; (c) the short duration of the initial spikes, consistent with the propagation with Alfvén speed of the magnetic instability over the whole neutron star surface (Thompson & Duncan 1995).

A strong dipole field also provides a natural way to slow-down a neutron star to a long period within a relatively short time: their small-scale height on the Galactic plane and their tendency to be found in regions close to clusters of very massive stars (see Section 1.3.1) indicate that magnetars are young objects. In the case of SGR 0526–66, spinning at 8 s, the associated supernova remnant implies an age of $\sim$5000 years. In order for this to be compatible with the spin-down age, the magnetic field must be $\approx 10^{15}$ G.

Finally, an independent evidence for superstrong magnetic fields in SGRs

[9]Eddington luminosity (sometimes also called the Eddington limit) is the largest luminosity that can pass through a layer of gas in hydrostatic equilibrium, supposing spherical symmetry (Eddington 1926). If the luminosity of a star exceeds the Eddington luminosity of a layer on the stellar surface, the gas layer is ejected from the star. This limit is obtained by equating the radiation pressure with gravitational forces. The exact value of Eddington luminosity depends on the chemical composition of the gas layer and the spectral energy distribution of the emission. If the Thomson scattering cross-section is used and the gas is assumed to be purely made of ionized hydrogen, the Eddington Luminosity is given by $L_{\mathrm{Edd}} = \frac{4\pi c G M m_p}{\sigma_T}$, where c is the speed of light, G is the gravitational constant, M is the mass of the body, m_p is the mass of a proton, and σ_T is the Thomson cross section.

has been recently pointed out by Vietri et al. (2007) who considered the high frequency 'quasi-periodic oscillations' (QPOs) observed in the giant flare of SGR 1806–20. The 625 and 1 840 Hz QPOs involve extremely large and rapid luminosity variations, with $\Delta L/\Delta t$ as large as several 10^{43} erg s^{-2}. This value exceeds the Cavallo-Rees luminosity-variability limit $\Delta L/\Delta t < 2\eta \times 10^{42}$ erg s^{-2}, where η is the efficiency of matter to radiation conversion (Cavallo & Rees 1978). The relativistic effects generally invoked to circumvent this limit in blazars and gamma-ray bursts are unlikely to be at work in the SGR QPO phenomenon. Vietri et al. (2007) instead propose that the Cavallo-Rees limit does not apply owing to the reduction in the photon scattering cross section induced by the strong magnetic field. In this way a lower limit of $\sim 2\,([10\,\mathrm{km}]/R)^3(0.1/\eta)^{1/2} \times 10^{15}$ G for the surface magnetic field is derived.

Duncan & Thompson (1992) and (Thompson & Duncan 1993) pointed out that very high magnetic fields, in principle up to $([3\,\mathrm{ms}]/P_\circ) \times 10^{17}$ G, can be formed through an efficient dynamo if the neutron stars are born with sufficiently small periods, of the order of $P_\circ \sim 1$–2 ms for a magnetic field in the range 10^{14}–10^{15} G, and if convection is present. The dynamo effect (comparable to the solar dynamo at a different scale) will be active only for a few seconds, but this can be sufficient to boost the internal (toroidal) magnetic field up to $B \sim 10^{16}$ G.

The dynamo is only effective within a small range of initial birth parameters and especially a short rotation period and therefore this mechanism is debated. In particular, population studies of radio pulsars indicate that such fast initial periods are not common (the birth spin periods inferred from a few young pulsars are of the order of a few tens of milliseconds; Faucher-Giguère & Kaspi 2006).

An alternative formation scenario is based on magnetic flux conservation arguments and postulates that the distribution of field strengths in neutron stars (and white dwarfs) simply reflects that of their progenitors. In this 'fossil field' model, the magnetars would simply be the descendent of the massive stars with the highest magnetic fields. The wide distribution of field strengths in magnetic white dwarfs is thought to result from the spread in the magnetic fields of their progenitors. Extrapolating this result to the more massive progenitors of neutron stars could explain the origin of magnetars (Ferrario & Wickramasinghe 2006). On average, higher magnetic fluxes are expected in the more massive progenitors. The young clusters of massive stars found close to the locations of the SGRs seem to support this scenario.

Different possibilities have been proposed to explain the observed persistent X-ray emission in magnetars. In the magnetar model, the pulsed X-rays are likely the combined result of surface thermal emission with a non thermic high-energy tail resulting from resonant scattering of thermal photons off magnetospheric currents.

Magnetic field decay can provide a significant source of internal heating. While ohmic dissipation and Hall drift dominate the field decay, respectively, in weakly ($\lesssim 10^{11}$ G) and moderately magnetized (10^{12}–10^{13} G) neutron stars, the most relevant process in magnetars is ambipolar diffusion, which has a characteristic time-scale $\tau_{\rm amb} \sim (B_{\rm core}/[10^{15}\,{\rm G}])^{-2} \times 10^4$ years (Goldreich & Reisenegger 1992; Thompson & Duncan 1996). This internal heating source yields a surface temperature higher than that of a cooling neutron star of the same age but of smaller magnetic field. Furthermore, the enhanced thermal conductivity in the strongly magnetized envelope, contributes to increase the surface temperature (Heyl & Hernquist 1997; Heyl & Kulkarni 1998).

The short, soft bursts can be triggered by cracking of the crust caused by the strong magnetic field (Thompson & Duncan 1996). The crust fractures perturb the magnetosphere and inject fireballs. The bursts duration is dictated by the cooling time, but it depends also on the vertical expansion of surface layers (Thompson 2002) and/or depth of heating (Lyubarsky 2002). Also a different burst mechanism could be at work in magnetars, producing bursts as result of magnetic reconnection events in the magnetosphere, with the release of energy stored in non-potential magnetic fields (Lyutikov 2002).

Thompson et al. (2002) explored thoroughly the conjecture that the magnetar internal field is tightly wound up in a toroidal configuration and is up to a factor $\sim$10 stronger than the external field. The unwinding of the internal field shears the neutron star crust. The rotational motions of the crust provide a source of helicity for the external magnetosphere by twisting the magnetic field which is anchored to the star surface (see Figure 1.7). A globally twisted magnetosphere, instead than a simple dipolar configuration, could be the main difference between magnetars and radio pulsars with $B \gtrsim B_{\rm QED}$.[10] The presence of a twisted magnetosphere ($B_\phi \neq 0$) has several important consequences. A twisted, force-free magnetosphere supports electrical currents several orders of magnitude larger than the Goldreich-Julian current flowing along open field lines in normal pulsars. The strong flow of charged particles heats the neutron star crust and produces a significant optical depth for resonant cyclotron scattering in the magnetosphere. Repeated scattering of the thermal photons emitted at the star surface can give rise to significant high-energy tails. The optical depth is proportional to the twist angle, thus a spectral hardening is expected when the twist increases. Another consequence of the twisted field is that the spin-down torque is larger than that of a dipolar field of the same strength. Given that both the spectral hardening and the spin-down rate in-

[10] Quantum electrodynamic effects appear around and above the critical magnetic field $B_{\rm QED} = m_e^2 c^3/\hbar e \simeq 4.413 \times 10^{13}$ G, at which the energy of the first Landau level for electrons equals their rest mass. They include that the vacuum becomes anisotropic and birefringent causing vacuum polarization(Duncan 2000). The light will become decomposed in ordinary (O) and extraordinary (E) photons and can cause magnetic lensing. Another effect is photon splitting (and merging; Adler et al. 1970) which is dominated by $E \rightarrow O+O$. Photon-electron scattering will be strongly suppressed in the E mode. Moreover, atoms in magnetic fields $\gtrsim 10^{10}$ G are distorted into long thin ('spaghetti-like') cylinders (Lai 2001).

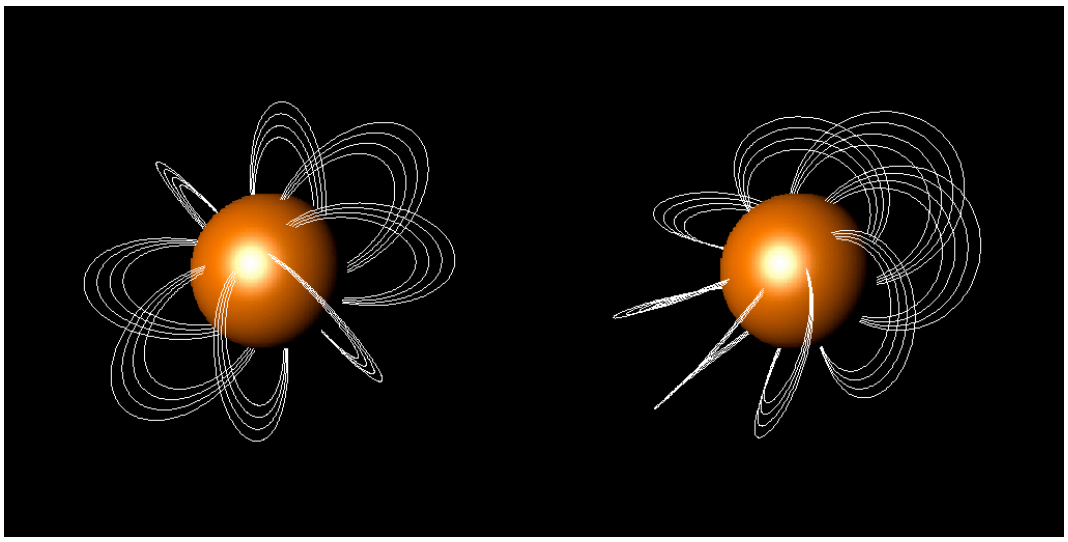

Figure 1.7 Comparison of a dipole magnetic field (*left*) with a twisted dipole magnetic field (*right*). Image credit: courtesy of R. Turolla.

crease with the twist angle, a correlation between these quantities is expected. In fact the presence of such a correlation has been reported by Marsden & White (2001) and Mereghetti et al. (2007). Since the stresses building up in the neutron star crust lead to crustal fractures which are at the base of the burst emission, it is also expected that a twist angle increase gives rise to an enhanced bursting activity. The overall evolution of SGR 1806–20 in the years preceding and following the giant flare of December 2004 seems to support these predictions (Mereghetti et al. 2005c, 2007).

In the context of the twisted magnetosphere model, two possibilities have been proposed to explain the high-energy emission from magnetars (Thompson & Beloborodov 2005; Beloborodov & Thompson 2007): (a) bremsstrahlung from a thin turbulent layer of the star's surface, heated to $k_BT \sim 100$ keV by magnetospheric currents, and (b) synchrotron emission from pairs produced at a height of $\sim$100 km above the neutron star. In the first case a cut-off at a few hundred keV is expected, while in the second case the spectrum should extend to higher energies, peaking around 1 MeV. The currently available data are insufficient to discriminate between the two cases by measuring the energy of the spectral cutoff, which is required to avoid exceeding the upper limits obtained with the Comptel instrument in the MeV range (den Hartog et al. 2006). Baring & Harding (2007) consider resonant, magnetic Compton upscattering to explain the hard X-ray emission. Ultra-relativistic electrons, accelerated along either open or closed magnetic field lines, upscatter the thermal soft X-ray atmospheric photons. This process is very effective close to the magnetar surface ($\lesssim 10 R_{\rm NS}$) where the magnetic field is still strong. The preliminary example spectra derived by Baring & Harding (2007) are however too soft and extend to energies much higher than can be permitted by the Compton upper limits.

1.3.3 Anomalous X-ray Pulsars

The AXP prototype 1E 2259+586 was discovered at the center of the supernova remnant G109.1-1.0 (Fahlman & Gregory 1981) and for many years it remained an isolated oddity in the 'zoo' of X-ray pulsars. A period derivative of $\sim 5 \times 10^{-13}$ s s^{-1} was measured by Koyama et al. (1987), but it was clear that, with a spin period of $\sim$7 s, the loss of rotational energy was orders of magnitude too small to power the observed luminosity of a few 10^{35} erg s^{-1}. Thus 1E 2259+586 was not a rotation powered pulsar and it also seemed different from the majority of accreting pulsars known at the time, due to its soft X-ray spectrum, lack of bright (and hence massive) companion star, and positive period derivative. Moreover, stringent limits on the mass of an unseen (possibly obscured by interstellar extinction) companion were derived from repeated measurements of the pulsation periods, which did not reveal any Döppler modulation produced by a possible binary orbit (Mereghetti et al. 1998).

Several additional sources were found with similar characteristics (in particular all the pulse periods were in the $\sim$5–10 s range) and recognized as a subclass of accreting X-ray pulsars (Mereghetti & Stella 1995; van Paradijs et al. 1995). In fact, the above limits did not rule out the presence of a very low mass companion star and this scenario was more plausible than an interpretation as isolated neutron stars. Mereghetti & Stella (1995) proposed that AXPs might have an intermediate magnetic field between that of the pulsars in high-mass X-ray binary systems and that of pulsars in low-mass X-ray binary systems, since a typical magnetic field of 10^{11} G would be able to explain the period clustering around $\sim$10 s, their typical luminosities of $\sim 10^{35}$ erg s^{-1}, and the presence of spin-down.[11]

The possible evidence that some AXPs are located in particularly dense regions suggested that they might be neutron stars accreting from the interstellar medium (Israel et al. 1994), but the very high densities required to produce their observed luminosity completely rules out this possibility. Other interpretations based on accretion but not requiring the presence of stellar companions were then proposed (see Mereghetti et al. 2002b, and references

[11] At the magnetospheric radius - where the magnetic pressure is equal to the ram pressure of the accreting matter - the disc is disrupted and the accretion flow is driven by the magnetic field lines. Entering the magnetosphere, the accreting matter transfers its angular momentum to the neutron star, that is anchored to its magnetic field lines and, if the inner edge of the accretion disc rotates faster than the magnetosphere, the neutron star is spun-up, as in fact observed in accretion-powered pulsars. If instead the neutron star rotates so fast that the velocity at the magnetospheric radius is higher than that of the disc, the accretion is centrifugally inhibited and the X-ray emission should stop. An equilibrium is therefore reached when the magnetosphere corotates with the inner edge of the accretion disc, i.e. for a period $P_{\rm eq} \simeq 3 (B/[10^{12}\,{\rm G}])^{6/7} (L/[10^{37}\,{\rm erg\,s^{-1}}])^{-3/7}$ s (since the mass accretion rate, and hence the luminosity, of X-ray binaries is rather variable, the accreting pulsars are not usually observed to regularly rotate at their equilibrium period). For a source with $L \approx 10^{35}$ erg s^{-1} and $B \approx 10^{11}$ G, one obtains $P_{\rm eq} \approx 10$ s. In a perfect equilibrium, no secular spin variations should be present, but a spin-down is nevertheless expected due to the torque exerted by the magnetic field lines threading the accretion disc (Ghosh & Lamb 1979).

therein). Most of them explained AXPs as isolated neutron stars accreting from a fossil disc formed by the fallback of material produced in the supernova explosion (Chatterjee et al. 2000; Alpar 2001; Marsden et al. 2001; Rothschild et al. 2002a,b).

Thompson & Duncan (1996) observed that AXPs share a number of properties with SGRs in their quiescent states. In particular, the inferred magnetic fields from the periods and period derivatives (see Figure 1.3) and anomalously high X-ray luminosities made also AXPs magnetar candidates. After the first AXPs exhibited bursting behaviour, the magnetar interpretation of AXPs become commonly accepted. 1E 1048.1–5937 was the first AXP to show two SGR-like short bursts (Gavriil et al. 2002) and soon thereafter 1E 2259+586 showed over 80 SGR-like short bursts (Kaspi et al. 2003; Gavriil & Kaspi 2004). Also large long-term torque variations and hard X-ray emission have now been observed from several AXPs, further supporting the SGRs-AXPs connection. Three AXPs have also shown remarkably bright bursts ($\sim$2 orders of magnitude brighter than normal AXP bursts; Woods et al. 2005). They all had SGR giant-flare-like characteristics (short bright peak and a long decaying tail lasting several hundred seconds in which the pulsar's spin periods were detected), except for the absolute scale: events during which luminosities $\gtrsim 10^{44}$ erg s^{-1} were reached have been observed so far only from SGRs.

1.4 Other classes of isolated neutron stars

Observations in the X-ray, gamma-ray and optical/infra-red bands have significantly changed the old paradigm of isolated neutron stars based mainly on the observations of the large population of radio pulsars. Different new manifestations of isolated neutron stars, besides AXPs and SGRs, have been recognized. Their existence might simply reflect a larger variety in the birth properties of neutron stars than previously thought, but it is also possible that some of these classes of neutron stars are linked by evolutionary paths.

The X-ray dim isolated neutron stars (XDINSs) are nearby ($\sim$100 pc) X-ray pulsars characterized by very soft thermal spectra with blackbody temperatures in the range 40–110 eV, X-ray luminosity of 10^{30}–10^{30} erg s^{-1}, faint optical counterparts ($V > 25$), and absence of radio emission (see Haberl 2007 for a recent review). A possible relation with the magnetars is suggested by the fact that all the XDINSs have spin periods in the 3–12 s range, and the period derivatives measured for two of them are of the order of 10^{-13} s s^{-1}. These P and $\dot{P}$ values give characteristic ages of $\sim$(1–2) $\times 10^6$ years and magnetic fields of a few 10^{13} G (assuming dipole radiation braking). Magnetic fields in the $\sim 10^{13}$–10^{14} G range are also inferred by the broad absorption lines observed in the X-ray spectra of most XDINSs, independently from their interpretation either as proton cyclotron features or atomic transition lines. The seven objects observed within a distance of a few hundreds parsecs imply that the space density of XDINSs is much higher than that of the active magnetars. XDINSs

could thus be the descendant of magnetars. Note that more distant XDINSs cannot be observed because their very soft X-ray emission is severely absorbed in the interstellar medium.

Periods similar to those of the magnetars are also seen in the rotating radio transients (RRATs) recently discovered in the Parkes Multibeam Survey (McLaughlin et al. 2006). These neutron stars emit short (2–30 ms) pulses of radio emission at intervals of minutes to hours. Their rotation periods, ranging from 0.4 to 7 s, could be inferred from the greatest common divisors of the time intervals between bursts. RRATs might represent a Galactic population as large as that of active radio pulsars, that remained undiscovered for a long time due to lack of radio searches adequate to detect them. The pulsed X-rays detected from one of these objects have a thermal spectrum (blackbody temperature $\sim$0.14 keV) and are consistent with cooling emission (McLaughlin et al. 2007). Period derivatives have been determined to date for three RRATs. Only one of these objects has a rather high inferred field $B = 5 \times 10^{13}$ G, while the other two have $B = 3 \times 10^{12}$ and 6×10^{12} G, similar to normal radio pulsars. Thus their relation, if any, with the magnetars is unclear.

The Compact Central Objects (CCOs) form a heterogeneous group of X-ray sources unified by their location at the center of supernova remnants and by the lack of radio detections (Pavlov et al. 2002, 2004; De Luca 2008). These properties are shared with some of the AXPs, indicating a possible connection between magnetars and CCOs. The presence of supernova remnants implies that these are very young objects (supernova remnants typically are detectable for only a few tens of thousands of years before they fade into the interstellar medium), maybe in an evolutionary stage preceding the AXP/SGR phase. However, the two CCOs for which pulsations have been determined do not support such a relation and rather indicate that these neutron stars are born with initial parameters opposite to those of magnetars. They have short spin periods (0.424 and 0.105 s) and undetectable spin-down rates ($\dot{P} < 2 \times 10^{-16}$ s s^{-1}), yielding estimated magnetic fields smaller than a few 10^{11} G (Gotthelf & Halpern 2007; Halpern et al. 2007). The resulting characteristic ages exceed by orders of magnitude their true ages, as inferred from the associated supernova remnants, implying that their initial rotational periods were not too different from the current values. The low magnetic field and long initial spin periods of these objects might be causally related. Similar P and $\dot{P}$ have not been found in all the other CCOs, despite intensive searches, and it cannot be excluded that some of them be magnetars. Suggestions in this sense have been put forward, e.g., for the CCOs in RCW 103 (De Luca et al. 2006) and in Cas A (Krause et al. 2005, but see also Kim et al. 2008).

In the last decade sensitive radio surveys led to the discovery of a few rotation powered pulsars with magnetic-field strengths approaching those of magnetars. However, no signs of magnetar-like activity, such as enhanced X-ray emission or bursts, were seen in the rotation-powered radio pulsars with the highest inferred magnetic fields (several 10^{13} G; e.g. Camilo et al. 2000; Gon-

zalez et al. 2005; Kaspi & McLaughlin 2005). For example, PSR J1814–1744, despite having P and $\dot{P}$ values very similar to those of the AXP 1E 2259+586 has a 2–10 keV luminosity smaller than 2×10^{33} erg s^{-1} (Pivovaroff et al. 2000). These findings seem to indicate that the dipole magnetic field intensity is not by itself the only element responsible for differentiating magnetars from ordinary radio pulsars.

Very recently, short bursts have been discovered from the young pulsar at the center of the Kes 75 supernova remnant (Gavriil et al. 2008). This object, PSR J1846–0258 ($P = 0.326$ s), is the pulsar with the smallest known characteristic age ($\tau_c \simeq 884$ years) and has a high field of 5×10^{13} G. Its lack of radio emission was generally ascribed to beaming, but the discovery of magnetar-like activity now leads to consider also the possibility that this pulsar be truly radio silent. The bursts observed in PSR J1846–0258 are very similar to those seen in AXPs, and are accompanied by an enhancement of the persistent X-ray emission, a spectral softening and an increased timing noise (Gavriil et al. 2008). The important discovery that apparently normal rotation-powered pulsars can exhibit the same kind of magnetically driven activity seen in AXPs and SGRs points to a more strict connection between radio pulsars and magnetars than previously thought.

Chapter 2

Discovery of X-ray emission from the young radio pulsar PSR J1357–6429

We present the first X-ray detection of the very young pulsar PSR J1357–6429 (characteristic age of 7.3 kyr) using data from the *XMM-Newton* and *Chandra* satellites. We find that the spectrum is well described by a power-law plus blackbody model, with photon index $\Gamma = 1.4$ and blackbody temperature $k_B T = 160$ eV. For the estimated distance of 2.5 kpc, this corresponds to a 2–10 keV luminosity of $\sim 1.2 \times 10^{32}$ erg s^{-1}, thus the fraction of the spin-down energy channeled by PSR J1357–6429 into X-ray emission is one of the lowest observed. The *Chandra* data confirm the positional coincidence with the radio pulsar and allow to set an upper limit of 3×10^{31} erg s^{-1} on the 2–10 keV luminosity of a compact pulsar wind nebula. We do not detect any pulsed emission from the source and determine an upper limit of 30% for the modulation amplitude of the X-ray emission at the radio frequency of the pulsar.

2.1 Introduction

X-ray observations of radio pulsars provide a powerful diagnostic of the energetics and emission mechanisms of rotation-powered neutron stars. Due to the magnetic dipole braking, a pulsar loses rotational kinetic energy at a rate $\dot{E} = 4\pi^2 I \dot{P} P^{-3}$, where I is the moment of inertia of the neutron star, assumed to be 10^{45} g cm^2, and P is the rotation period. Though pulsars have traditionally been mostly studied at radio wavelengths, only a small fraction (10^{-7} to 10^{-5}, e.g., Taylor et al. 1993) of the 'spin-down luminosity' $\dot{E}$ emerges as radio pulsations. Rotation power can manifest itself in the X / γ-ray energy range as pulsed emission, or as nebular radiation produced by a relativistic wind of particles emitted by the neutron star. Residual heat of formation is

also observed as soft X-ray emission from young neutron stars. Such thermal radiation, however, can also be produced as a result of reheating from internal or external sources. The growing list of observable X-ray emitting rotation-powered pulsars allows the study of the properties of the population as a whole. Young pulsars constitute a particularly interesting subset to investigate owing to their large spin-down luminosities ($\gtrsim 10^{36}$ erg s^{-1}).

The discovery of PSR J1357–6429 during the Parkes multibeam survey of the Galactic plane (see Lorimer et al. 2006 and references therein) is reported in Camilo et al. (2004). The pulsar is located near the supernova remnant candidate G309.8−2.6 (Duncan et al. 1997) for which no distance or age information is available. With a spin period of 166 ms, a period derivative of 3.6×10^{-13} s s^{-1}, and a characteristic age $\tau_c = P/2\dot{P} \simeq 7300$ yr, this pulsar stands out as one of the ten youngest Galactic radio pulsars known (see the ATNF Pulsar Catalogue[1], Manchester et al. 2005). The other main properties of this source derived from the radio observations are the spin-down luminosity of 3.1×10^{36} erg s^{-1} and the surface magnetic field strength of 7.8×10^{12} G, inferred under the assumption of pure magnetic dipole braking. Based on a dispersion measure of ∼127 cm^{-3} pc (Camilo et al. 2004), a distance of ∼2.4 kpc is estimated, according to the Cordes-Lazio NE2001 Galactic Free Electron Density Model.[2]

Here we report the first detection of PSR J1357–6429 in the X-ray range using the *XMM-Newton* observatory and we present its spectral properties in the 0.5–10 keV energy band. We also made use of two short *Chandra* observations to confirm the identification and to probe possible spatial extended emissions, taking advantage of the superb angular resolution of the *Chandra* telescope.

2.2 *XMM-Newton* observation and data analysis

In this section we present the results obtained with the EPIC instrument on board the *XMM-Newton* X-ray observatory. EPIC consists of two MOS (Turner et al. 2001) and one pn CCD detectors (Strüder et al. 2001) sensitive to photons with energies between 0.1 and 15 keV. All the data reduction was performed using the XMM-Newton Science Analysis Software[3] (SAS version 7.0). The raw observation data files were processed using standard pipeline tasks (EPPROC for pn, EMPROC for MOS data). Response matrices and effective area files were generated with the SAS tasks RMFGEN and ARFGEN.

The observation was carried out on 2005 August 17 and had a duration of 15 ks, yielding net exposure times of 11.7 ks in the pn camera and 14.5 ks in

[1]See http://www.atnf.csiro.au/research/pulsar/psrcat .
[2]See http://rsd-www.nrl.navy.mil/7213/lazio/ne_model and references therein.
[3]See http://xmm.vilspa.esa.es/ .

the two MOSs. The pn and the MOSs were operated in Full Frame mode (time resolution: 73.4 ms and 2.6 s, respectively) and mounted the medium thickness filter. PSR J1357–6429 is clearly detected in the pn and MOS images (see Figure 2.1) at the radio pulsar position (Right ascension = $13^{\rm h}\,57^{\rm m}\,02.4^{\rm s}$, Declination = $-64^\circ\,29'\,30.2''$ (epoch J2000.0); Camilo et al. 2004). The source spectra

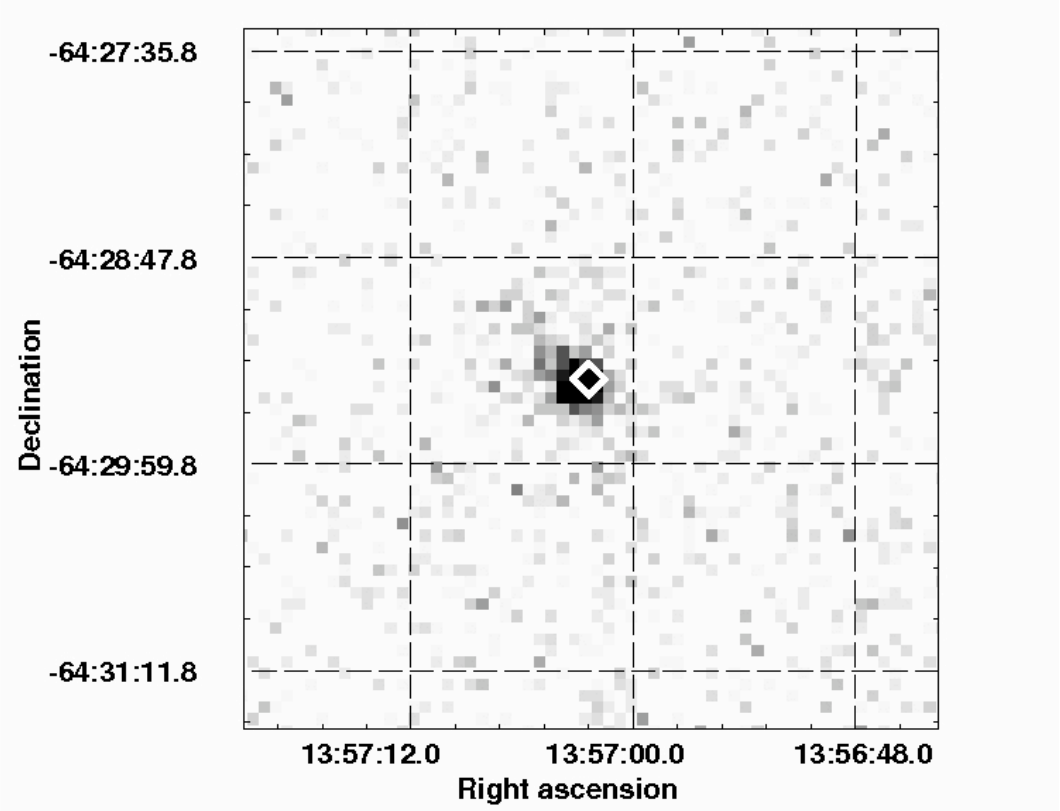

Figure 2.1 Field of PSR J1357–6429 as seen by the EPIC cameras in the 0.5–10 keV energy range. The radio pulsar position (Camilo et al. 2004) is marked with the white diamond sign. The angular separation of the centroid of the X-ray source (computed using the SAS task EMLDETECT) from the radio pulsar position is $(3.5 \pm 0.6)''$ ($1\,\sigma$ statistical error). Considering the *XMM-Newton* absolute astrometric accuracy of $2''$ (r.m.s.), the X-ray and radio positions are consistent.

were extracted from circular regions centered at the position of PSR J1357–6429. The whole observation was affected by a high particle background that led to the selection of a $20''$ radius circle in order to increase the signal-to-noise ratio in the pn detector, particularly sensitive to particle background, and a $40''$ radius for both the MOS cameras. The background spectra were extracted from annular regions with radii of $140''$ and $220''$ for the MOSs, and from two rectangular regions with total area of $\sim 10^4$ arcsec^2 located on the sides of the source for the pn. We carefully checked that the choice of different background extraction regions does not affect the spectral results. We selected events with

Table 2.1 Summary of the *XMM-Newton* spectral results. The abundances of Anders & Grevesse (1989) are used throughout. Errors are at the 90% confidence level for a single interesting parameter.

Parameter	Value	
	PL	PL+BB
$N_{\rm H}$ (10^{22} cm^{-2})	$0.14^{+0.07}_{-0.06}$	$0.4^{+0.3}_{-0.2}$
Γ	$1.8^{+0.3}_{-0.2}$	1.4 ± 0.5
k_BT (keV)	–	$0.16^{+0.09}_{-0.04}$
R_{BB}[a] (km)	–	$1.4^{+2.9}_{-0.2}$
Flux[b] (10^{-13}erg cm^{-2} s^{-1})	2.3	3.6
Blackbody flux[b] (10^{-13}erg cm^{-2} s^{-1})	–	1.3
χ^2_r / d.o.f.	1.00 / 72	0.85 / 70

[a] Radius at infinity assuming a distance of 2.5 kpc.

[b] Unabsorbed flux in the 0.5–10 keV energy range.

pattern 0–4 and pattern 0–12 for the pn and the MOS, respectively. The resulting background subtracted count rates in the 0.5–10 keV energy range were $(4.2 \pm 0.3) \times 10^{-2}$ cts s^{-1} in the pn and $(1.9 \pm 0.2) \times 10^{-2}$ cts s^{-1} in the two MOS cameras, while the background rate expected in the source extraction regions is about 50% of these values. The spectra were rebinned to have at least 20 counts in each energy bin. Spectral fits were performed using the XSPEC version 12.3 software[4] (Arnaud 1996).

The spectra from the three cameras were fitted together in the 0.5–10 keV energy range with a power law and with a power-law plus blackbody model (see Table 2.1). The latter model provides a slightly better fit, with less structured residuals (see Figure 2.2). Furthermore, considering the distance of 2.5 kpc, the interstellar absorption along the line of sight derived with the power-law fit is too low if compared to the typical column density of neutral absorbing gas in that direction of approximately 10^{22} cm^{-2} (Dickey & Lockman 1990). The resulting best-fit parameters for the power-law plus blackbody model are photon index $\Gamma = 1.4$, blackbody temperature $k_BT = 0.16$ keV, and absorption $N_{\rm H} = 4 \times 10^{21}$ cm^{-2} with a reduced χ^2 of 0.85 for 70 degrees of freedom. The corresponding luminosity in the 0.5–10 keV band is 2.7×10^{32} erg s^{-1}.

Young pulsars are often associated with pulsar wind nebulae: complex structures that arise from the interaction between the particle wind powered by the pulsar and the supernova ejecta or surrounding interstellar medium (see Gaensler & Slane 2006 for a review). Inspecting the EPIC images in various energy bands, we find only a marginal ($\approx 3\,\sigma$) evidence of diffuse emission, in the 2–4 keV energy band consisting of a faint elongated ($\sim$20 arcsec to the north-

[4] See http://heasarc.gsfc.nasa.gov/docs/xanadu/xspec/ .

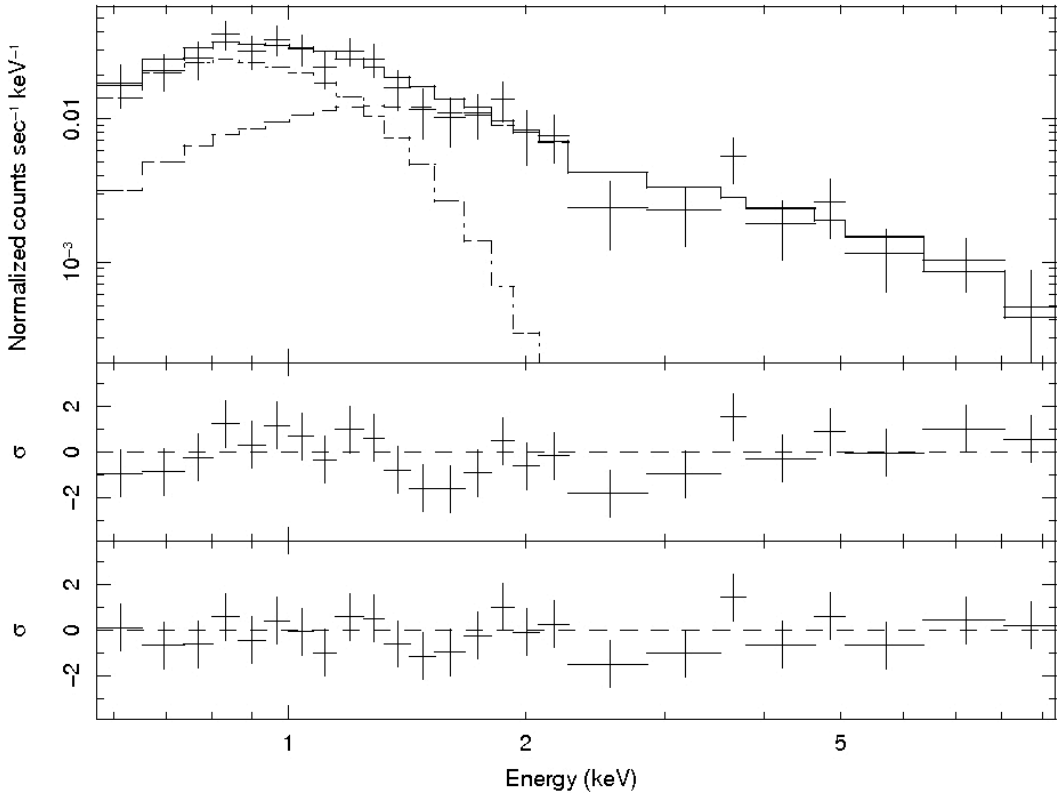

Figure 2.2 EPIC pn spectrum of PSR J1357–6429. *Top:* Data and best-fit power-law (dashed line) plus blackbody (dot-dashed line) model. *Middle:* Residuals from the power-law best-fit model in units of standard deviation. *Bottom:* Residuals from the power-law plus blackbody best-fit model in units of standard deviation.

east, see Figure 2.1) structure starting from PSR J1357–6429. We took that excess as an upper limit for a diffuse emission: assuming the same spectrum as the point source, it corresponds to a 2–10 keV luminosity of $\approx 6 \times 10^{31}$ erg s^{-1}.

For the timing analysis we applied the solar system barycenter correction to the photon arrival times with the SAS task BARYCEN. We searched the data for pulsations around the spin frequency at the epoch of the *XMM-Newton* observations, predicted assuming the pulse period and the spin-down rate measured with the Parkes radio telescope (Camilo et al. 2004). As glitches and / or deviations from a linear spin-down may alter the period evolution, we searched over a wide period range centered at the value of $\sim$166 ms. We searched for significant periodicities using two methods: a standard folding technique and the Rayleigh statistic. No pulsation were detected near to the predicted frequency with either method but, since the pn timing resolution (73 ms) allows to only poorly sample the 166 ms pulsar period, a reliable upper limit on the pulsed fraction cannot be set.

2.3 *Chandra* observations and data analysis

PSR J1357–6429 was observed by means of the *Chandra X-ray Observatory* during two exposures of ∼17 ks duration each on 2005 November 18 and 19. The observations were carried out with the Spectroscopic array of the High Resolution Camera (HRC-S; Murray et al. 2000) used without transmission gratings. The HRC is a multichannel plate detector sensitive to X-ray over the 0.08–10 keV energy range, although essentially no energy information on the detected photons is available. The HRC-S time resolution is 16 μs.

We started from 'level 1' event data calibrated and made available through the Chandra X-ray Center.[5] The level 1 event files contain all HRC triggers with the position information corrected for instrumental (degap) and aspect (dither) effects. After standard data processing with the Chandra Interactive Analysis of Observations (CIAO ver. 3.3), a point-like source has been clearly detected in both the observations at a position consistent with that of PSR J1357–6429 (see Figure 2.3).

For the timing analysis we corrected the data to the solar system barycenter with the CIAO task AXBARY and then we followed the same procedure described in Section 2.2, but we again did not detect the source pulsation. By folding the light curve of PSR J1357–6429 on the radio frequency and fitting it with a sinusoid, we determine a 90% confidence level upper limit of ∼30% on the amplitude of a sinusoidal modulation. We stress that this upper limit depends sensitively on data time binning and on the assumed pulse shape.

We used the CIAO task MERGE_ALL to generate a combined image of the source. Our main purpose was to search for diffuse structures on scales smaller than the *XMM-Newton* angular resolution. We compared the radial profile of the pulsar emission with the *Chandra* High-Resolution Mirror Assembly point-spread function at 1 keV generated using Chandra Ray Tracer (ChaRT) and Model AXAF Response to X-rays (MARX). We found that the emission we detect from PSR J1357–6429 (∼100 counts concentrated within a ∼0.5″ radius circle) is consistent with that from a point source.

We used the *Chandra* data and the PIMMS software[6] to determine an upper limit on the luminosity of a possible spatial extended emission. The $3\,\sigma$ upper limit on a pulsar wind nebula brightness (in counts s^{-1}) has been estimated as $3(bA)^{1/2}\tau^{-1}$, where b is the background surface brightness in counts arcsec^{-2}, A is the pulsar wind nebula area, and τ is the exposure duration. Assuming the interstellar absorption value from the *XMM-Newton* best-fit model ($N_{\rm H} = 0.4 \times 10^{22}$ cm^{-2}, see Section 2.2) and typical parameters for a pulsar wind nebula (radius of $\sim 2 \times 10^{17}$ cm, that corresponds to ∼5″ for a distance of 2.5 kpc, and power-law spectrum with photon index $\Gamma = 1.6$, see, e.g., Gotthelf (2003)), this upper limit corresponds to a 2–10 keV luminosity of $\approx 3 \times 10^{31}$ erg s^{-1} for a uniform diffuse nebula. No significant diffuse excess

[5] See http://cxc.harvard.edu/.

[6] See http://heasarc.gsfc.nasa.gov/docs/tools.html .

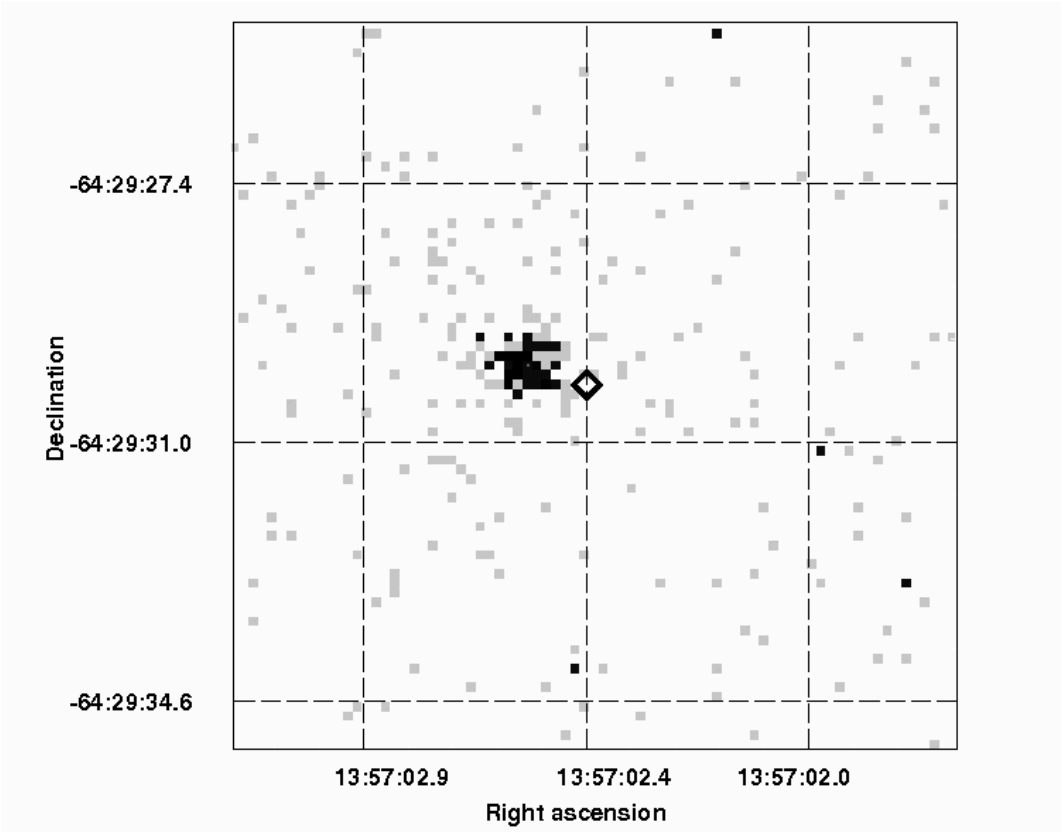

Figure 2.3 *Chandra* 0.08–10 keV HRC-S image centered on the radio pulsar position, marked with a diamond sign (Camilo et al. 2004). The CIAO CELLDETECT routine yields a best-fit position for the X-ray source at an angular distance of $(0.9 \pm 0.2)''$ ($1\,\sigma$ statistical error) from the radio pulsar. This value consistent with the *Chandra* pointing accuracy of $0.8''$ (99% confidence level).

was found even at larger angular scale, but the corresponding upper limit for diffuse emission is less constraining than that derived using the *XMM-Newton* data.

2.4 Discussion and conclusions

We have presented the results of the first X-ray observations of PSR J1357–6429 by means of the *XMM-Newton* and *Chandra* observatories. The source has been positively detected in all the instruments although, probably due to the low statistics, we could not detect the source pulsation. The high angular resolution *Chandra* observations favor the picture in which most of the counts belong to a point source. We found that the spectrum is well represented by either a power-law with photon index $\Gamma = 1.8^{+0.3}_{-0.2}$ or by a power-law plus blackbody model. In the latter case the best-fit parameters are for the power-law component a photon index $\Gamma = 1.4 \pm 0.5$ and, for the blackbody component,

radius[7] of $\sim 1.4^{+2.9}_{-0.2} d_{2.5}$ km and temperature corresponding to $k_B T = 0.16^{+0.09}_{-0.04}$ keV.

It is generally believed that a combination of emission mechanisms are responsible for the detected X-ray flux from rotation-powered pulsars (see, e.g., Kaspi et al. 2006 for a review). The acceleration of particles in the neutron star magnetosphere generates non thermal radiation by synchrotron and curvature radiation and / or inverse Compton processes, while soft thermal radiation could result by cooling of the surface of the neutron star. A harder thermal component can arise from polar-cap reheating, due to return currents from the outer gap or from close to the polar-cap. The dominant emission mechanism is likely related to the age of the pulsar. In pulsar younger than $\approx 10^4$ yr the strong magnetospheric emission generally prevails over the thermal radiation, making difficult to detect it.

As discussed in Section 2.2, we tend to prefer the power-law plus blackbody spectral model for PSR J1357–6429. The resulting blackbody size of $\sim 1.5 d_{2.5}$ km may suggest that the soft emission ($\lesssim$2 keV) is coming from hot spots on the surface due to backflowing particles, rather than from the entire surface. However this hint should be considered with caution, as the surface temperature distribution of a neutron star is most likely non uniform (since the heath conductivity of the crust is higher along the magnetic field lines) and the small and hot blackbody could result from a more complicated distribution of temperature. Moreover, currently we lack of reliable models of cooling neutron star thermal emission and thus we cannot exclude that the soft component is emitted from surface layers of the whole neutron star.

To date, thermal emission has been detected in only a few young radio pulsars. Among these, the properties of PSR J1357–6429 are similar to those of the young pulsars Vela (PSR B0833−45; $\tau_c = 11$ kyr, $P = 89$ ms, $\dot{E} = 6.9 \times 10^{36}$ erg s^{-1}, and distance $d \simeq 0.2$ kpc; Pavlov et al. 2001) and PSR B1706–44 ($\tau_c = 17.5$ kyr, $P = 102$ ms, $\dot{E} = 3.4 \times 10^{36}$ erg s^{-1}, and $d \simeq$ 2.5 kpc; Gotthelf et al. 2002). Notably, the efficiency in the conversion of the spin-down energy loss into X-ray luminosity for PSR J1357–6429 is $L_{0.5-10\,\mathrm{keV}}/\dot{E} \simeq 8 d_{2.5}^2 \times 10^{-5}$, significantly lower than the typical value of $\approx 10^{-3}$ (Becker & Truemper 1997), and similar to that of PSR B1706–44 ($\sim 10^{-4}$) and Vela ($\sim 10^{-5}$).

Although a pulsar wind nebula would not came as a surprise for this young and energetic source, we did not find clear evidence of diffuse X-ray emission associated with PSR J1357–6429. However, some known examples of wind nebulae (see Gaensler & Slane 2006), rescaled to the distance of PSR J1357–6429, would hide below the upper limits derived from the *XMM-Newton* and *Chandra* data.

New deeper exposures using *XMM-Newton* or *Chandra* would help determine if a thermal component is present in the emission of PSR J1357–6429 as our spectral analysis suggests, and possibly detect a pulsed emission. High

[7] We indicate with d_{N} the distance in units of N kpc.

sensitivity observations would also serve to address the issue of the presence of a pulsar wind nebula. Although there is not any EGRET γ-ray source coincident with PSR J1357–6429 (Hartman et al. 1999), young neutron stars and their nebulae are often bright γ-ray sources and PSR J1357–6429 in particular, given its high 'spin-down flux' $\dot{E}/d^2$ and similarity with Vela and PSR B1706–44, is likely to be a good target for the upcoming *AGILE* and *GLAST* satellites and the ground based Cherenkov air showers telescopes.

Chapter 3

Five years of SGR 1900+14 observations with *BeppoSAX*

We present a systematic analysis of all the *BeppoSAX* data of the soft gamma-ray repeater SGR 1900+14: these observations allowed us to study the long term properties of the source quiescent emission. In the observation carried out before the 1998 giant flare the spectrum in the 0.8–10 keV energy range was harder and there was evidence for a 20–150 keV emission, possibly associated with SGR 1900+14. This possible hard tail, if compared with the recent *INTEGRAL* detection of SGR 1900+14, has a harder spectrum (power-law photon index ∼1.6 versus ∼3) and a 20–100 keV flux ∼4 times larger. In the last *BeppoSAX* observation (April 2002), while the source was entering the long quiescent period that lasted until 2006, the 2–10 keV flux was ∼25% below the historical level. We also studied in detail the spectral evolution during the 2001 flare afterglow. This was characterized by a softening that can be interpreted in terms of a cooling blackbody-like component.

3.1 Introduction

Soft Gamma-ray Repeaters (SGRs) are a small group of high-energy sources, originally discovered through the emission of their characteristic short γ-rays bursts. Only four confirmed SGRs are known, plus two candidates. SGR bursts have typical duration of the order of 0.1 s, peak luminosity in the 10^{39}–10^{42} erg s^{-1} range, and are emitted during 'active' periods that can last from weeks to months. Exceptionally large outbursts are also observed in SGRs. These rare events have properties clearly different from those of the usual short γ-ray bursts. Based on their intensities, they can be classified either as 'giant' flares, with total released energy up to 10^{47} erg, or 'intermediate' flares, with total energy smaller by orders of magnitude (10^{41}–10^{43} erg). In the classical X-ray range (∼1–10 keV) SGRs are relatively steady sources with luminosity in the 10^{35}–10^{36} erg s^{-1}range (although fainter states have also been

observed, see Kouveliotou et al. 2003 and Mereghetti et al. 2006) and showing periodic pulsations with periods of several seconds and secular spin-down of $\sim 10^{-11}$–10^{-10} s s^{-1}.

It is generally thought that SGRs, as well as a group of similar pulsars known as Anomalous X-ray Pulsars (AXPs), are magnetars, i.e. isolated neutron stars with strong magnetic fields (see Woods et al. 2004 for a review of this class of objects). In the magnetar model both the persistent X-ray emission and the bursts are powered by magnetic energy (Duncan & Thompson 1992; Thompson & Duncan 1995, 1996). If the secular spin-down observed in SGRs is attributed to dipole radiation losses, as in ordinary radio pulsars, magnetic fields of the order of 10^{14}–10^{15} G are inferred.

In this paper we focus on SGR 1900+14, reporting all the observations of this source carried out with the *BeppoSAX* satellite. Although some of these data have been already published (Woods et al. 1999a, 2001; Feroci et al. 2003), we reanalyzed all the data sets following the same procedure, in order to compare them in a consistent way. In fact these observations, spanning five years and covering different states of bursting / flaring activity, give the possibility to investigate the long term spectral and flux variability of the source with a homogeneous data set.

In Section 3.2 we briefly review some results on SGR 1900+14, in the context of the activity history of the source. The spectral and timing analysis are reported in Sections 3 and 4, where we focus on the long term changes in the 1–10 keV emission properties. In Section 5 we report evidence for the detection of SGR 1900+14 in the 20-150 keV band during one of the *BeppoSAX* observations. In Section 6 we concentrate on the spectral variability on short time-scales following the April 2001 intermediate flare.

3.2 SGR 1900+14: activity episodes and *BeppoSAX* observations

This SGR was discovered in 1979 when a few bursts were recorded with the *Venera 11* and *Venera 12* probes (Mazets et al. 1979). No other bursts were detected until thirteen years later, when four more events were seen with the BATSE instrument on the *Compton Gamma Ray Observatory* in 1992 (Kouveliotou et al. 1993). The X-ray counterpart, discovered with *ROSAT* (Vasisht et al. 1994), was observed a first time with *BeppoSAX* (Woods et al. 1999a). The periodic pulsations in the X-ray counterpart (period of $\sim$5.2 s) were discovered with the *ASCA* satellite during an observation in April 1998 (Hurley et al. 1999d), which took place just three weeks before the burst reactivation of the SGR (Hurley et al. 1999b). Subsequent observations with the *RossiXTE* satellite confirmed the pulsations and established that the source was spinning down rapidly, with a period derivative of $\sim 10^{-11}$ s s^{-1} (Kouveliotou et al. 1999).

The peak of the bursting activity for SGR 1900+14 was reached on 1998 August 27, when a giant flare was recorded by numerous instruments. This flare started with a short (∼0.07 s) soft spike (often referred to as the 'precursor'), followed by a much brighter hard pulse (duration ∼1 s) that reached at least $\sim 10^{45}$ erg s^{-1} and a soft γ-ray tail modulated at 5.2 s (Hurley et al. 1999a; Mazets et al. 1999b; Feroci et al. 2001). The oscillating tail decayed quasi-exponentially over the next ∼6 minutes (Feroci et al. 2001). Integrating over the entire flare assuming isotropic emission, at least 10^{44} erg were released in hard X-rays above 15 keV (Mazets et al. 1999b). Another bright burst was detected on August 29 (Ibrahim et al. 2001), scaled down by a factor of ∼100 in peak luminosity and duration, compared to the August 27 flare. The second *BeppoSAX* observation was done less than one month after these events when the source was still active and showed an enhanced X-ray emission (Woods et al. 1999a).

After almost two years of quiescence, during which two *BeppoSAX* observations were carried out (Woods et al. 2001), SGR 1900+14 emitted an intermediate flare on 2001 April 18 (Guidorzi et al. 2001). This event, which prompted the two following *BeppoSAX* observations (Feroci et al. 2003, 2004; Woods et al. 2003), had a duration of ∼40 s and a total fluence of 1.6×10^{-4} erg cm^{-2}. Another bright flare, but of comparatively smaller fluence ($\sim 9 \times 10^{-6}$ erg cm^{-2}), occurred after 10 days (Lenters et al. 2003). The last bursts reported from SGR 1900+14, before its recent reactivation (Palmer et al. 2006; Golenetskii et al. 2006) occurred in November 2002 (Hurley et al. 2002).

All the *BeppoSAX* observations of SGR 1900+14 are listed in Table 3.1.[1] In each observation the SGR was aligned with the optical axis of the instruments. In summary: three observations were triggered by the occurrence of flares (B, E and F), and took place while the source was still active, as testified by the detection of bursts in the *BeppoSAX* data, while all the other observations can be considered as representative of the source quiescent state emission.

3.3 Spectral Analysis

The results presented in this section were obtained with the Low Energy Concentrator Spectrometer (LECS) and the Medium Energy Concentrator Spectrometer (MECS) instruments (Parmar et al. 1997; Boella et al. 1997). Both are imaging detectors operating in the 0.1–10 keV and 1.8–10 keV energy ranges respectively.

We used source extraction regions with radii of 4′ and 8′ for the MECS and the LECS, respectively. Because of the low Galactic latitude of SGR 1900+14, in order to properly account for the presence of the diffuse emission from the Galactic Ridge, concentric rings of 6'.4–9'.6 and 9′–13′ were chosen from each

[1] Observations G and H are listed for completeness, but are of scarce utility due to their short integration time and presence of contaminating sources in the PDS instrument; they will not be discussed further.

Table 3.1 Summary of the *BeppoSAX* observations of SGR 1900+14.

Obs.	Date	MJD	LECS exposure	MECS exposure	PDS exposure	Period[a]
A	1997-05-12	50580	19.9 ks	45.8 ks	20.1 ks	5.15719(3) s
B	1998-09-15	51071	13.8 ks	33.3 ks	15.8 ks	5.16026(2) s
C	2000-03-30	51633	14.4 ks	40.3 ks	18.3 ks	5.16709(3) s
D	2000-04-25	51659	17.4 ks	40.5 ks	18.8 ks	5.16765(3) s
E	2001-04-18	52017	20.4 ks	46.4 ks	16.7 ks	5.17277(1) s
F	2001-04-29	52028	25.7 ks	57.6 ks	25.6 ks	5.17298(1) s
G	2001-11-05	52218	–	1.3 ks	0.5 ks	–
H	2002-03-09	52342	–	–	47.6 ks	–
I	2002-04-27	52391	–	82.9 ks	–	5.18019(2) s

[a] $1\,\sigma$ errors in the last digit are quoted in parenthesis.

pointing for background subtraction with the MECS and the LECS, respectively. The bursts in observations B, E and F were excluded from the analysis.[2] This was done by extracting light curves with a bin size of 1 s and applying intensity filters. All the spectra were rebinned to achieve at least 30 counts in each spectral channel and to oversample by a factor 3 the instrumental energy resolution. The fits were performed simultaneously, over the energy ranges 1.8–10 keV (MECS) and 0.8–4.0 keV (LECS), and including a constant factor to account for normalization uncertainties between the instruments (this factor was constrained to be within its usual range[3]). Spectral analysis has been performed with the XSPEC v.11.3.2 software package (Arnaud 1996).

In some observations a fit with an absorbed power-law yields unacceptable χ^2 values, therefore we explored a power-law plus blackbody model which gave good fits for all the data sets. Since there is no obvious physical reason for the absorption to change, at least while the source is in quiescence, we fitted all the data sets also with a common value for the $N_{\rm H}$. The value of 2.6×10^{22} cm^{-2} has been derived fitting simultaneously the spectra of the observations performed while the source was in quiescence. The blackbody temperature ($\sim$0.4 keV) and emitting area[4] (R$\sim$6-7 km) do not vary much, except during observation E. This observation was performed during the afterglow of the 2001 April 18 flare, and shows clear evidence for spectral variations within the observation (see Section 3.6). In Figure 3.1 we have plotted the long term evolution of the flux and spectral parameters obtained in the power-law plus blackbody fits and all the best fit parameters are reported in Table 3.2. They are consistent

[2]The spectral results for the bursts detected in observation E are reported in Feroci et al. (2004).

[3]See the Cookbook for *BeppoSAX* NFI Spectral Analysis, http://www.asdc.asi.it/bepposax/software/cookbook/

[4]We assume for SGR 1900+14 a distance of 15 kpc (Vrba et al. 2000).

with those obtained by Woods et al. 1999a (for observations A and B), Woods et al. 2001 (C and D), and Feroci et al. 2003 (E and F).

The observations in which SGR 1900+14 had the highest X-ray flux are those following the two flares (B and E). The flux in the last observation (I), whose analysis is reported here for the first time, is instead ∼25% lower than in the other quiescent observations. The fading is also confirmed by a simple comparison of the MECS count rates of observations I and D, which differ at $>10\,\sigma$ level. During observation I the transient source XTE J1908+94 (in't Zand et al. 2002), located 24′ from the SGR (i.e. just inside the MECS field of view), was in a high state. Therefore we carefully checked our flux estimate for SGR 1900+14 by exploring different background and source extraction regions. Our conclusion is that the observed decrease in the flux is real.

Figure 3.1 also shows that the power-law component during observation A was slightly harder than in all the following quiescent state observations, performed after the 1998 August 27 giant flare. In order to compare the hardness of the overall spectra of the quiescent observations, we have simultaneously fit them with the same parameters (introducing a normalization factor to account for the flux change) and we note that the spectra C, D, F, and I give an acceptable fit, while the addition of spectrum A makes the simultaneous fit unacceptable, due to the high energy excess shown in figure 3.2. This means that the pre-flare spectrum was significantly harder than the average quiescent spectrum of SGR 1900+14 measured by *BeppoSAX* after the giant flare.

3.4 Timing analysis

For the timing analysis we first corrected the time of arrival of the MECS events to the solar system barycenter, and then used standard folding techniques to measure the source spin period. For observation I we find a period of 5.18019 ± 0.00002 s, and for all the other observations our values (reported in Table 3.1 and in Figure 3.1) are in agreement with those of Woods et al. (1999a, 2001) and Feroci et al. (2002). In Figure 3.3 we show the background-subtracted phase-folded profiles and the pulsed fractions for the seven data sets. We derived the pulsed fractions and the relative errors fitting the pulse profiles with a constant plus one or two (for observation A) sinusoidal functions and computing the ratio between the sin amplitude and the constant. Although SGR 1900+14 has been extensively monitored with the *RossiXTE* satellite and there are detailed studies of its light curve and pulsed flux evolution (see e.g. Woods et al. 1999b and Göğüş et al. 2002), the results presented here, being obtained with an imaging instrument, have the advantage of providing absolute flux and pulsed fraction measurements.

We note that the changes in the spectrum and in the pulse profile after the giant flare were not accompanied by significant variations in the pulsed fractions. The only significant change has been measured during observation E, when the pulsed fraction was higher (∼25%) then the average value of ∼17%

Table 3.2 Summary of the spectral results in the 0.8–10 keV energy range. The abundances of Anders & Grevesse (1989) are used throughout. Errors are given at the 90% confidence level.

Obs.	Model	$N_{\rm H}$ (10^{22} cm^{-2})	Γ	k_BT (keV)	$R_{\rm BB}$[a] (km)	Flux[b] (10^{-11} erg cm^{-2} s^{-1})	χ^2_r (d.o.f.)
A	PL	1.4 ± 0.2	1.9 ± 0.1	–	–	$0.92^{+0.04}_{-0.03}$	1.60 (98)
	PL+BB	$1.6^{+0.6}_{-0.4}$	$0.9^{+0.3}_{-0.4}$	0.5 ± 0.1	4^{+2}_{-1}	1.0 ± 0.1	1.12 (96)
	PL+BB	2.6 (fixed)	$1.1^{+0.3}_{-0.2}$	$0.44^{+0.03}_{-0.05}$	7^{+2}_{-1}	1.11 ± 0.06	1.16 (97)
B	PL	2.4 ± 0.2	2.2 ± 0.1	–	–	2.6 ± 0.1	1.22 (113)
	PL+BB	$1.7^{+0.6}_{-0.5}$	$1.5^{+0.5}_{-0.6}$	0.7 ± 0.1	3 ± 1	2.5 ± 0.2	1.16 (111)
	PL+BB	2.6 (fixed)	2.0 ± 0.2	0.5 ± 0.1	5 ± 2	2.7 ± 0.2	1.21 (112)
C	PL	$2.0^{+0.4}_{-0.3}$	2.3 ± 0.1	–	–	0.95 ± 0.04	1.29 (84)
	PL+BB	2 ± 1	$1.7^{+0.3}_{-0.6}$	0.5 ± 0.1	5^{+7}_{-2}	$1.0^{+0.1}_{-0.2}$	1.09 (82)
	PL+BB	2.6 (fixed)	1.7 ± 0.3	0.45 ± 0.05	6^{+2}_{-1}	1.1 ± 0.1	1.08 (83)
D	PL	2.1 ± 0.3	2.4 ± 0.1	–	–	0.90 ± 0.05	1.06 (83)
	PL+BB	$2.2^{+0.9}_{-0.7}$	$2.0^{+0.4}_{-0.5}$	0.5 ± 0.1	4^{+8}_{-2}	$0.9^{+0.1}_{-0.2}$	1.00 (81)
	PL+BB	2.6 (fixed)	2.1 ± 0.3	0.4 ± 0.1	7^{+4}_{-2}	1.0 ± 0.1	0.99 (82)
E	PL	3.6 ± 0.2	2.2 ± 0.1	–	–	3.5 ± 0.1	1.18 (121)
	PL+BB	$2.6^{+0.7}_{-0.9}$	$1.8^{+0.3}_{-0.8}$	$0.9^{+0.2}_{-0.1}$	$1.6^{+0.6}_{-0.8}$	$3.1^{+0.3}_{-0.2}$	1.13 (119)
	PL+BB	2.6 (fixed)	$1.7^{+0.1}_{-0.2}$	0.9 ± 0.1	$1.7^{+0.4}_{-0.5}$	3.1 ± 0.2	1.12 (120)
F	PL	$2.4^{+0.3}_{-0.2}$	2.3 ± 0.1	–	–	$1.06^{+0.04}_{-0.03}$	1.35 (105)
	PL+BB	$2.4^{+0.8}_{-0.5}$	1.4 ± 0.4	0.5 ± 0.1	5^{+3}_{-1}	$1.1^{+0.1}_{-0.2}$	1.06 (103)
	PL+BB	2.6 (fixed)	1.5 ± 0.3	$0.51^{+0.03}_{-0.05}$	5 ± 1	1.1 ± 0.1	1.05 (104)
I	PL	1.9 ± 0.3	2.4 ± 0.1	–	–	0.62 ± 0.03	1.06 (94)
	PL+BB	3 ± 1	2.2 ± 0.3	0.3 ± 0.1	8^{+25}_{-4}	$0.73^{+0.04}_{-0.09}$	0.94 (92)
	PL+BB	2.6 (fixed)	2.1 ± 0.2	$0.37^{+0.04}_{-0.06}$	8^{+4}_{-2}	0.69 ± 0.04	0.93 (93)

[a] Radius at infinity assuming a distance of 15 kpc.

[b] Flux in the 2–10 keV range, corrected for the absorption.

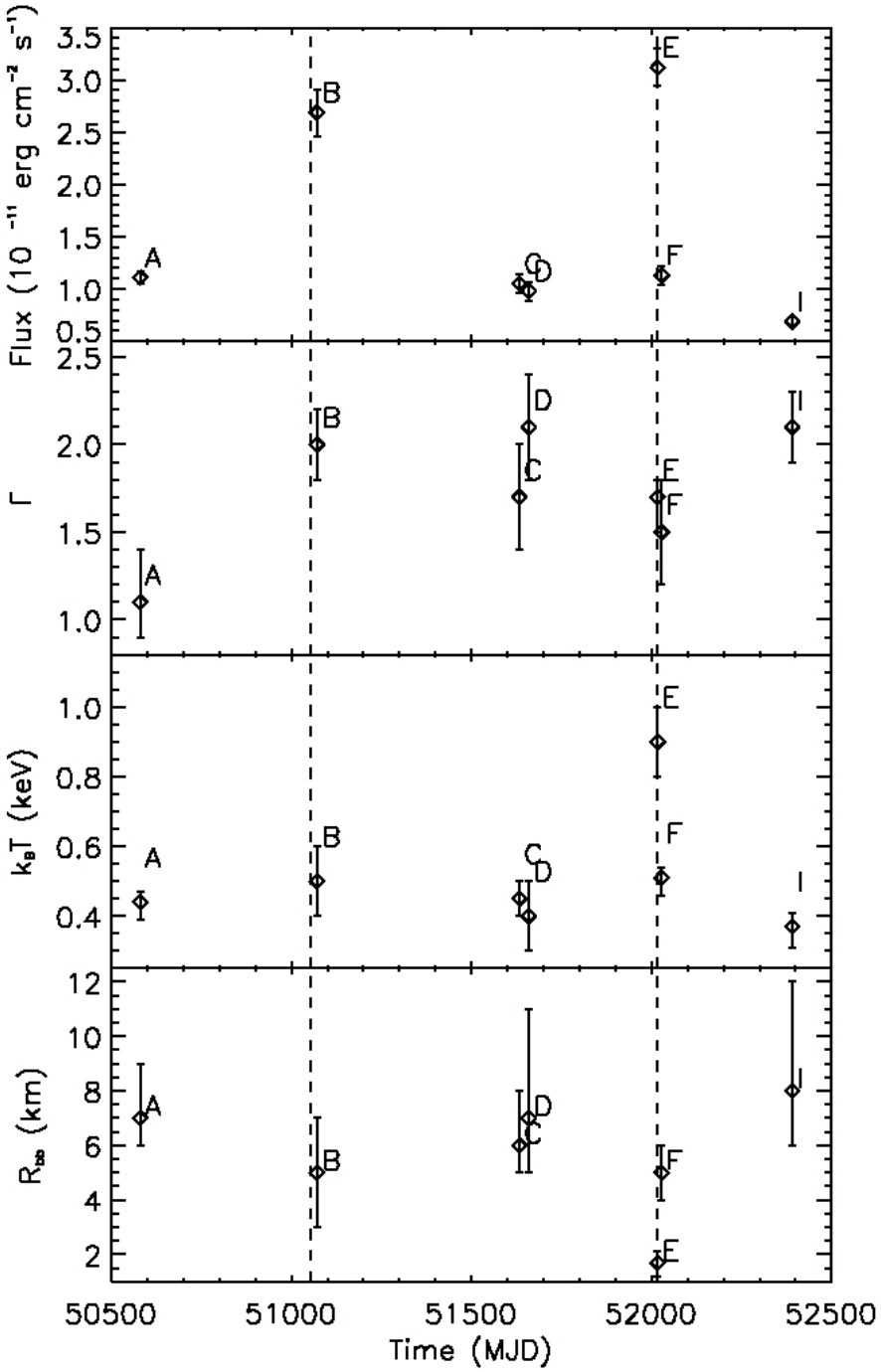

Figure 3.1 Long term evolution of the 2–10 keV unabsorbed flux and of the spectral parameters of SGR 1900+14 (assuming for the absorption the value of 2.6×10^{22} cm^{-2}). The vertical dashed lines indicate the time of the 1998 August 27 giant flare and of the 2001 April 18 intermediate flare. The error bars are at the 90% confidence level.

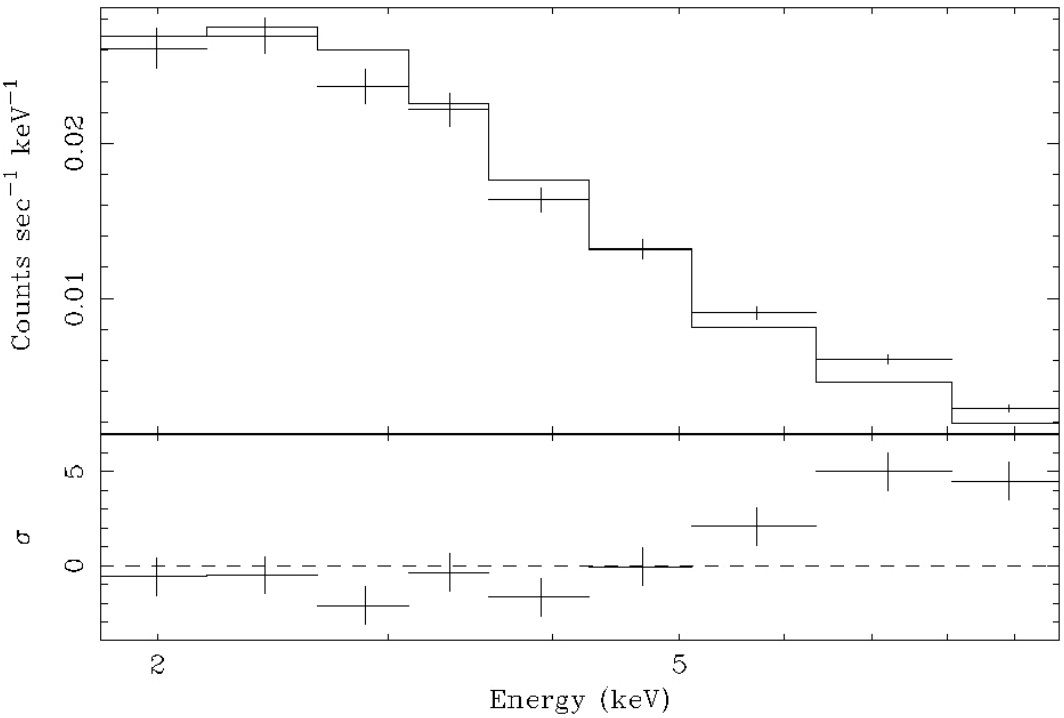

Figure 3.2 *BeppoSAX* / MECS spectrum of observations A and residuals with respect to the simultaneous fit of the spectra of observation A, C, D, F, and I with an absorbed power-law plus blackbody model with only an overall normalization factor left free to vary. The data have been rebinned graphically to emphasize the trend in the spectral residuals.

(this enhancement, related to the afterglow emission, has been discussed in Feroci et al. 2003). In contrast the pulse shape of SGR 1806–20, the only other SGR observed before and after a giant flare, was only slightly different after the event, and its pulsed fraction remained small (∼4%, Tiengo et al. 2005; Rea et al. 2005b) until two months after the flare and then increased to the pre-flare value (∼10%, Rea et al. 2005b; Woods et al. 2007).

3.5 Hard X-ray detection

The PDS instrument (Phoswich Detection System, Frontera et al. 1997) extended the spectral and timing capabilities of *BeppoSAX* to the 15–300 keV band. This non-imaging spectrometer had a field of view of 1.3° (FWHM) and the background subtraction was done with a rocking system, which switched between the source and two background regions offset by 3.5° every 96 s.

In all the PDS exposures listed in Table 3.1 we detected a significant hard X-ray emission. However three transient X-ray sources, the pulsars 4U 1907+97 (Giacconi et al. 1971b; Liu et al. 2000) and XTE J1906+09 (Marsden et al. 1998), and the black hole candidate XTE J1908+94 (in't Zand et al. 2002), are located at a small angular distance from SGR 1900+14 (47′, 33′ and 24′ respec-

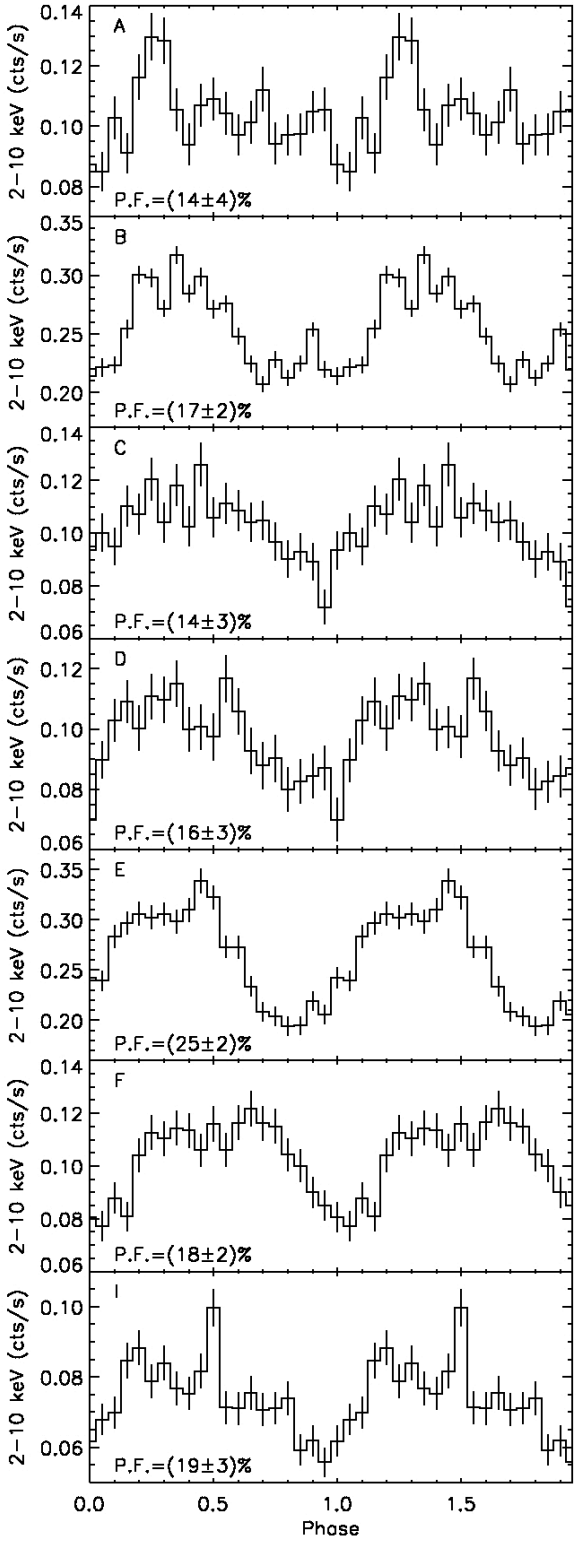

Figure 3.3 MECS pulse profiles (not phase-connected) and pulsed fraction of SGR 1900+14 in the seven observations (as indicated in the panels).

tively). When in high state, they can reach fluxes above $\sim 10^{-9}$ erg cm^{-2} s^{-1} in the 20–100 keV range, preventing a sensitive search for a (presumably dimmer) emission from SGR 1900+14. XTE J1908+94 during a bright state is clearly identifiable in the MECS and LECS, since it lies within the field of view of these imaging instruments. This was the case of observation I, performed shortly after the discovery of that source (Woods et al. 2002). The presence of the other two sources has been identified from the detection in the PDS of periodicity at their known pulse periods (∼89 s for XTE J1906+09 and ∼440 s for 4U 1907+97) in all the PDS data sets except in the first one. Therefore only for the 1997 observation there is no evidence of contamination from one of these three sources. Given that SGR 1900+14 lies at a low Galactic latitude (b=0.77°), we might worry that the flux observed in the PDS during observation A could result from diffuse emission from the Galactic Ridge. Since this emission is constant in time, the lowest count rate observed in later observations (see Table 3.3) allows us to set an upper limit to its contribution in observation A. This upper limit is of ∼60% of the detected flux in the 20–50 keV band and of ∼10% in the 50–150 keV band. Although we cannot rule out the possibility of contamination from unknown transient sources, we conclude that the flux measured in observation A up to ∼150 keV is very likely due to SGR 1900+14.

We extracted the PDS background subtracted spectrum and using the most recent response matrix, we fitted the logarithmically rebinned PDS spectrum in the range 15–150 keV. With a simple power-law model we obtained a photon index $\Gamma = 1.6 \pm 0.3$ and a 20–100 keV flux of $(6 \pm 1) \times 10^{-11}$ erg cm^{-2} s^{-1} with a χ^2_r value of 0.98 for 40 d.o.f. . We also fitted the PDS spectrum simultaneously with the LECS and MECS spectra, using a blackbody plus power-law model. We included a factor to account for normalisation uncertainties between the low-energy instruments and the PDS. This factor assumed the value of 0.90 (the range of acceptable values is 0.77–0.95). The resulting best fit parameters (photon index $\Gamma = 1.04 \pm 0.08$, blackbody temperature $k_B T = 0.50 \pm 0.06$, radius $R_{\rm BB} = 5 \pm 2$ km, and absorption $N_{\rm H} = (1.8 \pm 0.5) \times 10^{22}$ cm^{-2}) are consistent with an extrapolation of the power-law component measured at lower energy (Figure 3.4, upper panel). We also checked a broken power-law plus blackbody model and, although the improvement in the goodness of the fit, as measured by the F-test statistic, is marginal, we obtained a slightly lower χ^2 value (1.11 for 135 d.o.f. instead of 1.17 for 137 d.o.f.) with a photon index of ∼0.7 up to ∼25 keV and of ∼1.7 above, and with a similar blackbody component (Figure 3.4, bottom panel). Motivated by the structured residuals from ∼15 keV to ∼35 keV, where, as discussed above, some contamination from the Galactic diffuse emission cannot be excluded, we performed also a fit using the PDS data only above 35 keV. The resulting parameters are photon index $\Gamma = 1.15 \pm 0.10$, blackbody temperature $k_B T \simeq 0.5$ keV and $R_{\rm BB} \simeq 5$ km, with a χ^2_r value of 1.08 for 123 d.o.f. . The 20–100 keV flux derived from all the fits is $(7 \pm 1) \times 10^{-11}$ erg cm^{-2} s^{-1}.

Table 3.3 PDS count rates for the 'off' and 'on' source positions during the observations of SGR 1900+14. Errors are given at $1\,\sigma$.

Region	Energy band (keV)	Obs. A (cts / s)	Obs. B (cts / s)	Obs. C (cts / s)	Obs. D (cts / s)	Obs. E (cts / s)	Obs. F (cts / s)	Obs. H (cts / s)
OFF −	20–50	4.88 ± 0.02	4.67 ± 0.02	3.75 ± 0.01	3.69 ± 0.01	3.37 ± 0.01	3.38 ± 0.01	3.35 ± 0.01
	50–150	6.87 ± 0.02	6.51 ± 0.02	5.23 ± 0.02	5.27 ± 0.02	4.75 ± 0.01	4.75 ± 0.01	4.73 ± 0.01
OFF +	20–50	4.91 ± 0.02	4.67 ± 0.02	3.74 ± 0.02	3.71 ± 0.01	3.38 ± 0.01	3.40 ± 0.01	3.35 ± 0.01
	50–150	6.83 ± 0.02	6.44 ± 0.02	5.24 ± 0.02	5.21 ± 0.02	4.76 ± 0.01	4.78 ± 0.01	4.75 ± 0.01
ON[a]	20–50	0.27 ± 0.03	0.79 ± 0.04	0.11 ± 0.03	0.36 ± 0.03	0.45 ± 0.03	0.43 ± 0.02	9.33 ± 0.02
	50–150	0.21 ± 0.04	0.12 ± 0.04	< 0.03	< 0.02	0.11 ± 0.03	0.06 ± 0.03	4.48 ± 0.02

[a] Background subtracted values.

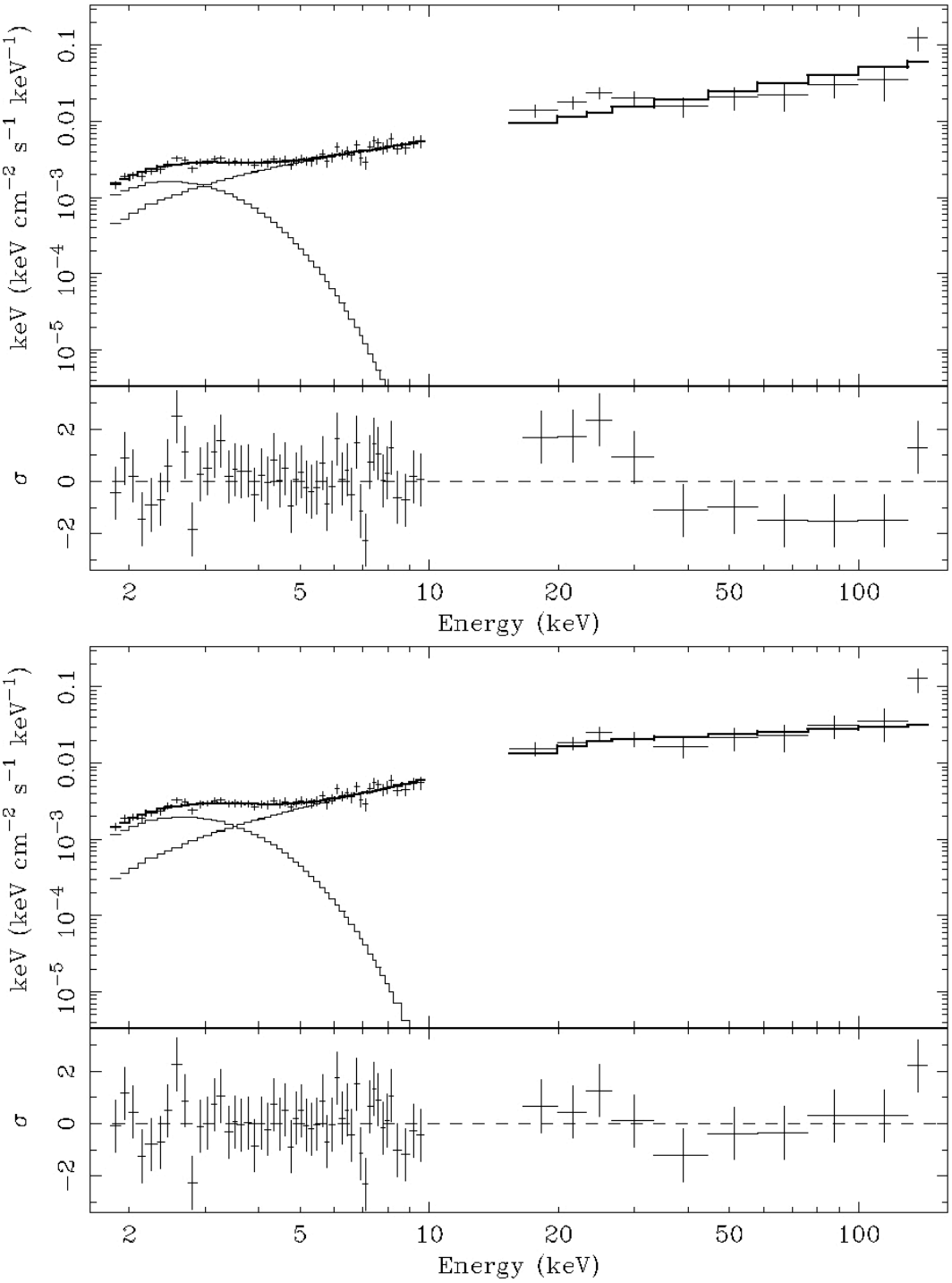

Figure 3.4 Broad band spectrum and residuals from the data of the observation A fitted with a power-law plus blackbody model (*top panel*) and with a broken power-law plus blackbody model (*bottom panel*). The data points are from the MECS and PDS instruments and the thick line represents the total model, while the thin lines represent its absorbed power-law and blackbody components.

In order to search for pulsations in the hard X-ray range we folded the PDS data at the period of 5.15719 s measured with the MECS, but no significant periodic signal was detected. The $3\,\sigma$ upper limit on the source pulsed fraction derived by a sinusoidal fit is ≈50%.

Except for observation H, whose high count rate is due to XTE J1908+94,[5] all the post-giant flare observations show a lower count rate in the 50–150 keV band with respect to observation A. The consistent count rates obtained in every observations from the two uncorrelated regions used for background subtractions (see Table 3.3) assure that this decrease does not result from bright sources in the background pointings. Moreover, the contamination in this band from the X–ray pulsars is expected to be negligible in all observations, since their spectrum in outburst is characterized by a high energy cutoff at 10–15 keV (Wilson et al. 2002; Baykal et al. 2006).

This considerations lead us to conclude that SGR 1900+14 became less bright in the 50–150 keV band after its giant flare. The fact that the 20–50 keV count rate during observation C was lower than in observation A, even though the pulsar XTE J1906+09 was active, might indicate that the flux of SGR 1900+14 in this softer energy band had also significantly decreased.

3.6 Spectral variability in the afterglow of the 18 April 2001 flare

Flux and spectral variations as a function of time within the individual observations (except for the bursts) were evident, as mentioned above, only for the data collected ∼7.5 hours after the onset of the 2001 April 18 flare (observation E). While evidence for this based only on hardness ratio analysis was reported in Feroci et al. (2003), here we present, for the first time, a time resolved spectral analysis of the afterglow lightcurve.

The SGR 1900+14 light curve for this observation, binned in 5 000 s intervals, is shown in the top panel of Figure 3.5. A detailed study of the flux decay, using also data from *RossiXTE* and *Chandra* that filled the time gap between observations E and F, has been reported by Feroci et al. (2003). They showed that, after subtracting a constant flux corresponding to the pre-flare quiescent level, the light curve is well described by a power-law with $F \propto t^{-0.9}$, with superimposed a broad 'bump' (visible at $t \sim 80\,000$ s in Figure 3.5).

Following this approach, we assumed that the variable 'afterglow' emission is present on top of a 'quiescent' emission that shows only moderate variations on long time-scales. We therefore extracted the source spectra for five different time intervals (our selection is visible in Figure 3.5) and fitted them with a model consisting of a power-law plus blackbody with fixed parameters, plus a third variable component to model the afterglow emission. As representative

[5]The source went in outburst in February 2002 and reached its flux peak about two months later (in't Zand et al. 2002).

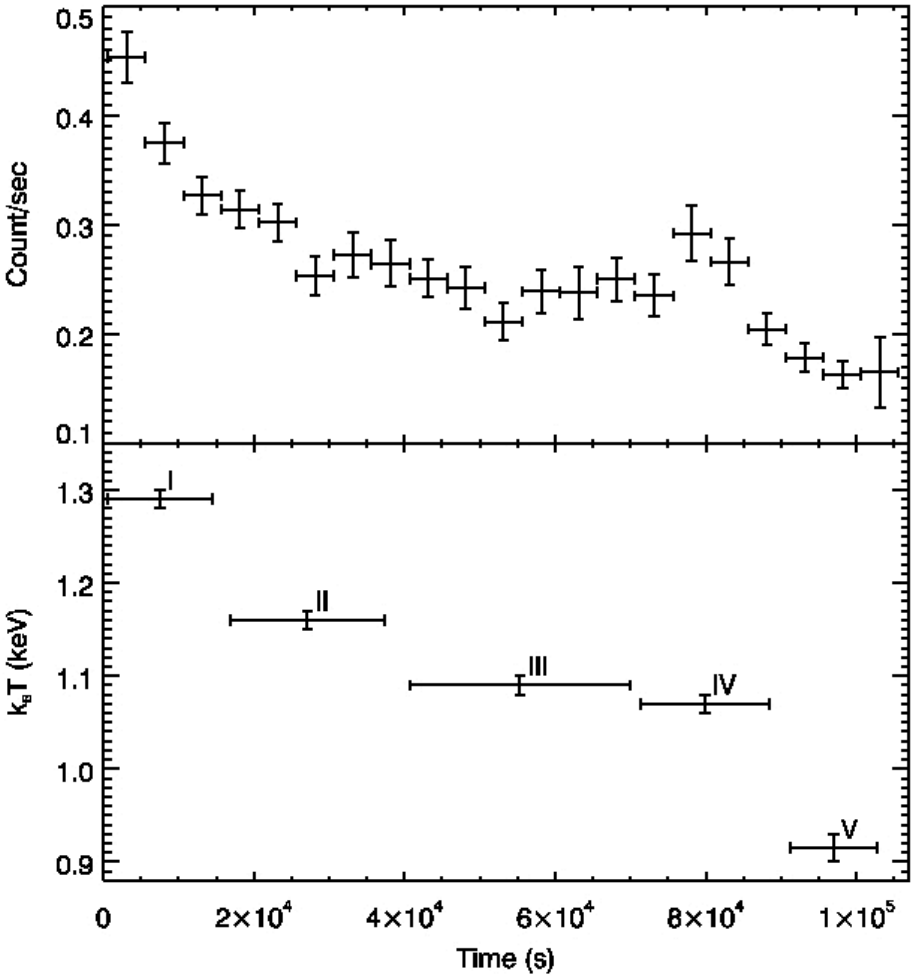

Figure 3.5 Background subtracted MECS 2–10 keV light curve and blackbody temperature observed on 2001 April 18 about 7.5 hours after the flare. See Table 3.4 for the latter values, obtained from the addition of a new blackbody component with fixed emitting area. The time intervals with bursts have been excluded. Error bars are at $1\,\sigma$.

parameters and normalization of the fixed emission we used values consistent with those seen in the last observations before the flare (C and D), i.e. $\Gamma \simeq 2$, $k_B T \simeq 0.4$ keV and $R_{\rm BB} \simeq 7$ km. We found that the variable component was better described by a blackbody than by a power-law (typical χ^2_r values of $\sim$1.1 and $\sim$1.7, respectively). The results for the blackbody fits are reported in Table 3.4. Relatively good fits were also obtained by imposing either a constant temperature or a constant emitting area along the whole observation. The temperatures derived in the latter case (that generally gives lower χ^2 values) are plotted in the bottom panel of Figure 3.5. These results show that a cooling blackbody emission from a region of constant surface could account for both

Table 3.4 Time resolved spectral results for observation E. The table gives the parameters of a blackbody component added to a fixed component with $N_{\rm H} = 2.6 \times 10^{22}$ cm^{-2}, $\Gamma = 2$, $k_BT = 0.4$ keV, and $R_{\rm BB} = 7$ km (see Section 3.6 for details). Errors are given at $1\,\sigma$.

Time interval	k_BT (keV)	$R_{\rm BB}$[a] (km)	χ^2_r (d.o.f.)
I	$1.23^{+0.02}_{-0.03}$	1.8 ± 0.1	1.03 (69)
	1.1 (fixed)	$2.17^{+0.03}_{-0.02}$	1.35 (70)
	1.29 ± 0.01	1.6 (fixed)	1.09 (70)
II	$1.15^{+0.03}_{-0.02}$	1.6 ± 0.1	1.21 (74)
	1.1 (fixed)	$1.77^{+0.02}_{-0.03}$	1.24 (75)
	1.16 ± 0.01	1.6 (fixed)	1.20 (75)
III	1.16 ± 0.04	1.4 ± 0.1	0.98 (64)
	1.1 (fixed)	$1.56^{+0.02}_{-0.03}$	1.01 (65)
	1.09 ± 0.01	1.6 (fixed)	1.04 (65)
IV	1.10 ± 0.05	$1.5^{+0.2}_{-0.1}$	1.31 (45)
	1.1 (fixed)	1.50 ± 0.03	1.28 (46)
	1.07 ± 0.01	1.6 (fixed)	1.29 (46)
V	0.94 ± 0.07	$1.5^{+0.3}_{-0.2}$	1.25 (29)
	1.1 (fixed)	1.09 ± 0.04	1.35 (30)
	$0.92^{+0.01}_{-0.02}$	1.6 (fixed)	1.21 (30)

[a] Radius at infinity assuming a distance of 15 kpc.

the flux decrease and the spectral softening observed during the afterglow.

However we note that, due to the relatively low statistics of the time resolved spectra, other spectral decompositions are consistent with the data. One possibility is for example to use the power-law plus blackbody model adopted for the time integrated emission with only either the power-law or the blackbody parameters free to vary.

3.7 Discussion and Conclusions

Our re-analysis of the *BeppoSAX* data of SGR 1900+14 confirms the spectral variability found in this source by Woods et al. (1999a, 2001), and Feroci et al. (2003) on yearly time-scale. Since they found that in some observations an additional blackbody component was required, we were interested in a more thorough assessment of its possibly persistent presence. Such a two-components spectrum is one of the characteristics of the AXPs (Mereghetti et al. 2002a) and has also been observed in the other well studied soft gamma-ray repeater SGR 1806–20 (Mereghetti et al. 2005c). Although formally required only in two (possibly three) observations, that component might well be a permanent fea-

ture, always present in this source. In fact, except during the aftermath of the April 2001 flare, its temperature (∼0.4 keV) and emitting area (∼6–7 km) are consistent with all the spectra. If we assume an underlying and nearly steady blackbody, it might be that, as proposed by Woods et al. 1999a and Kouveliotou et al. 2001, this spectral component is visible only in the observations that offer both a low power-law flux and good statistics.

The long term spectral variability seems to correlate with the occurrence of the giant and intermediate flares and, in a more complex way, with the ordinary bursting activity. Comparing the only *BeppoSAX* pre-flare observation with the quiescent post-flare ones, there is evidence for a softening in the spectrum. Also SGR 1806–20 after its 2004 December 27 giant flare displayed a softer spectrum with respect to the 2004 levels (Rea et al. 2005b). This is qualitatively consistent with the magnetar scenario, in which the spectral hardening is linked to the increasing torque of the twisted magnetosphere, that finally drives the SGR to a giant flare (Thompson et al. 2002; Mereghetti et al. 2005c). Then, after the flare, the source magnetosphere is foreseen to relax into a less twisted configuration, with a softer spectrum.

The most recent *BeppoSAX* observation of SGR 1900+14 (Observation I, April 2002), shows a small but statistically significant fading compared to the preceding observations. A long term monotonic decrease of the X–ray emission has been observed in SGR 1627–41 (Kouveliotou et al. 2003; Mereghetti et al. 2006) from 1998 to 2004. During this period no bursts were recorded from SGR 1627–41, and its fading has been interpreted as due to the cooling of the neutron star surface after the heating occurred when the source was active in 1998. SGR 1900+14 was still moderately active during 2002 (Hurley et al. 2002), but then no bursts were observed for several years. The smaller luminosity in the last *BeppoSAX* observation might thus correspond to the initial part of a cooling and fading phase, at least qualitatively similar to that observed in SGR 1627–41, but now interrupted by the recent (March 2006) reactivation (Palmer et al. 2006; Golenetskii et al. 2006).

During the afterglow of the 2001 April 18 flare, Feroci et al. (2003) found a flux decrease and a spectral softening. Our re-analysis shows that the variable spectral component can be well modeled as an additional blackbody emitted from a smaller and hotter (but rapidly cooling) region of the neutron star surface. Successful attempts to explain observations of afterglow flux decays in magnetars by means of a cooling thermal component are described in Ibrahim et al. (2001), Lenters et al. (2003), and Woods & Thompson (2006); all these works point out evidence of cooling hot spots on the surface of the neutron star exposed to a fireball. However we note that the occurrence of the bump in the light curve of the afterglow is an anomaly in the picture of the cooling of a thermal emission, since it requires a re-injection of energy; we refer to Feroci et al. 2003 for an extensive discussion of this issue.

Evidence for persistent emission above 20 keV for SGR 1900+14 has recently been obtained with *INTEGRAL* observations (Götz et al. 2006). We

found that a hard tail was visible also in the 1997 *BeppoSAX* PDS data. If this emission is indeed due to SGR 1900+14, our 50 ks long observation indicates significant differences with respect to the average properties obtained with *INTEGRAL*, based on the sum of many observations performed discontinuously from March 2003 to June 2004. The PDS 20–100 keV flux is ∼4 times larger[6] and the spectrum is harder (photon index ∼1.1) than that measured with *INTEGRAL* (photon index ∼3). Even considering our fit based only on the PDS instrument, the difference in the hard X-ray spectral index is significant (photon index ∼1.6 versus ∼3). Another interesting indication from the PDS data is a decrease of the 50–150 keV flux of SGR 1900+14 after the giant flare: it is possible that the hard X-ray flux decrease and softening in SGR 1900+14 was a consequence of the 1998 August 27 giant flare.

The only other SGR established as a persistent hard X-ray source to date is SGR 1806–20 (Mereghetti et al. 2005a; Molkov et al. 2005). For this source observations carried out with *XMM-Newton*in the April 2003–October 2004 period, showed a progressive spectral hardening in the 1–10 keV band, as the source increased its burst rate before the giant flare (Mereghetti et al. 2005c). The *INTEGRAL* observations displayed some evidence of a similar behaviour above 20 keV. In fact its photon index varied from ∼1.9 in the period March 2003–April 2004 to ∼1.5 in September–October 2004 (Mereghetti et al. 2005a). A comparison of the hard X-ray luminosity of the two SGRs in the 'pre-flare' state is subject to uncertainties in their distances. For SGR 1900+14 a distance of 15 kpc has been derived based on its likely association with a young star cluster (Vrba et al. 2000), while for SGR 1806–20 the distance is rather debated and has been variously estimated from 6.4 kpc to 15 kpc (Cameron et al. 2005; McClure-Griffiths & Gaensler 2005). If we assume a distance of 15 kpc for both sources we obtain similar 20–100 keV luminosities: $(1.5 \pm 0.3) \times 10^{36}$ erg s^{-1} for SGR 1900+14 and $(1.2 \pm 0.1) \times 10^{36}$ erg s^{-1} for SGR 1806–20.

These results, together with the recent detections of several AXPs in the hard X-ray range (Molkov et al. 2004; Kuiper et al. 2004; Revnivtsev et al. 2004; den Hartog et al. 2006; Kuiper et al. 2006) with 20–100 keV luminosities similar or larger than those below 10 keV, indicate that non thermal magnetospheric phenomena are energetically important in magnetars. Soft X-rays give only a partial view and broad band observations are required for a better understanding of the physical processes occurring in these sources. In this respect, SGR 1900+14, being probably the first magnetar showing evidence for variability in the hard X-ray range and currently in a moderately active state, is a good target to further explore possible correlations between the persistent emission and the bursting activity.

[6]The uncertainty in the relative calibration of the two satellite in the energy band considered here is of ≈10% (Kirsch et al. 2005).

Chapter 4

SGR 1806–20 about two years after the giant flare: *Suzaku*, *XMM-Newton* and *INTEGRAL* observations

In December 2004, the soft gamma-ray repeater SGR 1806–20 emitted the most powerful giant flare ever observed. This probably involved a large-scale rearrangement of the magnetosphere leading to observable variations in the properties of its X-ray emission. Here we present the results of the first *Suzaku* observation of SGR 1806–20, together with almost simultaneous observations with *XMM-Newton* and *INTEGRAL*. The source seems to have reached a state characterized by a flux close to the pre-flare level and by a relatively soft spectrum. Despite this, SGR 1806–20 remained quite active also after the giant flare, allowing us to study several short bursts observed by *Suzaku* in the 1–100 keV range. We discuss the broad-band spectral properties of SGR 1806–20, covering both persistent and bursting emission, in the context of the magnetar model, and consider its recent theoretical developments.

4.1 Introduction

The four known Soft Gamma-ray Repeaters (SGRs) were discovered as transient sources of high-energy photons; they emit sporadic and short ($\sim$0.1 s) bursts of (relatively) soft gamma-rays with luminosity $L \sim 10^{40}$–10^{41} erg s^{-1} during periods of activity, that are often broken by long intervals of quiescence. Three 'giant' flares with luminosity $\gtrsim 10^{43}$ erg s^{-1} have also been observed to date, each one from a different SGR: on March 5, 1979 from SGR 0526–66 in the Large Magellanic Cloud (Mazets et al. 1979), on August 27, 1998 from SGR 1900+14 (Hurley et al. 1999a), and on December 27, 2004 from SGR 1806–20 (Hurley et al. 2005). Persistent emission with $L \sim 10^{35}$ erg s^{-1} is also ob-

served from SGRs in the soft X–ray range (<10 keV) and, for SGR 1806–20 and SGR 1900+14, also in the hard X-ray range (Mereghetti et al. 2005a; Götz et al. 2006). In three cases, periodic pulsations at a few seconds have been detected. The bursts, the giant flares, the quiescent X-ray counterparts, and the pulsations have been interpreted in the framework of the magnetar model (see Thompson et al. 2002, and references therein). Magnetars are highly magnetized neutron stars with field strengths of 10^{14}–10^{15} G, larger than those of the majority of radio pulsars. The ultimate source of energy for the bursts and the quiescent emission is believed to be the ultra-strong magnetic field.

SGR 1806–20 was discovered in 1979 (Laros et al. 1986, 1987) and its persistent X-ray counterpart was observed for the first time with the *ASCA* satellite in 1993 (Murakami et al. 1994). A *RossiXTE* observation led to the discovery of pulsations in the persistent emission with period $P \simeq 7.47$ s and period derivative $\dot{P} \simeq 2.6 \times 10^{-3}$ s yr^{-1} (Kouveliotou et al. 1998a). Under the assumption of pure magnetic dipole braking, these values imply a surface magnetic field strength of 8×10^{14} G, strongly supporting the magnetar model. Both the burst rate and the X-ray persistent emission of SGR 1806–20 started increasing during 2003 and throughout 2004 (Mereghetti et al. 2005c; Tiengo et al. 2005; Mereghetti et al. 2007; Woods et al. 2007), culminating with the giant flare of December 27, 2004, during which $\sim 10^{47}$ erg were released[1] (Hurley et al. 2005; Mereghetti et al. 2005b; Terasawa et al. 2005). This giant flare was exceptionally intense, ∼100 times more energetic than those from SGR 0526–66 and SGR 1900+14. Observations with *RossiXTE* unveiled, for the first time in an isolated neutron star, rapid quasi-periodic oscillations in the pulsating tail of the flare, likely related to global seismic oscillations on the neutron star surface (Israel et al. 2005b). The flare produced a hard X-ray (>80 keV) afterglow lasting a few hours (Mereghetti et al. 2005b; Frederiks et al. 2007) and a radio afterglow that faded in a few days (Cameron et al. 2005). The small positional uncertainty of the radio observations permitted to identify the likely IR counterpart of the SGR (Kosugi et al. 2005; Israel et al. 2005a). The fluxes observed in the IR and gamma energy bands show a variability correlated with that observed in the 2–10 keV energy range (Mereghetti et al. 2007).

After the giant flare, the persistent X-ray flux of SGR 1806–20 started to decrease from its outburst level, and its X-ray spectrum to soften (Rea et al. 2005b,a; Mereghetti et al. 2007; Tiengo et al. 2005; Woods et al. 2007). A Similar flux decrease have been observed from its radio afterglow (Gaensler et al. 2005; Taylor et al. 2005) and its newly discovered IR counterpart (Israel et al. 2005a; Rea et al. 2005a; Mereghetti et al. 2007).

Here we present the results of the first *Suzaku* observation of SGR 1806–20, covering both persistent and bursting emission in the 1–100 keV energy band. We also report on the analysis of a simultaneous observation performed with *XMM-Newton* and the latest outcomes of the monitoring of SGR 1806–20 with

[1] Assuming isotropic luminosity and for a distance $d = 15$ kpc (Corbel et al. 1997; McClure-Griffiths & Gaensler 2005).

INTEGRAL, comparing them with what is seen in the same energy ranges with *Suzaku*.

4.2 *Suzaku* observation and analysis

The *Suzaku* observation of SGR 1806–20 started on September 09, 2006 at 23:13 UT and ended on September 11, at 04:01 UT. The *Suzaku* X-ray observatory (Mitsuda et al. 2007) carries on board the XIS spectrometers (Koyama et al. 2007) operating in the 0.2–12 keV energy band, and the HXD collimated detector (Takahashi et al. 2007), which covers the 10–70 keV energy range with PIN diodes and the 40–600 keV with GSO scintillators. Four X-ray telescopes with a spatial resolution (half-power diameter) of 2′ (XRTs; Serlemitsos et al. 2007) focus X-rays onto the four sensors (XIS 0, 1, 2, and 3) that constitute the XIS instrument. Each XIS contains 1024 by 1024 pixel rows covering a $18' \times 18'$ field of view, and features an energy resolution of ∼140 eV at 6 keV. XIS 0, 2, and 3 are front-illuminated (FI) CCDs, while XIS 1 is a back-illuminated (BI) CCD, that features an enhanced soft X-ray response. The XRT/XIS combination yields effective area per detector of ∼330 cm^2 (FI) or ∼370 cm^2 (BI) at 1.5 keV, and of ∼160 cm^2 (FI) or ∼110 cm^2 (BI) at 8 keV.

The 50 ks long observation was carried out with SGR 1806–20 at the 'HXD nominal' pointing position. The XIS was operated in the normal mode with the 3×3 editing mode (time resolution of 8 s). The data sets were processed using the version 6.1 of the FTOOLS package and the most recent available calibration files available at the time the reduction was performed (November 2006). The XIS pipeline products were affected by an imperfect charge transfer inefficiency (CTI) correction, resulting in a systematically lower energy scale. The error has been corrected by applying the CTI correction tool XISPI again with correct CTI parameters.

For the XISs, source spectra were extracted from circular regions with radii of 3′ centered at the position of SGR 1806–20, while the background spectra from composite regions (far enough from SGR 1806–20 to prevent contamination by its photons). We screened the XIS events based on standard criteria:[2] only events with GRADE 0, 2, 3, 4 and 6 were considered; the CLEANSIS script was used to remove hot or flickering pixels; data collected within 256 s of passage through the South Atlantic Anomaly (SAA) were discarded; data were selected to be at more than 5° in elevation above the Earth rim (20° above the day Earth rim). This resulted in a net exposure time of 46.4 ks and about 57,000 net counts. The response matrices and effective area files were generated independently for each XIS with the tasks XISRMFGEN and XISSIMARFGEN (the ARF generator takes into account the level of hydrocarbon contamination on the optical blocking filter). The spectra were binned with GRPPHA following indications from the XIS Team; furthermore, the data were

[2]See The Suzaku Data Reduction Guide,
http://suzaku.gsfc.nasa.gov/docs/suzaku/analysis/abc/ .

further rebinned to have at least 200 source events per bin.

The HXD data were selected according to the following standard criteria: at least 500 s after the SAA passages, day and night Earth elevation angles each $\geqslant 5^\circ$, and geomagnetic cut-off rigidity to be at least 8 GeV c^{-1}. The exposure was corrected for the instrument dead time, for a net exposures of 48.4 ks in the PIN and 48.8 ks in the GSO. The HXD PIN and GSO instrumental background events were provided by the HXD Team (the instrumental background is due to events created by particles in the vicinity of the instrument). The source and background spectra (generated with the same good-time intervals) were both binned with GRPPHA following recommendations from the HXD Team.

To study the properties of the persistent emission of SGR 1806–20, we cleaned the event list from bursts by applying intensity filters (with a negligible reduction of the net integration time). Spectral fits were performed using the XSPEC version 12.3 software (Arnaud 1996). The analysis of the bursts is presented in Section 4.2.3.

4.2.1 Results in the 1–10 keV energy range

Owing to the high interstellar absorption, very few counts were detected from SGR 1806–20 at low energies and thus we limited the spectral analysis to the 1.5–12 keV energy range. *Suzaku* is placed in a near-circular orbit around the Earth with an orbital period of about 96 minutes. Due to the source occultation by the Earth in each orbit, the data-gathering required $\sim$1.2 days. Apart from the bursts, no variability in the XIS light curves of SGR 1806–20 was detected. The 8 s time resolution of the XIS data does not allow to detect the $\sim$7.6 s pulsations. We also investigated the possibility of spectral variability by splitting the observation in three intervals of equal duration, with negative results.

We fit simultaneously the XIS spectra (with relative normalization factors to account for the calibration uncertainties between the four cameras, see Section 4.3 for details) adopting a power-law and a power-law plus blackbody model. The reduced χ^2 of the former fit, $\chi^2_r = 1.16$ for 283 degrees of freedom (d.o.f.), corresponding to a null hypothesis probability of 0.03, is not completely satisfactory. The power-law plus blackbody model provided a better fit, with $\chi^2_r = 0.98$ for 281 d.o.f. (null hypothesis probability = 0.6). The best fit parameters are photon index $\Gamma = 1.8 \pm 0.1$, blackbody temperature $k_B T = 0.49^{+0.08}_{-0.07}$ keV, and absorption $N_{\rm H} = 7.1^{+0.6}_{-0.5} \times 10^{22}$ cm^{-2} (Table 4.1). The presence of the blackbody component is consistent with the findings of deeper *XMM-Newton* observations (Mereghetti et al. 2007, see also Section 4.3).

Table 4.1 Summary of the spectral results for the persistent emission in the 1.5–12 keV energy range with *Suzaku*/XIS and *XMM-Newton*/pn instruments. The abundances of Anders & Grevesse (1989) are used throughout. Errors are quoted at the 90% confidence level for a single parameter.

Model[a]	Instruments	$N_{\rm H}$ (10^{22} cm^{-2})	Γ	k_BT (keV)	$R_{\rm BB}$[b] (km)	Flux[c] (10^{-11} erg cm^{-2} s^{-1})	χ^2_r (d.o.f.)
PL	XIS	6.4 ± 0.2	2.03 ± 0.04	–	–	1.90 ± 0.04	1.16 (283)
	pn	6.5 ± 0.2	1.78 ± 0.05	–	–	1.74 ± 0.04	1.25 (71)
	XIS+pn	6.5 ± 0.1	1.95 ± 0.03	–	–	1.73 ± 0.03	1.56 (356)
PL+BB	XIS	$7.1^{+0.6}_{-0.5}$	1.8 ± 0.1	$0.49^{+0.08}_{-0.07}$	5^{+9}_{-2}	2.1 ± 0.1	0.98 (281)
	pn	$6.7^{+0.6}_{-0.7}$	$1.6^{+0.1}_{-0.3}$	$0.6^{+0.2}_{-0.1}$	2^{+3}_{-1}	$1.8^{+0.1}_{-0.2}$	1.09 (69)
	XIS+pn	6.9 ± 0.4	1.6 ± 0.1	0.55 ± 0.07	$3.7^{+1.6}_{-0.8}$	1.8 ± 0.1	1.33 (354)

[a] Model applied in XSPEC notation: PL=PHABS*POWERLAW and PL+BB=PHABS*(POWERLAW+BBODYRAD).

[b] Radius at infinity assuming a distance of 15 kpc.

[c] Flux in the 2–10 keV range, corrected for the absorption.

4.2.2 Results in the 10–100 keV energy range and broad-band spectral results

The advantages of *Suzaku*/HXD over previous non imaging instruments are its small field of view ($34' \times 34'$ FWHM below $\sim$100 keV) and a low instrumental background. The images obtained from *INTEGRAL* very deep exposures do not show contaminating point sources within the HXD field of view (see Mereghetti et al. 2005a, Figure 1) and no bright and hard X-ray sources below 10 keV have been found either in the *ASCA* Galactic Plane survey (Sugizaki et al. 2001) or in the SIMBAD database.[3] However, given that SGR 1806–20 lies at low Galactic latitude and longitude ($b \simeq 0^\circ$ and $l \simeq 10^\circ$), the study of its emission in the hard X / soft gamma-ray band is complicated by the presence of the diffuse emission from the Galactic Ridge (see Lebrun et al. 2004, and references therein).

After standard data processing, a positive flux possibly associated with SGR 1806–20 is detected in the HXD-PIN data up to $\sim$40 keV (apart from the bursts, no significant emission is detected in the GSO data). The instrumental background counts obtained by simulations based on the present knowledge of HXD in-orbit performances, are about 70% of the $\sim$26,400 total counts in the 12–40 keV band. To estimate the cosmic X-ray background level in the HXD-PIN band we took the spectrum reported in Gruber et al. (1999), of the form $7.877\, E^{-0.29} e^{-E/41.13\,\mathrm{keV}}$ keV keV^{-1} cm^{-2} s^{-1} sr^{-1}. To model the Galactic Ridge emission we used the spectrum reported in Valinia & Marshall (1998) for their R1 region (Central Ridge: $-1.5^\circ < b < 1.5^\circ$ and $-45^\circ < l < 45^\circ$), where the SGR is located: a power-law with photon index $\Gamma = 2.1$ and surface brightness of 4.9×10^{-8} erg cm^{-2} s^{-1} sr^{-1} in the 10–35 keV band.

However, the R1 region is wide and, since the Galactic Ridge emission strongly varies with latitude and longitude (Lebrun et al. 2004), this estimate of the Galactic Ridge contribution to the background could be severely inaccurate. Therefore, we analyzed a 43 ks long pointing carried out with *Suzaku* on April 07, 2007 at the coordinates $b \simeq 0^\circ$ and $l \simeq 8^\circ$, to provide a background field for the observation of the TeV source HESS J1804−216 (reported in Bamba et al. 2007). After a data processing and instrumental background subtraction performed as described above, we fit the spectrum with a power-law with photon index fixed to 2.1. The ratio between the measured power-law normalization and the one reported for the average spectrum in Valinia & Marshall (1998) is 0.9 ± 0.3 (90% confidence level). So, these data indicate that the emission from the Galactic Ridge at a longitude closer to that of SGR 1806–20 is not significantly different from the average value in the R1 region. We remark that this result relies on the accuracy of the instrumental background estimate, at present $\lesssim$5% (Kokubun et al. 2007). In fact, using a 5% higher background we obtain a nearly null Galactic Ridge emission, whereas a 5% smaller background yields a Galactic Ridge flux 2.0 ± 0.4 times higher than

[3] See http://simbad.u-strasbg.fr/simbad/ .

that of Valinia & Marshall (1998).

We note that to account for the whole signal detected in the HXD-PIN instrument, the Galactic Ridge emission in the HXD field of view should be ∼7 times higher than that reported by Valinia & Marshall (1998). This seems very unlikely to us and therefore we consider significant the detection of SGR 1806–20. However, both its spectral shape and flux are subject to the uncertainty reflecting the coarse knowledge of the Galactic Ridge contribution to the background.

Including the cosmic diffuse and Galactic Ridge emission as fixed components, we fitted the HXD-PIN spectrum in the 12–40 keV band to a power-law model. The best-fit parameters are $\Gamma = 2.0 \pm 0.2$ and flux in the 20–60 keV of $(3.0 \pm 0.5) \times 10^{-11}$ erg cm^{-2} s^{-1} ($\chi^2_r = 0.90$ for 10 d.o.f.). The source, with a net count rate of ∼0.11 counts s^{-1}, accounts for ∼70% of the counts remained after the subtraction of the instrumental background. Varying the assumed instrumental background by ±5% we obtain best-fit fluxes of $(3.7 \pm 0.5) \times 10^{-11}$ erg cm^{-2} s^{-1} and $(2.4 \pm 0.4) \times 10^{-11}$ erg cm^{-2} s^{-1}.

Fitting together the HXD-PIN and XIS[4] spectra, we find that the HXD-PIN data must be scaled downward by a factor of ∼2 to be consistent with the parameters derived in the 1.5–12 keV energy range. This scaling factor is unacceptably large, since the uncertainty in the relative calibration of the two instruments in the energy band considered here is of $\lesssim$20% (Kokubun et al. 2007). To better reproduce the broad-band spectrum we tried a broken power-law plus blackbody model, with a normalization factor between the instruments kept at <1.2. We find an acceptable fit ($\chi^2_r = 1.09$ for 354 d.o.f.; null hypothesis probability = 0.13) with the photon index changing from 1.0 ± 0.1 below the break at 16 ± 2 keV to $2.2^{+0.4}_{-0.2}$ above it, $k_B T = 0.8 \pm 0.1$ keV, $R_{\rm BB} = 2.5^{+0.4}_{-0.3}$ km (at 15 kpc), and $N_{\rm H} = 5.6^{+0.3}_{-0.4} \times 10^{22}$ cm^{-2} (see Figure 4.1). The corresponding 2–10 keV and 20–60 keV unabsorbed fluxes are $\sim 2 \times 10^{-11}$ erg cm^{-2} s^{-1} and $\sim 3 \times 10^{-11}$ erg cm^{-2} s^{-1}, respectively. The normalization factor assumed the value of 1.195, very close to the allowed maximum.

We did not find a significant pulsation in the HXD-PIN data (time resolution of 61 μs). However, given the low signal-to-noise ratio, we do not expect to detect a clear signal if the pulsed fraction is ∼10% (with a sinusoidal profile) as in the 2–10 keV energy range, or smaller. By folding the HXD-PIN light curve on the SGR 1806–20 pulsation period measured in simultaneous *XMM-Newton* data (Section 4.3) and fitting it with a sinusoid, we determine a $3\,\sigma$ confidence level upper limit of ≈20% on the amplitude of a sinusoidal modulation (Galactic Ridge emission subtracted). This upper limit is consistent with the preliminary results obtained with *INTEGRAL* in the 20–60 keV energy range (Götz et al. 2008).

[4]For the broad-band analysis we added the spectra of the three FI CCDs (XIS 0, 2, and 3) using the FTOOL MATPHA. We generated the instrumental responses by summing the redistribution matrices and the effective area files using the FTOOLS ADDRMF and ADDARF.

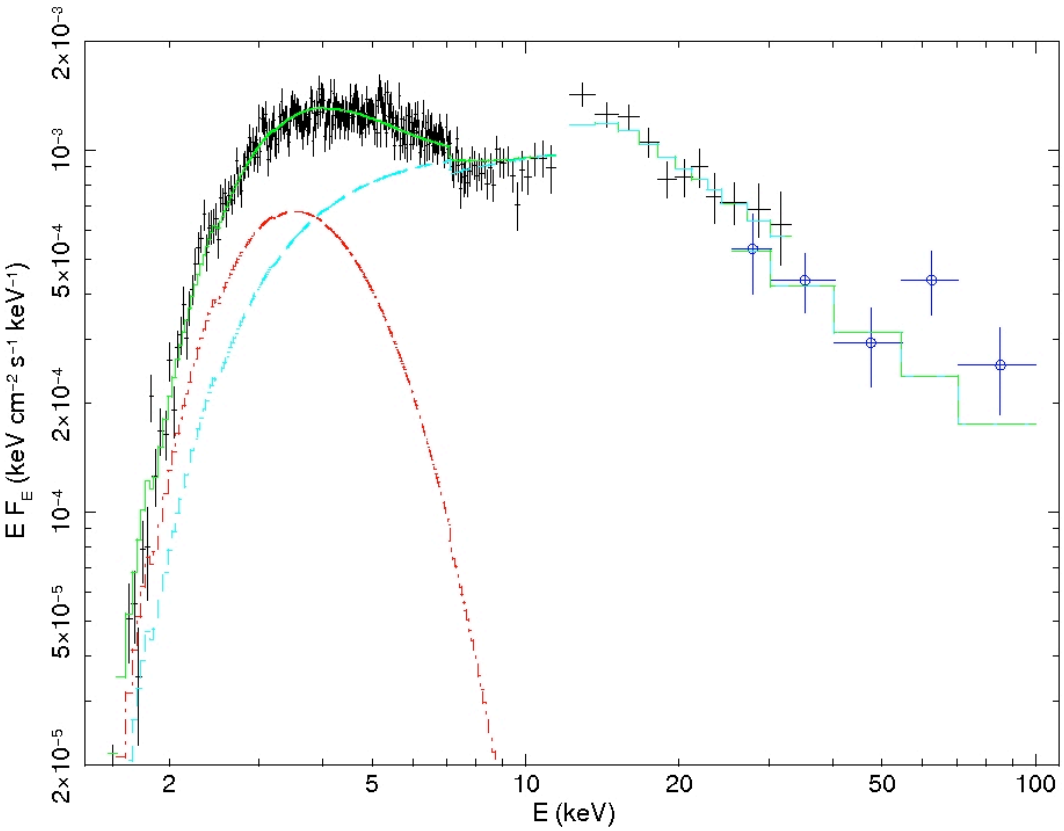

Figure 4.1 Broad-band *Suzaku* spectrum of SGR 1806–20 (see the online edition of the article for a color version of this figure). The *Suzaku*'s XIS 023 and HXD-PIN data (in black) are fit with the broken power-law (light blue dashed line) plus blackbody (red dot-dashed line) model. The XIS 1 data are not shown for clarity. We also plotted the *INTEGRAL* data (see Section 4.4) using the blu circle marks.

4.2.3 Analysis of the bursts

The *Suzaku* (XIS, PIN, and GSO) light curves show many short bursts (Figure 4.2). To obtain significant constraints on spectral fit parameters, we considered only the events with more than 50 counts in the HXD-PIN band. Thus, we selected only two bursts, indicated by the labels A and C in Figure 4.2 and shown in Figure 4.3.

Since the frame-time of the XIS instruments (8 s) is much larger than the burst duration, we measured the duration of the bursts in the high time resolution HXD-PIN light curve (∼0.5 s for burst A and ∼0.4 s for burst C) and we set the integration time of the XIS spectra to these values.[5] The threshold above which the photon pileup becomes significant in the XIS cameras is ∼100 counts frame^{-1} for a point source, and both bursts had a count rate above this

[5]During the two 8 s frames containing bursts A and C, less than 1.5% of the total XIS counts can be attributed to the persistent source plus background emission. Thus, the effect of this emission on the XIS spectra of the bursts is negligible.

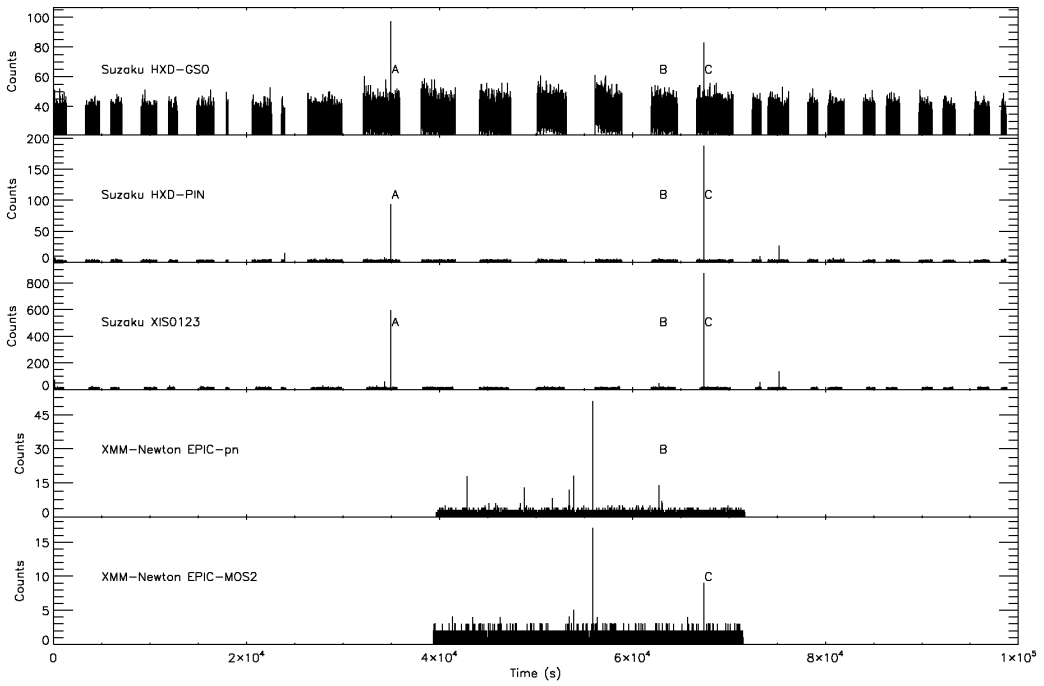

Figure 4.2 Temporal coverage of the *Suzaku* and *XMM-Newton* data (source plus background counts). Several bursts have been detected in the various instruments, but the brigh burst C is not visible in *XMM-Newton*/pn because it is too strong and saturated the detector. Despite this, the burst rate in the *XMM-Newton*/pn is higher than in in the *Suzaku*/XIS, with 0.5 ± 0.2 burst ks^{-1} versus 0.15 ± 0.06 burst ks^{-1}. The difference is likely due to faint bursts undetected in the XIS owing to the long frame-time (8 s). The *Suzaku* arrival times of the photons were barycentered to the Solar System using the task AEBARYCEN. The comparison between the *Suzaku*/HXD and *XMM-Newton*/EPIC times of bursts B and C proves a relative timing accuracy better than 0.2 s.

value. After a careful analysis of the distribution of the counts in the pixels, we excluded a circular region with radius of $15'$ at the image center from the event extraction region to minimize the pileup effects. To increase the statistics in the spectra we added the four XIS spectra using the FTOOL MATPHA. We calculated the corresponding instrumental responses by summing the redistribution matrices and the new effective area files for the annular regions using the FTOOLS ADDRMF and ADDARF. XIS and HXD spectra were rebinned to have a minimum number of 20 counts in each bin. For the background subtraction, under the usual working hypothesis that the bursting emission is present on top of the quiescent one, we used the spectra of the whole observation, cleaned from all the bursts.

The column density of neutral absorbing gas along the line of sight is a critical parameter for the spectral fitting. The most precise measurement of this parameter comes from modeling the persistent X-ray emission: for SGR 1806–

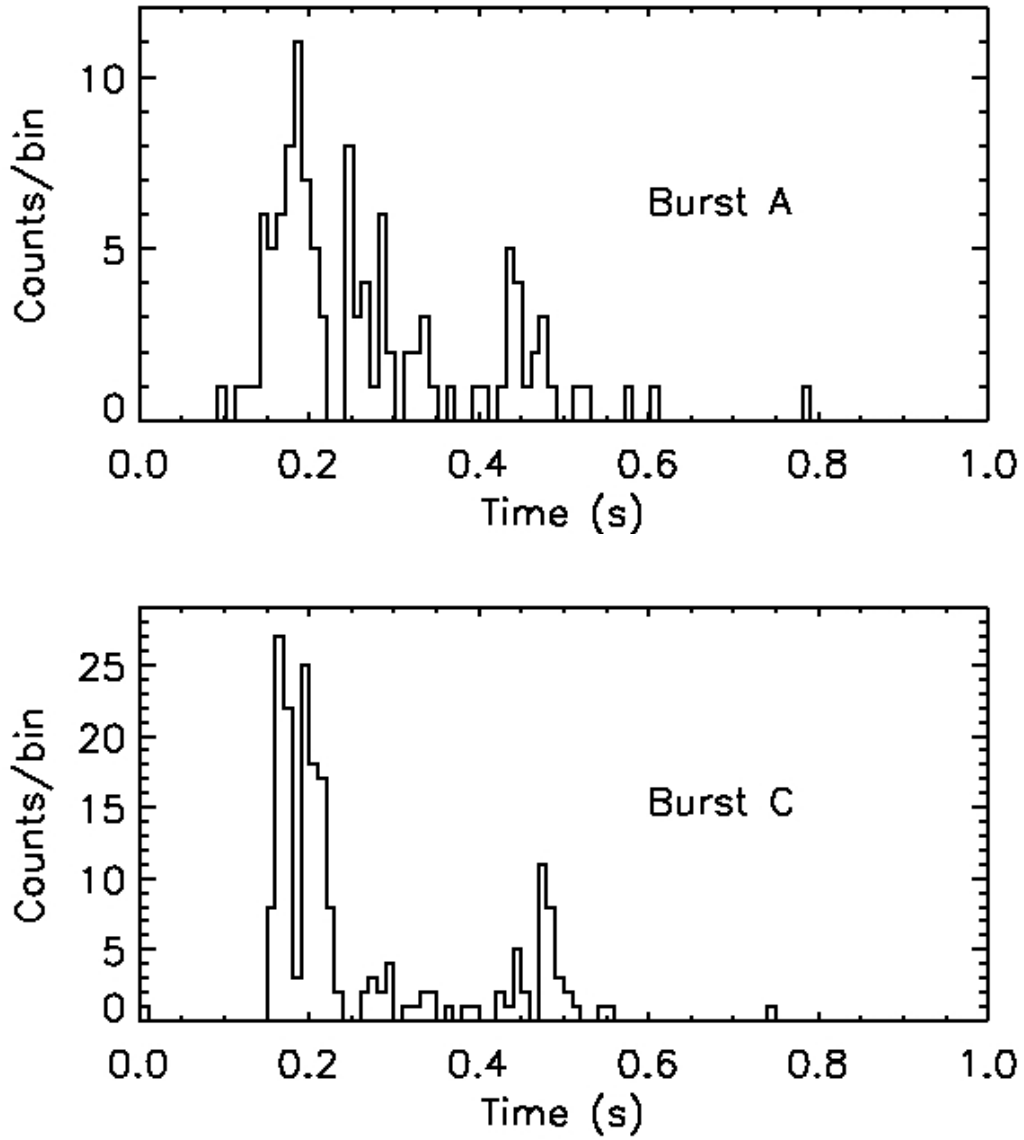

Figure 4.3 HXD-PIN light curves of the bursts A and C in the energy range 12–50 keV. The origins of the time axis are arbitrary and the time bin size is 10 ms.

20 the column density is consistently measured at $N_{\rm H} \simeq 6.5 \times 10^{22}$ cm^{-2} (see Table 4.1 and Mereghetti et al. 2007). To test different spectral models we therefore decided to fix the equivalent hydrogen column at the value measured for the persistent source before and after the bursts. Spectral fits with power-law or thermal bremsstrahlung models, with the $N_{\rm H}$ value fixed at 6.5×10^{22} cm^{-2}, yield unacceptable χ^2 values. Good fits with either the power-law or bremsstrahlung, if the $N_{\rm H}$ is left free to vary, require large absorp-

tion: $N_{\rm H}$ values of 1.7×10^{23} cm^{-2} and 1.4×10^{23} cm^{-2}, respectively. Similar results were obtained by Fenimore et al. (1994) and by Feroci et al. (2004) for the soft gamma-ray repeater SGR 1900+14. A single blackbody spectrum gives a formally acceptable fit in the soft range, but it severely underestimates the observed flux at higher photon energies. Another possible thermal model is the sum of two blackbodies, as used by Olive et al. (2004) and Feroci et al. (2004) to fit bursts from SGR 1900+14. We found that this two components model provided good fits to the bursts, with the parameters summarized in Table 4.2. We tried other types of spectral models, obtaining almost equally good fits with either a blackbody plus power-law model or a blackbody plus thermal bremsstrahlung model (see Table 4.2 and Figure 4.4).

4.3 *XMM-Newton* observation and comparison with *Suzaku*

The *XMM-Newton* observation of SGR 1806–20 started on September 10, 2006 at 10:11 UT and ended at 19:04 UT. It is therefore simultaneous to part of the *Suzaku* observation, as shown in Figure 4.2. Here we present the analysis of the data collected with the EPIC instrument, which consists of two MOS (Turner et al. 2001) and one pn (Strüder et al. 2001) cameras sensitive to photons with energies between 0.1 and 15 keV. The pn was operated in Small Window mode (time resolution 6 ms), while the MOS 1 unit was in Timing mode (time resolution 1.5 ms) and the MOS2 in Full Frame mode (time resolution 2.6 s); all the detectors mounted the medium thickness filter. The data reduction was performed following the procedure described in Tiengo et al. (2005) but using the XMM-Newton Science Analysis Software (SAS) version 7.0.

By an inspection of the *XMM-Newton* lightcurves we found several bursts (see Figure 4.2), but the *XMM-Newton* data do not provide significant improvement on the results obtained from the *Suzaku* data (Section 4.2.3). In fact burst A occurred before the start of the *XMM-Newton* exposure, while burst C was too bright for the pn (the two MOSs registered few counts only), saturating the instrument telemetry.[6] Only burst B was observed by both satellites (see Figure 4.2), but it was too faint for a spectral study. To obtain the results presented in this section, we excluded the bursts from the analysis by applying intensity filters. A further cleaning was necessary because of the presence of soft proton flares during the observation. On the whole, the net exposure time was reduced from ∼22.3 ks to ∼21.6 ks for the pn detector.

We fit in the 1.5–12 keV range the spectrum obtained with the pn camera adopting the same models used for the *Suzaku* spectral analysis. We again

[6] If the count rate in the pn is higher than the telemetry limit (∼600 counts s^{-1} for the imaging modes), then the so-called 'counting mode' is triggered and for some time the science data are lost.

Table 4.2 Burst spectral parameters for the two component models (assuming for the absorption the value of 6.5×10^{22} cm^{-2}). Errors are quoted at the 90% confidence level for a single parameter.

Burst	Model[a]	k_BT_1 (keV)	$R_{\rm BB\,1}$[b] (km)	k_BT_2 (keV)	$R_{\rm BB\,2}$[b] (km)	$k_BT_{\rm BR}$ (MeV)	Γ	Flux[c] (erg cm^{-2} s^{-1})	χ^2_r (d.o.f.)
A	BB+BB	$2.3^{+0.6}_{-0.4}$	15^{+5}_{-4}	10 ± 2	$1.5^{+0.7}_{-0.6}$	–	–	1.3×10^{-7}	1.15 (47)
	BB+BR	$4.6^{+1.2}_{-0.8}$	5 ± 2	–	–	$0.10^{+0.06}_{-0.03}$	–	1.2×10^{-7}	1.08 (47)
	BB+PL	$4.5^{+0.8}_{-0.7}$	5^{+2}_{-1}	–	–	–	$1.5^{+0.2}_{-0.1}$	1.1×10^{-7}	1.19 (47)
C	BB+BB	$2.2^{+0.5}_{-0.4}$	20^{+5}_{-4}	7 ± 1	4 ± 1	–	–	2.1×10^{-7}	0.95 (63)
	BB+BR	$4.2^{+0.5}_{-0.4}$	9 ± 2	–	–	$0.11^{+0.29}_{-0.06}$	–	2.0×10^{-7}	1.09 (63)
	BB+PL	4.2 ± 0.4	9 ± 2	–	–	–	1.4 ± 0.2	2.0×10^{-7}	1.12 (63)

[a] Model applied in XSPEC notation: BB+BB=PHABS*(BBODYRAD+BBODYRAD), BB+BR=PHABS*(BBODYRAD+BREMSS), and BB+PL=PHABS*(BBODYRAD+POWERLAW).

[b] Radius at infinity assuming a distance of 15 kpc.

[c] Flux in the 2–100 keV range, corrected for the absorption.

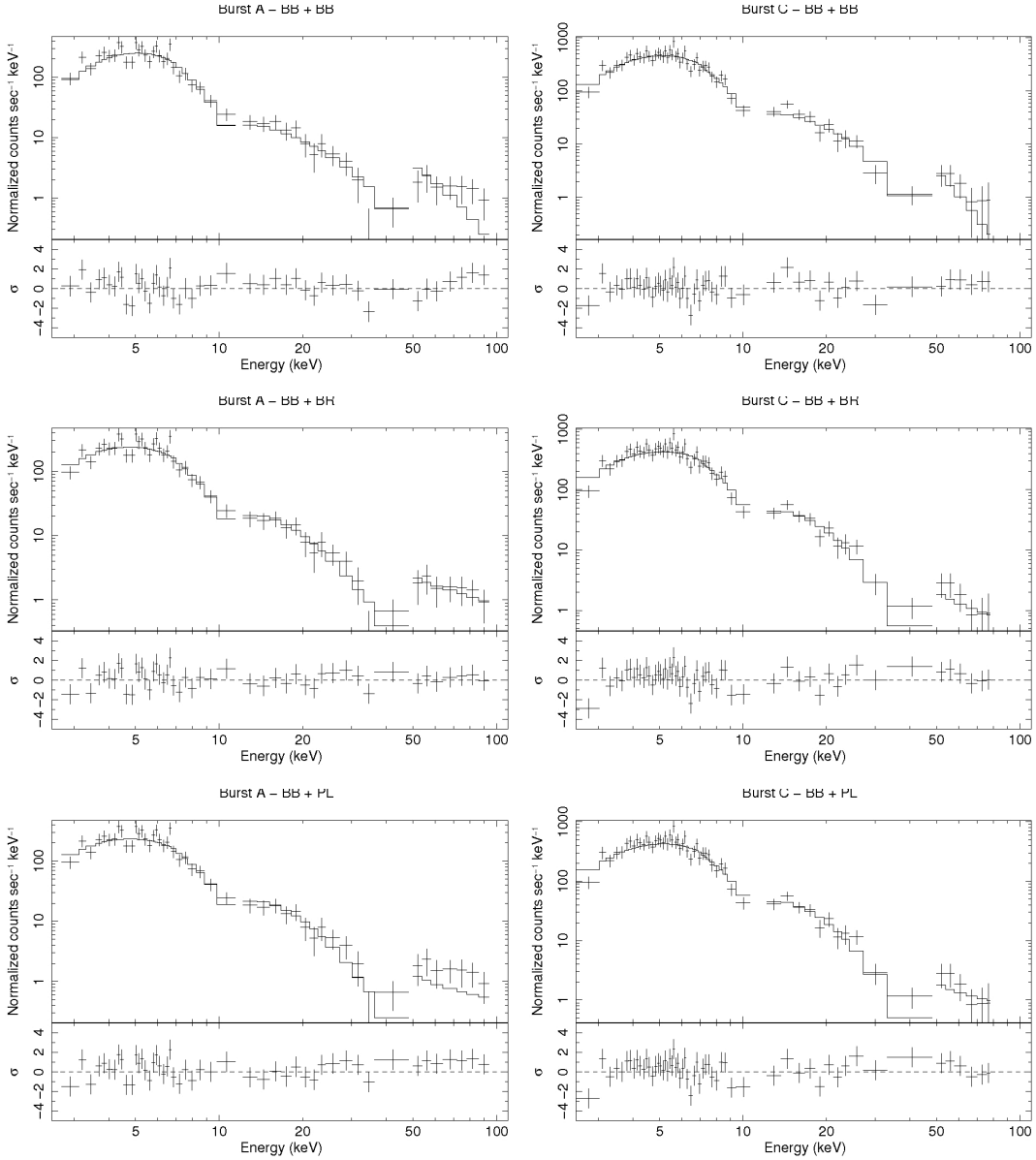

Figure 4.4 *Suzaku* broad-band spectra and residuals of the bursts A and C (XIS 1.5–12 keV, HXD-PIN 12–50 keV and HXD-GSO 50–100 keV). The model adopted is indicated on each panel (see also Table 4.2)

Table 4.3 Normalization factors for the *Suzaku*/XIS cameras with respect to the *XMM-Newton*/pn (see Section 4.3 for details).

Detector	Energy range			
	1.5–12 keV	1.5–4 keV	4–8 keV	8–12 keV
XIS 0	1.11 ± 0.02	1.23 ± 0.04	1.05 ± 0.03	1.1 ± 0.1
XIS 1	1.08 ± 0.02	1.19 ± 0.04	1.00 ± 0.03	1.1 ± 0.2
XIS 2	1.17 ± 0.02	1.26 ± 0.04	1.13 ± 0.03	1.1 ± 0.1
XIS 3	1.19 ± 0.02	1.33 ± 0.04	1.12 ± 0.03	1.1 ± 0.1

found that the power-law plus blackbody model provides a slightly better fit (see Table 4.1); the best-fit parameters are $\Gamma = 1.6$, $k_B T = 0.6$ keV, and $N_{\rm H} = 6.7 \times 10^{22}$ cm^{-2}, with a χ^2_r of 1.09 for 69 d.o.f.. The corresponding luminosity in the 2–10 keV band is $5 \times 10^{35} d^2_{15}$ erg s^{-1}, where we indicate with $d_{\rm N}$ the distance in units of N kpc. This luminosity is slightly higher than that of the previous *XMM-Newton* observation performed on April 4, 2006 (Mereghetti et al. 2007), as also supported by a simple comparison of the pn net count rates (0.993 ± 0.007 counts s^{-1} with respect to 0.946 ± 0.007 counts s^{-1}), while the other spectral parameters are consistent. We also analyzed in a similar way the spectra obtained with the MOS cameras, finding results consistent with the pn ones.

Given the simultaneity of the *XMM-Newton* and *Suzaku* observations, we have tried to fit together the *XMM-Newton*/pn and *Suzaku*/XIS spectra, with a normalization factor to account for the uncertainty in the absolute flux estimate of the different instruments. In Table 4.1 we report the results of such analysis using either a power-law or a power-law plus blackbody model. We note that the χ^2 values are unacceptable. Since no intrinsic spectral variability during the non-coincident exposure windows of the two satellites is expected (the bursts have been removed in both datasets), this simultaneous fit can be used to evaluate the cross-calibration discrepancies between the *XMM-Newton*/pn and the four *Suzaku*/XIS detectors. Fixing the *XMM-Newton*/pn normalization factor to 1 and linking all the other parameters, we derive the normalization factors reported in Table 4.3, either for the whole energy range or restricting the fit to three energy bands. These values show that the four XIS detectors measure a systematically higher flux with respect to the pn, especially in the soft energy range. However we note that the cross-calibration accuracy between the pn and the XIS is, especially above 4 keV, of the same order of the discrepancies between the different XIS units.

To derive the period of SGR 1806–20 we used the pn data. Photon arrival times were converted to the Solar System barycenter using the SAS task BARYCEN. With a standard folding analysis of the light curves, we measured a spin period of 7.5891 ± 0.0002 s. The resulting peak-to-trough pulsed fraction $PF_{\rm pt} \equiv (F_{\rm max} - F_{\rm min})/(F_{\rm max} + F_{\rm min})$, where $F_{\rm max}$ and $F_{\rm min}$ are the ob-

served background-subtracted count rates at the peak and at the minimum, is $(11 \pm 2)\%$ in the 2–10 keV band.[7]

4.4 *INTEGRAL* observations and broad-band spectral analysis

We analyzed the *INTEGRAL*'s AO-4 Key Project (KP) observation of the Galactic Centre, and report here results obtained with ISGRI, the low energy detector plane (15 keV–1 MeV; Lebrun et al. 2003) of *INTEGRAL*'s imager IBIS[8] (Ubertini et al. 2003). The IBIS/ISGRI data were reduced using the Off-line Scientific Analysis package (OSA version 6.0). Thanks to IBIS large field of view ($29^\circ \times 29^\circ$), SGR 1806–20, which is located $\sim 10^\circ$ from the Galactic Centre, was almost constantly observed during the KP. This project was divided in two parts: the first one lasted from September 12 to October 5, 2006, yielding an effective exposure time of $\sim$750 ks on the source, while the second one lasted from February 28 to March 25, 2007 for an exposure of $\sim$550 ks. Our data set consists of about 700 individual pointings, but due to the faintness of the source we could not extract the spectra from the individual pointings. We extracted the images for each pointing in 10 energy bands between 20 and 300 keV and added all the individual images in order to produce two mosaics (one for each part of the KP observation). We then extracted the fluxes from the mosaics in each energy band in order to derive the source spectrum, and rebinned the ISGRI response matrix to match our energy bands. Since the fluxes were found not to vary within the errors between the two parts of the KP, we added the two spectra in order to increase our statistics.

The IBIS/ISGRI spectrum can be well fit ($\chi^2_r = 0.85$ for 5 d.o.f.) with a single power-law, with $\Gamma = 1.7 \pm 0.3$, and a 20–60 keV flux of $(2.8 \pm 0.4) \times 10^{-11}$ erg cm^{-2} s^{-1}. The power-law parameters obtained in the hard X-ray band with IBIS/ISGRI and the *Suzaku*/HXD (Section 4.2.2) are consistent within the errors. The joint fit of the IBIS/ISGRI and *Suzaku*'s XIS and HXD-PIN data to the broken power-law plus blackbody model adopted in Section 4.2.2 yields virtually identical best-fit parameters, with $\chi^2_r = 1.09$ for 358 d.o.f..

We also fit the IBIS/ISGRI spectrum simultaneously with the *XMM-Newton* pn spectrum described in the previous section, using a blackbody plus power-law model. The resulting best-fit parameters ($\Gamma = 1.55 \pm 0.08$, blackbody temperature $k_B T = 0.6 \pm 0.1$ keV and radius $R_{\rm BB} = 2^{+2}_{-1}$ km (at 15 kpc), and $N_{\rm H} = 6.6^{+0.5}_{-0.4} \times 10^{22}$ cm^{-2}, with $\chi^2_r = 1.27$ for 107 d.o.f.) are consistent with

[7] Note that here we use a different definition of the pulsed fraction than in Mereghetti et al. (2007). Using the old definition based on a sinusoidal fit to the profile, the estimated pulsed fraction in the same energy range is $(8 \pm 1)\%$.

[8] The direction of SGR 1806–20 was scarsely covered by *INTEGRAL*'s X-ray monitor JEM-X (Lund et al. 2003), due to its smaller (with respect to that of IBIS) field of view (7° diameter). As a consequence, only about 200 ks of exposure were available, and this was unsufficient for a detection.

an extrapolation of the low-energy model (Figure 4.5).

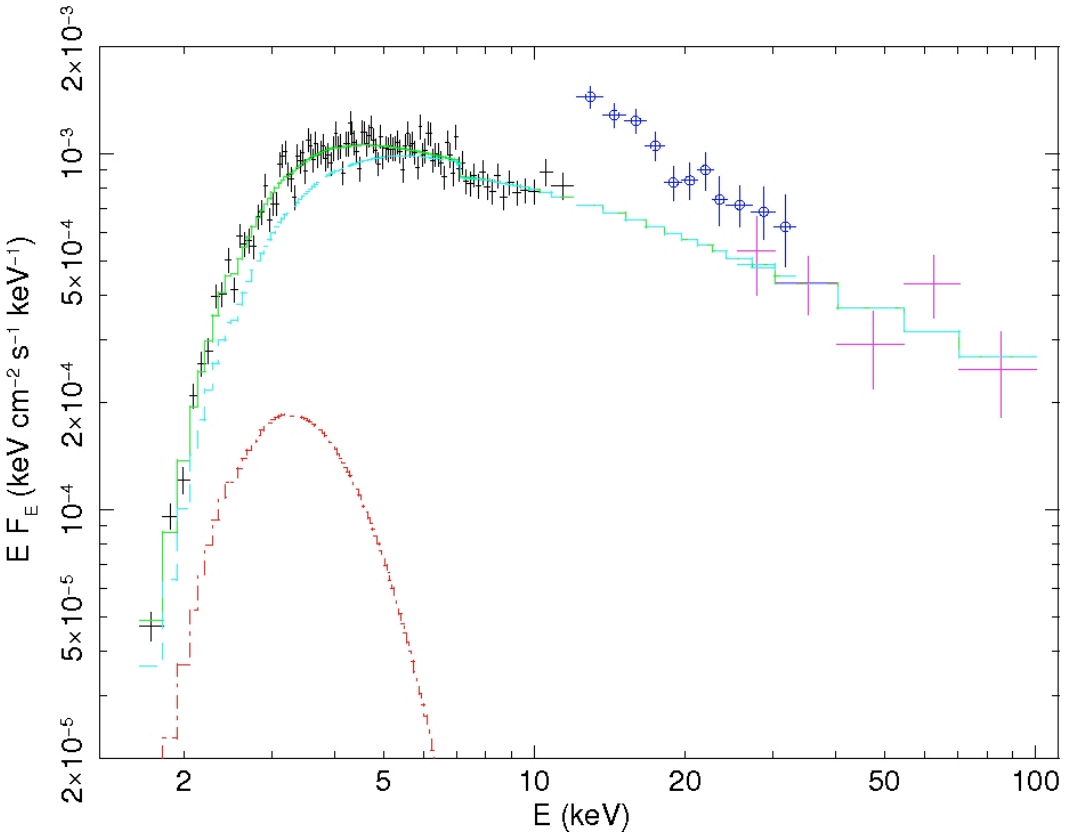

Figure 4.5 *XMM-Newton* and *INTEGRAL* broad-band spectrum of SGR 1806–20 (see the online edition of the article for a color version of this figure). The data from *XMM-Newton*/pn (black) and *INTEGRAL*/IBIS (lilac) are fit with the power-law (light blu dashed line) plus blackbody (red dot-dashed line) model. We also plotted *Suzaku*/HXD-PIN data using the blu circle marks.

4.5 Discussion and conclusions

The *Suzaku*, *XMM-Newton*, and *INTEGRAL* observations reported here represent a complementary data set that allows us to study the spectral properties of SGR 1806–20 in the broad 1–100 keV energy range. Although the *Suzaku*/HXD does not have imaging capabilities, we know thanks to *INTEGRAL* that no other bright hard X-ray sources are present in its field of view. The uncertainties in the instrumental background (currently at the ∼5% level) and in the modelling of the Galactic Ridge emission are a more relevant concern. Future improvements in the knowledge of these components may eventually allow us to obtain more robust conclusions. Thanks to its imaging capabilities, background issues do not affect the *INTEGRAL* observations. However, the IBIS/ISGRI data required long integration times, with discontinuous ob-

servations spanning several months. Thus they provide information on the average properties only. The possible presence of long term variability was in fact one of the main motivations to perform the *Suzaku* and *XMM-Newton* observations simultaneously. With all these caveats in mind we proceed now to discuss the broad band spectrum of SGR 1806–20.

The *XMM-Newton* and *INTEGRAL* spectra are consistent with an extrapolation of the power-law plus blackbody model measured in the 2–10 keV band. Between 12 and 30 keV the *Suzaku*/HXD sensitivity is better than that of *INTEGRAL*, allowing to detect SGR 1806–20 during a single 50 ks long observation. With respect to the *XMM-Newton* and *INTEGRAL* joint fit, the HXD data show an 'excess' (see Figure 4.5) that cannot be completely ascribed to calibration uncertainties between the various instruments.

Given the lack of a direct measure of the Galactic Ridge emission around SGR 1806–20, we cannot exclude that this excess is due to an underestimation of such contribution to the background. If instead the excess is a real feature of the spectrum of SGR 1806–20, its broadband spectrum could be empirically modeled adopting a power-law with the photon-index changing from $\sim$1 to $\sim$2 at $\sim$16 keV, and a blackbody component with $k_BT \sim 0.8$ keV. This would agree with the results reported by Götz et al. (2006), who point out that the hard tails of the SGRs are softer than the power-law components measured below 10 keV.

The presence of a down-break in the 10–20 keV spectrum of SGR 1806–20 would have remarkable physical implications. The soft X-ray emission from magnetar candidates (SGRs and AXPs) is usually interpreted within the twisted magnetosphere model as due to resonant cyclotron up-scattering of soft photons from the star surface onto charges flowing into the magnetosphere (Thompson et al. 2002). Detailed calculations of resonant compton scattering (RCS) spectra have been recently performed (Lyutikov & Gavriil 2006; Fernández & Thompson 2007) and successfully applied to fit AXP spectra (Rea et al. 2007). Quite interestingly, some of the model spectra presented by Fernández & Thompson (2007) exhibit a downward break in the tens of keV range. Their overall shape is quite reminiscent of the *Suzaku* XIS/HXD-PIN spectrum of SGR 1806–20, and, as noted by Fernández & Thompson (2007), they may also play a role in the interpretation of the broadband X-ray spectrum of SGR 1900+14. In particular, when assuming a (non-thermal) top-hat or a broadband velocity distribution for the magnetospheric charges, multiple peaks can appear in the spectrum (see their Figure 6 and Figure 11). The downturn possibly present in our data may then be due the presence of a second 'hump' (in addition to the main thermal one) in the range 10–20 keV. Nobili et al. (2008a,b) assuming a 1-D thermal electron distribution superimposed to a (constant) bulk velocity, found also double humped spectra. In this case the second (and only) hump occurs when resonant scattering is efficient enough to fill the Wien peak at the temperature of the comptonising particles. A spectral break at $\sim$15 keV would translate then in a temperature of $\sim$5 keV

for the magnetospheric electrons. If a more refined treatment of background subtraction confirms the spectral break in the X-ray data of SGR 1806–20 this would provide important diagnostics for the physical parameters of the model.

In 2003 we started a long-term monitoring program to study the time evolution of the spectral properties of SGR 1806–20 using the *XMM-Newton* X-ray satellite. The December 27, 2004 giant flare was a fortunate occurrence that allowed us to observe how the source properties evolved in the two years leading up to the flare and how they changed after this dramatic event (see Mereghetti et al. 2005c, 2007; Rea et al. 2005a; Tiengo et al. 2005, for details). The *XMM-Newton* data showed a doubling of the flux in the September–October 2004 followed by a gradual recovery to the 'historical' level after the giant flare. A direct comparison of the *XMM-Newton*/pn count rates measured in the different observations shows that before the giant flare the flux of SGR 1806–20 in the 1–10 keV band was monotonically increasing, while the three observations after the flare, and preceding the one reported here, followed a steady decreasing trend. The September 2006 observation breaks this long term decay, having a count rate higher by 5% with respect to the last *XMM-Newton* observation performed 5 months before. This slight (but statistically significant) re-brightening might indicate either a temporary oscillation around an equilibrium flux level or the start of a new monotonic flux increase, similar to the one that preceded the December 2004 giant flare. This phenomenon was interpreted as due to the building up of a magnetospheric twisting, that determined also the hardening of the X-ray spectrum, an increase of the spin-down and a more intense bursting activity (Mereghetti et al. 2005c). The relatively high burst rate observed during the *XMM-Newton* and *Suzaku* observations of September 2006 (see Section 4.2.3) is therefore another indication of a possible increase of the magnetospheric twisting in SGR 1806–20, but, before a new *XMM-Newton* observation will be performed, only the monitoring of the frequency and intensity of SGR 1806–20 bursts can tell us if the evolution is erratic or follows a stable trend. The recent report of a bright burst from SGR 1806–20 (Golenetskii et al. 2007; Perotti et al. 2007) seems actually to favour the second hypothesis.

Two of the bursts detected during the *Suzaku* observation were bright enough to allow spectral analysis. In both cases, the broadband spectrum (2–100 keV) revealed the presence of two components: a soft component which is well reproduced by a blackbody with $k_BT \sim$ 2–4 keV, and a harder one whose spectral shape is not firmly established and can be equally well fit with a power-law, a hot bremsstrahlung or a second blackbody (See Table 4.2 and Figure 4.4). In absence of robust theoretical predictions, we can not exclude that a two component model simply reflects our ignorance of the correct spectral shape, and has therefore a purely phenomenological significance. However, it is worth noticing that, from their recent analysis of a sample of 50 bursts detected from SGR 1806–20 with *HETE-2* from 2001 to 2005, Nakagawa et al. (2007) have suggested the presence of a time delay between the 30–100 keV

and the 2–10 keV emission. Although such a delay can be attributed to an intrinsic, rapid spectral softening, an alternative, and simpler, interpretation invokes the presence of two separate emitting regions.

Let us consider a scenario in which the two components are physically distinct and let us consider the hard component first. In the magnetar scenario, short bursts are usually ascribed to either reconnection phenomena in the external magnetosphere (eventually modulated by a tearing instability, see Lyutikov 2003) or movements of the footprints of the external magnetic field, produced by crustal deformations or fractures driven by the stress exerted by the internal field helicity (Thompson & Duncan 1995, 2001; Thompson et al. 2002). Both kind of processes lead to the generation and launch of an Alfvèn wave, which produces and accelerates a particle cascade, and ultimately is detected as a burst. The emerging spectrum is expected to be synchrotron dominated, unless the Alfvèn wave is temporarily trapped in a fireball and thermalized. Therefore, both the BB+PL and BB+BB spectral fits are consistent with a scenario in which such an Alfvèn wave is responsible for the hard component. We notice that, although a fireball formation is not required to explain short bursts (and therefore usually not invoked in such cases), to our knowledge there is no a priori reasons why a small fireball can not be created and evaporated in a sub-second time scale, giving rise to a thermal spectrum. A point in favour of this interpretation is that, in the BB+BB fit, the temperature of the hot blackbody is remarkably close to the minimal temperature above which a fireball thermalizes, $k_B T \approx 11\,(R_{\rm NS}/10\,{\rm km})^{-1/5}$ keV, according to Thompson & Duncan (2001), eq. [71] (see also Olive et al. 2004, for similar findings based on longer duration burst). The third model of the hard component which is compatible with our data is a bremsstrahlung emission at $\sim$100 keV. Quite recently, Thompson & Beloborodov (2005) and Beloborodov & Thompson (2007) discussed the electrodynamics of the magnetar coronae and the production mechanisms for soft gamma-rays. In particular, their model predicts the existence of a thin transition layer between the corona and the thermal photosphere, where Langmuir turbulence can be excited by a downward beam of current-carrying charges. As a result, the transition layer can be heated up to a typical temperature of $\sim$100 keV, and emit, approximatively, an optically thin bremsstrahlung at a single temperature. Although Thompson & Beloborodov (2005) model was originally developed in connection with the persistent hard emission of magnetars, the predicted bremsstrahlung temperatures are remarkably close to those we detected during the two bursts, suggesting that a similar mechanism may instead be activated during periods of activity.

Our results about the spectral modelling of the soft X-ray component are more robust, inasmuch as all our spectral fits require the presence of a cold blackbody with $k_B T \sim 2$–4 keV. This is in agreement with similar findings by Olive et al. (2004), Nakagawa et al. (2007), and Feroci et al. (2004). This component is usually interpreted as due to emission from a fraction of the star

surface (which can be as large as the whole star in the case of our BB + BB fit) heated by returning currents. Alternatively, it has been suggested that the soft component may originate up in the magnetosphere ($\leq$700 km), presumably due to a delayed emission process (Nakagawa et al. 2007). Here we only notice that, although the spectra of our two events are compatible with emission from the star surface, the radius of the cold blackbody as measured during other short bursts can reach values much higher than 50–100 km (Nakagawa et al. 2007, similar findings have been found in the case of SGR 1900+14 bursts measured with *Swift*, Israel et al. 2008). One possible explanation is that part of the flare energy is intercepted and reprocessed in a larger region and re-emitted at a lower temperature. In such scenario, the radius of the reprocessing region can then vary depending on the fraction of material that is intercepted, and is not bounded by the value of the star radius. Thompson & Duncan (2001) considered the equilibrium state of a pair corona sufficiently extended that the local value of the magnetic field is $B \ll B_{\rm QED}$, so that photon splitting can be ignored (if the magnetic field scales as a dipole, this occurs above $\sim$3 star radii, for a polar surface value of $\sim 10^{15}$ G). They found that a stable balance between heating and diffusive cooling requires a continuous source of ordinary photons that can be provided, for instance, by external illumination. If the corona intercepts part of the flare beam (which in their treatment is assumed to originate in a trapped fireball, although in general this is not necessarily required), equilibrium is possible below a critical luminosity given by

$$L < L_{\rm max} = 1.5 \times 10^{42}\, \tau_{EO}^{-1} \left(\frac{k_B T_e}{20\ {\rm keV}}\right)^4 \left(\frac{R}{10\ {\rm km}}\right)^2\ {\rm erg\ s^{-1}}\,,$$

where T_e is the pair temperature in the corona, $\tau_{EO} \sim 1$ is the scattering depth for ordinary to extraordinary mode conversion and R the radius of the emitting part of the corona (see equations [84] and [89] in Thompson & Duncan (2001) and note that there is a typo in their equation [89]: it should contain R^2 instead of R^{-2}). Even for an emission region as small as 5–20 km (as inferred by our best fit of the low temperature blackbody) and a temperature of $k_B T \sim$ 2–4 keV, this is well above the luminosity emitted during the two bursts detected by *Suzaku*. Therefore, simply on the basis of energetics, relatively large emitting regions for the cold blackbody are compatible with the temporary formation of a pair corona, sustained by a fraction of the flare energy. When the heating rate ceases, the pair atmosphere contracts and quickly evaporates. In order to derive firmer conclusions a more detailed analysis is needed, mainly in assessing the possibility that the intercepted beam is thermalized and re-emitted as a blackbody. This study is beyond the purpose of this paper, and will be presented elsewhere (Israel et al. 2008).

Chapter 5

The 2008 May burst activation of SGR 1627–41

In May 2008 the soft gamma-ray repeater SGR 1627–41 resumed its bursting activity after nearly a decade of quiescence. After detection of a bright burst, *Swift* pointed its X-ray telescope in the direction of the source in less than five hours and followed it for over five weeks. In this paper we present an analysis of the data from these *Swift* observations and an *XMM-Newton* one performed when SGR 1627–41 was still in a quiescent state. The analysis of the bursts detected with *Swift*/BAT shows that their temporal and spectral properties are similar to those found in previous observations of SGR 1627–41 and other soft gamma-ray repeaters. The maximum peak luminosity of the bursts was $\sim 2 \times 10^{41}$ erg s^{-1}. Our data show that the outburst was accompanied by a fast flux enhancement and by a hardening of the spectrum with respect to the persistent emission.

5.1 Introduction

The soft gamma-ray repeater (SGR) SGR 1627–41 is likely to host a 'magnetar', i.e. an isolated neutron star believed to have an extremely strong magnetic field ($B \sim 10^{14}$–10^{15} G) powering their bright X-ray emission and peculiar bursting activity (e.g. Mereghetti 2008). Several magnetars, including SGR 1627–41, have been observed to emit short bursts (<1 s) in the hard X/soft gamma-ray band, with characteristic peak luminosities of the order of $\sim 10^{39}$–10^{41} erg s^{-1}. Besides short bursts, SGRs are known to emit intermediate and giant flares, with typical durations of 0.5–500 s, during which luminosities up to $\sim 10^{47}$ erg s^{-1} can be achieved.

SGR 1627–41 was discovered in 1998 by the *Compton Gamma Ray Observatory* because of the intense bursts it emitted at the time (Kouveliotou et al. 1998b). These bursts, more than a hundred in six weeks, were also observed by other X-ray satellites (Hurley et al. 1999c; Woods et al. 1999c; Feroci et al.

1998; Smith et al. 1999; Mazets et al. 1999a). Soon after the discovery of the bursts, the persistent X-ray emission of this SGR was detected by *BeppoSAX* at a luminosity of $\sim 10^{35}$ erg s^{-1} (assuming a distance to the source of 11 kpc; Corbel et al. 1999). The quiescent spectrum was well modelled by an absorbed power law ($N_{\rm H} \approx 8 \times 10^{22}$ cm^{-2} and photon index $\Gamma \approx 2.5$; Woods et al. 1999c). No further bursting activity has been reported since then, but several X-ray satellites observed the X-ray persistent counterpart of SGR 1627–41 in the past ten years (Kouveliotou et al. 2003; Mereghetti et al. 2006). Since its discovery, this persistent emission showed a slow luminosity decay, from about 10^{35} to 10^{33} erg s^{-1}, the lowest value ever observed for an SGR, and a spectral softening from $\Gamma \approx 2$ to 4 (Kouveliotou et al. 2003; Mereghetti et al. 2006). The post-burst cooling trend seen in X-rays is peculiar among SGRs; rather it resembles the behaviour of transient anomalous X-ray pulsars (AXPs), a sub-class of the magnetar family.

Here we report on the last observation of SGR 1627–41 performed at the end of the ten year long stretch of quiescence and on the burst re-activation of the source on 28 May 2008 (Palmer et al. 2008; Golenetskii et al. 2008; Woods et al. 2008a).

5.2 The February 2008 *XMM-Newton* observation

The last *XMM-Newton* (Jansen et al. 2001) observation of SGR 1627–41 before the May 2008 re-activation was carried out on 12–13 February 2008 and lasted about 80 ks. The EPIC pn and MOS cameras (sensitive in the 0.1–15 keV range) were operated in Full Frame mode with the medium optical filter. The data were processed using version 7.1.0 of the *XMM-Newton* Science Analysis Software (SAS). We selected events with patterns 0–4 and 0–12 for the pn and the MOS cameras, respectively. The data were filtered to reject intervals with soft-proton flares, reducing the net exposure time to 49.3 ks for the pn detector, 68.3 ks for the MOS 1, and 69.4 ks for the MOS 2.

Source spectra were accumulated for each camera from circular regions with a 25″ radius. The background counts were selected from a 70×150 arcsec^2 box centred at RA = $16^{\rm h}36^{\rm m}01.4^{\rm s}$, Decl. = $-47°34'27.6''$. About 330 counts above the background were collected from SGR 1627–41 by the pn between 2 and 10 keV, 150 by the MOS 1, and 160 by the MOS 2. Spectral redistribution matrices and ancillary response files were generated using the SAS tasks RMFGEN and ARFGEN. The spectral fitting was performed using the XSPEC fitting package version 12.4. The data were grouped so as to have at least 20 counts per energy bin and the spectra from the MOS 1, MOS 2, and pn in the 2–10 keV range were fit simultaneously (spectral channels having energies below 2 keV were ignored, owing to the very low signal-to-noise ratio). We fit an absorbed power-law model and obtained the following best-fit parameters ($\chi^2_{\rm r} = 0.98$ for

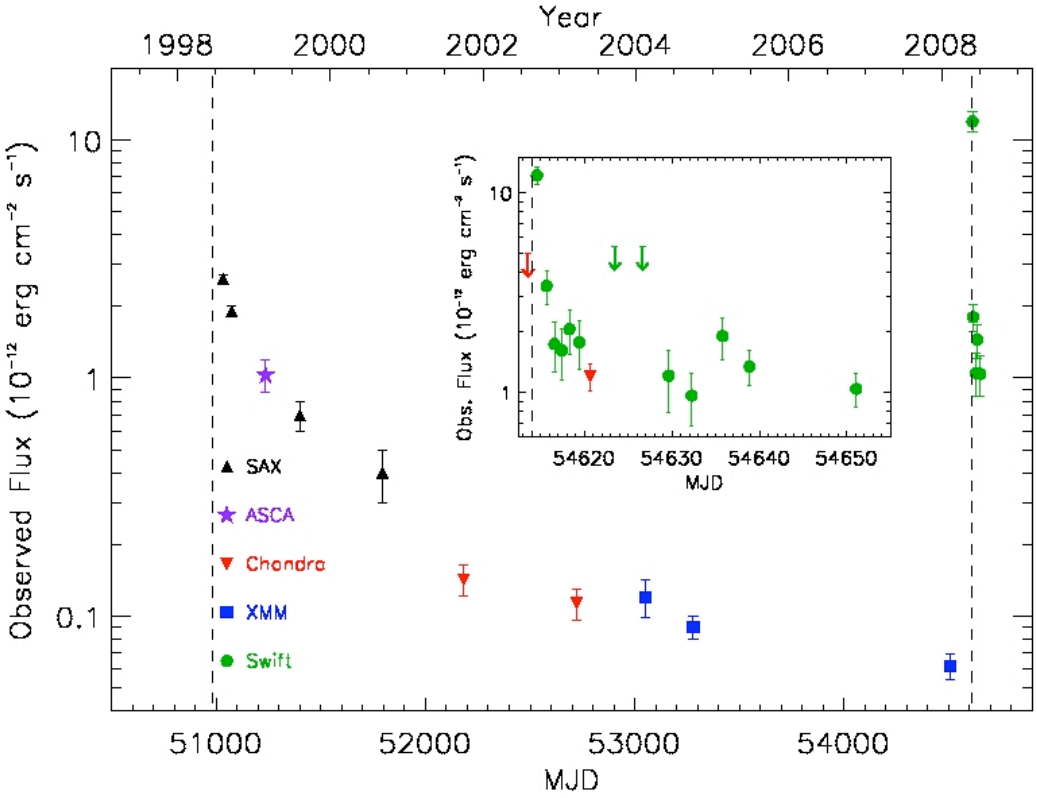

Figure 5.1 Long term light-curve of SGR 1627–41 based on data from different satellites (updated from Mereghetti et al. 2006). The vertical dashed lines indicate the onset of the two burst-active periods of the source. The inset shows in detail the light-curve around the 2008 reactivation, using also *Chandra* data from Tiengo et al. (2008) and Woods et al. (2008b). The down-arrows indicate upper limits at $3\,\sigma$ confidence level.

42 degrees of freedom): absorption $N_{\rm H} = (10 \pm 2) \times 10^{22}$ cm^{-2} and photon index $\Gamma = 3.3^{+0.6}_{-0.4}$ (hereafter all errors are at $1\,\sigma$ confidence level). The observed 2–10 keV flux was $(6 \pm 2) \times 10^{-14}$ erg cm^{-2} s^{-1}. For comparison with previous work (Kouveliotou et al. 2003; Mereghetti et al. 2006) we also fit the data keeping the absorption column fixed at $N_{\rm H} = 9 \times 10^{22}$ cm^{-2}, obtaining a similar photon index $\Gamma = 3.0 \pm 0.2$ and a flux of $(6 \pm 1) \times 10^{-14}$ erg cm^{-2} s^{-1}. This value (plotted in Figure 5.1) hints at a further luminosity decrease since the previous *XMM-Newton* observations (September 2004; Mereghetti et al. 2006).

5.3 *Swift* observations and data analysis

Swift (Gehrels et al. 2004) was specifically designed to study Gamma Ray Bursts (GRBs) and their afterglows, and its payload includes a wide-field instrument, the Burst Alert Telescope (BAT; Barthelmy et al. 2005), and two

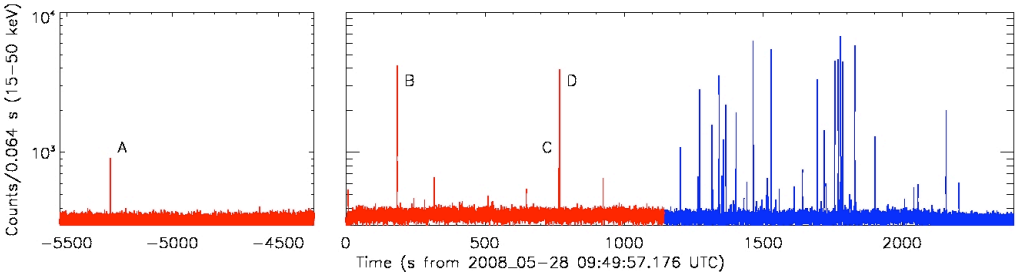

Figure 5.2 The time-line of the bursts detected by the *Swift* Burst Alert Telescope (generated on board, see Section 5.3.1). The portion plotted in red corresponds to the temporal range for which event data were available; for the portion in blue only rate and survey data were distributed.

narrow-field instruments, the X-Ray Telescope (XRT; Burrows et al. 2005) and the Ultraviolet/Optical Telescope (UVOT; Roming et al. 2005). In this Section we report on the results obtained from our analysis of the *Swift* BAT and XRT observations of SGR 1627–41 performed since its May 2008 re-activation. Given the extremely large optical extinction inferred from the X-ray absorption of the SGR 1627–41 spectrum ($A_V > 40$ mag; Wachter et al. 2004) the UVOT instrument cannot provide meaningful constraints on the ultraviolet/optical emission of SGR 1627–41.

5.3.1 Burst Alert Telescope data - Bursting emission

The coded mask gamma-ray (15–150 keV) BAT instrument spends a large fraction of its time waiting for the occurrence of a GRB in its field of view (FOV). Whenever a GRB or an interesting hard X-ray transient is detected, information for individual photons is sent to the ground in order to have the maximum energy and time resolution (event data). If no GRB is detected, the on board software accumulates the detector count map in 80-channel histograms with a typical integration time of ∼5 minutes (survey data). In this mode, continuous full-detector count rate information is available in 4 energy bands at 64 ms resolution, providing a light-curve for bright variable sources in the FOV.

On 28 May 2008 at 08:21:43 UT BAT triggered on and localised a bright burst from SGR 1627–41 (Palmer et al. 2008). Another bright burst was detected at 09:53:00 UT and was followed by tens of bursts extending to at least 10:25:54 UT (see Figure 5.2). Due to the non-continuous coverage, the net exposure time spent by BAT on the source was ∼3.4 ks. In this Section we present the study of bursts detected when event data were available (∼2.3 ks).

The data reduction was performed using version 2.8 of the standard *Swift*/BAT analysis software distributed within FTOOLS under the HEASOFT package (version 6.4.0). For each event file, the background-subtracted counts of the source were extracted from the detector pixels illuminated by the source by using the

mask-weighting technique. Light-curves in the 15–50 keV band showing the bursting activity were produced. For each burst, a spectrum of the entire bursting time interval was extracted.

We identified in the BAT data eight bursts with more than 500 counts in the 15–50 keV energy range. Their spectra were fit well by an optically-thin thermal bremsstrahlung (OTTB) model with temperatures ranging from about 10 to 70 keV and are overall similar to those detected during the previous outburst of SGR 1627–41 as well as the outbursts from other SGRs (Aptekar et al. 2001).

The main problem with the OTTB model is that, while it generally provides good fits to the spectra of SGR bursts in the hard X-rays ($\gtrsim$15 keV), it tends to overestimate the flux at low energies when broad band data are available (e.g. Olive et al. 2004; Feroci et al. 2004). Among numerous possible spectral models (see Israel et al. 2008, for a review), we tested the double blackbody model (2BB) that was successfully applied to the SGR bursting emission over broad energy ranges (e.g. Olive et al. 2004; Feroci et al. 2004; Nakagawa et al. 2007; Israel et al. 2008). In the case of SGR 1627–41 the 2BB model yielded a good description of the burst spectra as well (even though the additional free parameters with respect to the OTTB model were not statistically required); in Table 5.1 we show the spectral results for the brightest events. Similar to previous studies, our spectral fits show the presence of a 'cold' blackbody with $k_B T_1 \approx 4$ keV and emitting radius $R_1 \approx 30$ km and a hotter blackbody, with $k_B T_2 \approx 10$ keV and $R_2 \approx 4$ km.

For these bright bursts we also produced the spectra corresponding to the rise, peak, and decay phases. The maximum luminosity detected in the SGR 1627–41 data set was $\sim 2 \times 10^{41}$ erg s^{-1} (burst B, peak phase; in particular, the hard blackbody component, with $k_B T_2 \simeq 11$ keV and radius $R_2 \simeq 8$ km, reached a luminosity of $\sim 10^{41}$ erg s^{-1}). Small variations with time were detected, though all the spectra are consistent with the model parameters of the corresponding time-averaged spectrum (see Table 5.1) simply re-scaled in normalisation (to account for the luminosity evolution during the burst). The results of this analysis are reported in Figure 5.3 where the two blackbody equivalent surfaces are shown as a function of their temperatures (only time resolved spectra with well-constrained fitting parameter values are shown). For comparison, we also report the corresponding measurements obtained for the intense 'burst forest' emitted by SGR 1900+14 on 29 March 2006 and observed by BAT (Israel et al. 2008). Despite the small number of photons detected in the SGR 1627–41 bursts, their spectral properties are in good agreement with those of SGR 1900+14.

We also searched the data for a persistent emission from SGR 1627–41 during all the non-bursting intervals. For each event file, an image was generated excluding the burst time intervals and the BATCELLDETECT tool was run. We investigated two time intervals, the first one (see Figure 5.2) ranging from time $t = -5\,533$ to $-4\,331$ s (net exposure time 1 201 s) and the second one from

Table 5.1 Spectral fit results (in the 15–100 keV range) of the bright bursts detected by *Swift*/BAT (see Figure 5.2) for the double blackbody model. We assume a distance to the source of 11 kpc.

Burst	Net counts	Duration (s)	k_BT_1 (keV)	R_1 (km)	L_1[a] (erg s^{-1})	k_BT_2 (keV)	R_2 (km)	L_2[a] (erg s^{-1})	Fluence (erg cm^{-2})	χ^2_r (d.o.f.)
A	11 802	0.110	3.8 ± 0.7	35^{+26}_{-12}	3.2×10^{40}	8.4 ± 0.9	5 ± 2	1.6×10^{40}	2.0×10^{-7}	0.90 (34)
B	20 595	0.135	$4.0^{+0.5}_{-0.4}$	30^{+10}_{-7}	3.1×10^{40}	$10.7^{+0.7}_{-0.5}$	3.9 ± 0.6	2.6×10^{40}	3.5×10^{-7}	0.91 (34)
C	3 704	0.018	$3.9^{+0.8}_{-0.7}$	34^{+22}_{-12}	3.6×10^{40}	11^{+2}_{-1}	4 ± 1	4×10^{40}	0.6×10^{-7}	1.22 (34)
D	10 497	0.250	4.4 ± 0.5	15^{+4}_{-3}	1.1×10^{40}	10 ± 1	$2.0^{+0.9}_{-0.7}$	0.5×10^{40}	1.7×10^{-7}	1.07 (34)

[a] Bolometric luminosity of first/second blackbody.

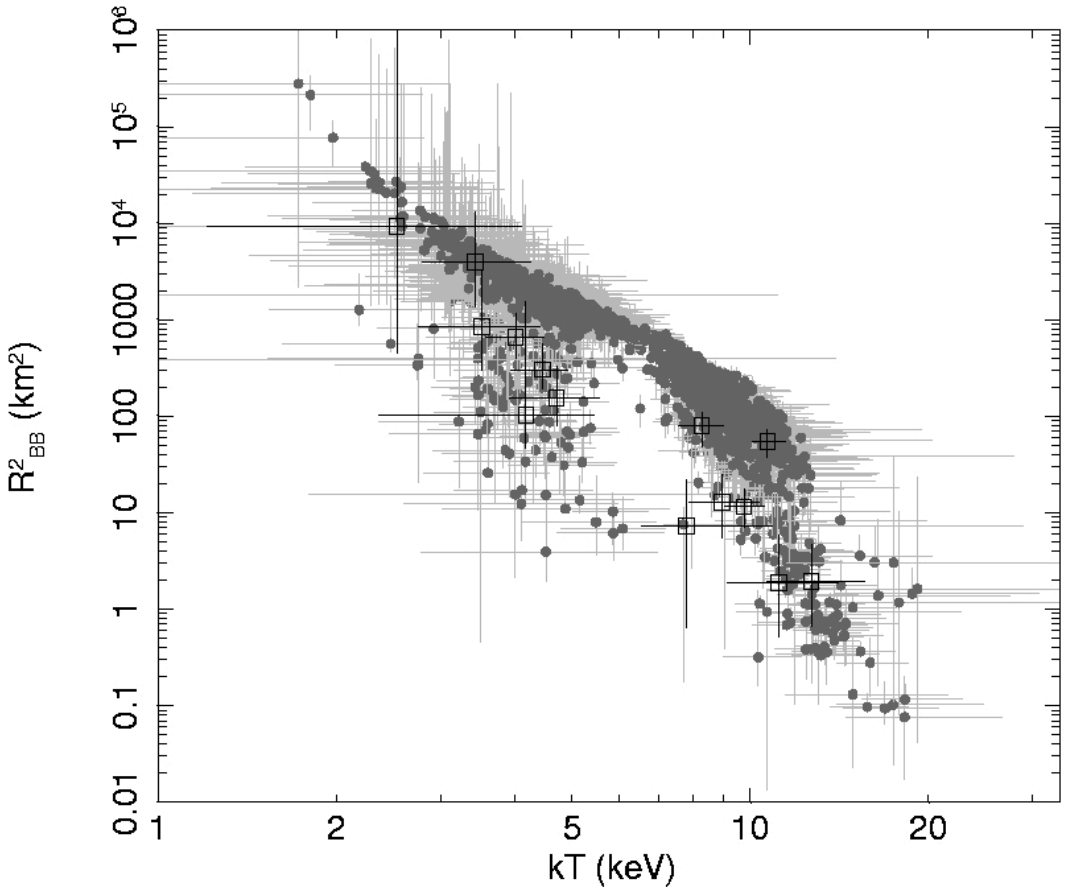

Figure 5.3 Square of radii for the 2BB model as a function of the corresponding temperatures for the time-resolved BAT data of bursts: empty squares mark the SGR 1627–41 events detected in 2008 May, grey data refer to the 2006 March 'burst forest' of SGR 1900+14 (Israel et al. 2008).

Table 5.2 Journal of the 2008 *Swift*/XRT observations. The observation sequence number is composed of 00312579 followed by the three digit segment number given here (e.g. 00312579001).

Obs.	Date	Start/End time (UT)		Exposure[a]	Count rate
	mm-dd	hh:mm:ss		(ks)	(counts s^{-1})
001	05-28	12:58:14	13:31:27	2.0	0.067 ± 0.003
002	05-29	14:47:17	16:30:39	2.0	0.015 ± 0.003
003	05-30	11:35:15	14:58:56	1.9	0.010 ± 0.003
004	05-31	08:49:41	10:37:58	1.8	0.007 ± 0.002
005	06-01	05:32:11	07:34:56	2.0	0.008 ± 0.002
006	06-02	08:37:17	19:18:48	2.1	0.011 ± 0.003
007	06-06	10:35:23	12:16:30	0.6	<0.03[b]
008	06-09	14:41:22	16:19:56	0.3	<0.03[b]
009	06-12	13:07:43	16:35:58	1.9	0.006 ± 0.002
010	06-15	03:34:10	08:50:57	3.8	0.006 ± 0.002
011	06-18	16:54:48	20:24:56	2.3	0.010 ± 0.002
012	06-21	18:46:38	23:39:55	5.2	0.008 ± 0.002
013	07-02	05:17:00	17:10:56	1.5	0.005 ± 0.002
014	07-05	15:29:07	21:59:57	5.6	0.005 ± 0.001

[a] The exposure time is usually spread over several snapshots (single continuous pointings at the target) during each observation.

[b] Upper limit at $3\,\sigma$ confidence level (following Gehrels 1986).

$t = 0$ to 1 146 s (net exposure 1 140 s). In both cases we found no significant emission; the $3\,\sigma$ upper limits on the flux in the 15–50 keV band for the above quoted intervals are 10^{-9} and 4×10^{-10} erg cm^{-2} s^{-1}, respectively (the large difference is due to the coded fraction at which the source was observed in the two cases).

5.3.2 X-Ray Telescope data - Persistent emission

The *Swift* XRT uses a CCD detector sensitive to photons with energies between 0.2 and 10 keV. Fourteen *Swift* observations of SGR 1627–41 were performed following the source re-activation. The XRT instrument was operated in photon counting (PC) mode. The first observation started about 4.6 hours after the first burst was detected by the BAT. Table 5.2 reports the log of the XRT observations used for this work. The data were processed with standard procedures using the FTOOLS task XRTPIPELINE (version 0.11.6). We selected events with grades 0–12 and limited the analysis to the 0.3–10 keV range, where the PC response matrices are well calibrated.

The source was significantly detected in all observations with exposure time

longer than 1 ks with the mean count rates given in Table 5.2. These values, corrected for the loss of counts caused by hot columns and pixels (the correction factor was calculated with XRTMKARF), are plotted in Figure 5.1 after conversion to flux as described below.

For the spectral analysis, we extracted the source events from a circular region with a radius of 20 pixels (1 pixel $\simeq 2.37''$), whereas the background events were extracted within an annular source-free region centred on SGR 1627–41 and with radii 50 and 75 pixels. Since individual data sets have too few counts for a meaningful spectral analysis, we extracted a cumulative spectrum. This corresponds to a total exposure of 32.9 ks and contains about 340 net counts in the 0.3–10 keV range. The data were rebinned with a minimum of 15 counts per energy bin. The ancillary response file was generated with XRTMKARF, and it accounts for different extraction regions, vignetting and point-spread function corrections. We used the latest available spectral redistribution matrix (swxpc0to12s6_20010101v010.rmf). Adopting an absorbed power-law model, we find the following best-fit parameters ($\chi^2_{\rm r} = 1.13$ for 21 d.o.f.): absorption $N_{\rm H} = 10^{+4}_{-3} \times 10^{22}$ cm^{-2} and photon index $\Gamma = 1.5^{+0.7}_{-0.4}$. We used the resulting observed 2–10 keV flux of $\sim 2.3 \times 10^{-12}$ erg cm^{-2} s^{-1} in order to derive the conversion factor 1 count s^{-1} $\simeq 1.8 \times 10^{-10}$ erg cm^{-2} s^{-1}.

Although the uncertainties in the spectral parameters are large, the *Swift*/XRT spectrum appears to be harder than the one observed by *XMM-Newton*/EPIC in February 2008. To better investigate whether this hardening is statistically significant, we simultaneously fit the XRT and EPIC spectra with an absorbed power-law model with linked parameters and a free normalisation factor. The resulting χ^2_r (1.60 for 65 d.o.f.) is unacceptable, while an acceptable fit ($\chi^2_r = 1.01$ for 64 d.o.f.) is obtained once the photon index is also left free to vary independently. The best-fit parameters of the latter fit are: a common absorption of $N_{\rm H} = (10^{+1}_{-2}) \times 10^{22}$ cm^{-2} and photon indices $\Gamma_{\rm XMM} = 3.5^{+0.1}_{-0.5}$ and $\Gamma_{\rm XRT} = 1.5^{+0.3}_{-0.5}$ for the EPIC and XRT spectra, respectively.

5.4 Discussion and conclusions

The recent, spectacular re-activation of SGR 1627–41, following a quiescent interval of nearly a decade, triggered the BAT instrument on board *Swift* on 28 May 2008. Tens of bursts were observed, with fluxes exceeding the underlying continuum by a factor $>10^5$. The bursts achieved a maximum luminosity of $\sim 10^{41}$ erg s^{-1} and had a duration of <0.5 s, typical of the bursts detected in SGRs. Thanks to the rapid response of *Swift*, the source was repeatedly observed with XRT in the days following the 'burst forest' emission, leading to the earliest post-burst observations ever obtained for this SGR. In fact, at the time of the previous active period, the persistent emission was observed only one month after the first burst detection (Woods et al. 1999c).

With respect to the last pre-burst *XMM-Newton* observation, the source

was detected in May–June 2008 at a much larger flux level (see Figure 5.1) and with a considerably harder spectrum. A serendipitous *Chandra* observation performed only 20 hours before the detection of the bursting activity provides a $3\,\sigma$ upper limit on the absorbed flux of 5×10^{-12} erg cm^{-2} s^{-1} (0.5–10 keV band; Tiengo et al. 2008), showing that most of the flux enhancement occurred in less than a day. These facts indicate a significant phase transition marked by the burst activation. The correlated spectral hardening/flux increase is in line with what is observed in the long term evolution of other magnetars (e.g. Mereghetti 2008), and expected in models in which the non thermal X-ray emission is due to resonant up-scattering by magnetospheric currents (Thompson et al. 2002).

The early flux decay of the source is shown in Figure 5.4, where, for comparison, we also plot the flux of the decay that followed the past bursting activity of SGR 1627–41 and those of two AXPs, CXOU J164710.2–455216 (Israel et al. 2007) and 1E 2259+586 (Woods et al. 2004). The SGR 1627–41 data taken after more than two days from the May 2008 trigger are well fit by a power-law decay (index ~ -0.2), but the XRT points at earlier times shows a marked excess over this trend, indicating a very steep initial decay. This behaviour closely resembles that of 1E 2259+586: in that case, after the June 2002 bursts active phase the source flux showed a double component decay, with a steep component that decayed rapidly during the first $\sim$2 days, followed by a slower year-long decay phase (Woods et al. 2004). Interestingly, the phase of steep flux decay (and harder spectra) was associated with a long-lasting period of bursting activity. This is consistent with what was observed in CXOU J164710.2–455216 and SGR 1627–41: in the former case, in which no steep/prompt decay was observed, the bursting activity was already over at the time of the first observation of the persistent flux. In the latter case, after the activation of June 1998 only a shallow decay was monitored >60 days from the first bursts. The light-curve of the recent SGR 1627–41 decay reveals both, the steep and shallow phase, and the last burst was detected by Konus/*Wind* between the first and the second XRT pointing (Golenetskii et al. 2008). The new observations support the presence of two distinct timescales (a short, $\sim$1 day, and a longer one, $\sim$month) in the flux decay following the outburst of a magnetar. In this respect, we notice that while a steep decay seems to point toward a magnetospheric effect (for instance following current dissipation or other forms of activity), the decay index of the shallow phase ranges from about -0.6 (in the case of SGR 1627–41, 1998) to -0.2 (for 1E 2259+586 and SGR 1627–41, 2008) and is roughly compatible with crustal cooling (considering the uncertainties in the theoretical models, see Eichler et al. 2006 and references therein). The energetics and relative importance of the steep/shallow decay phases, nevertheless, greatly vary from source to source. Indeed, in some cases this requires a powering mechanism for the tail emission much more energetic than the bursts energy deposition. This might be associated with magnetospheric current dissipation or crustal cooling fol-

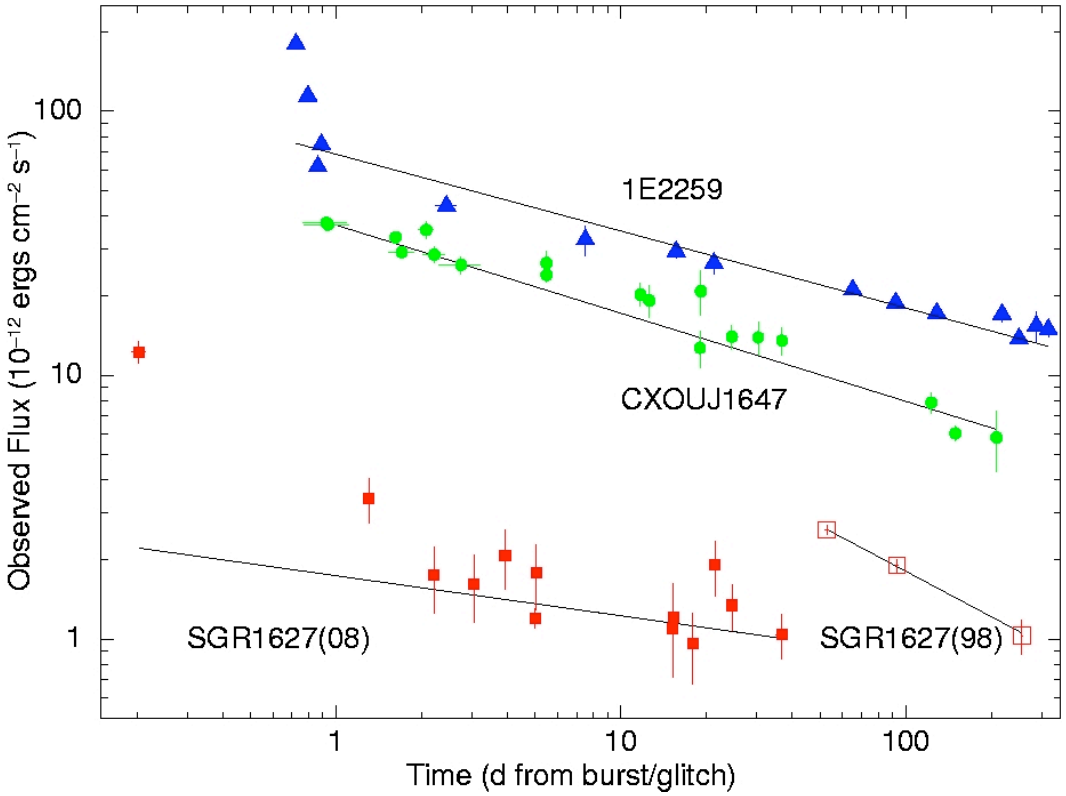

Figure 5.4 Comparison among flux decays of SGR 1627–41 (this work, Woods et al. 2008b, Mereghetti et al. 2006), CXOU J164710.2–455216 (Israel et al. 2007; filled circles) and 1E 2259+586 (Woods et al. 2004; filled triangles) following a period of bursts emission and/or glitch. In the case of SGR 1627–41 we report the available data for both the 2008 (filled squares) and 1998 (open squares) activation periods. The solid lines represent the power-law best-fits (see Section 5.4 for more details).

lowing an impulsive heat deposition.

For several bursts we had enough counts to perform a spectral analysis. The parameter values derived from the 2BB fits are in agreement with the results of a comprehensive analysis of a 'burst forest' emitted by SGR 1900+14 (Israel et al. 2008), which showed that the bursts populate almost homogeneously all temperatures between ∼2 and ∼12 keV, with a bimodal distribution behaviour and a sharp edge in the k_BT–R^2 plane. This supports the idea of two distinct emitting regions, a cold and larger one and a hot and smaller one which in turn may be associated to the escaping regions of two populations of photons, from the O- and E- polarisation modes. Interestingly, the bright bursts detected from SGR 1627–41 lie within the cloud of the SGR 1900+14 bursts (Figure 5.3) and the luminosities of the two blackbody components are in agreement with the relation shown in Figure 6 of Israel et al. (2008), suggesting that short bursts form a continuum in terms of spectral properties, duration and fluence. Finally, we notice that in the scenario proposed by Israel

et al. (2008), the luminosity of the hot blackbody is not expected to exceed the magnetic Eddington luminosity (Thompson & Duncan 1995). In the case of SGR 1627–41, where the maximum luminosity observed by the BAT for the hot blackbody is $\sim 10^{41}$ erg s^{-1}, this translates into a lower limit for the magnetic field of $B > 1.8 \times 10^{14}$ G.

Chapter 6

Unveiling the nature of RX J0002+6246 with *XMM-Newton*

The X-ray source RX J0002+6246 was discovered close to the supernova remnant CTB 1 in a *ROSAT* observation performed in 1992. The source phenomenology (soft spectrum, apparent lack of counterparts, possible pulsations at 242 ms, hints for surrounding diffuse emission) led to interpret it as an isolated neutron star in a new supernova remnant. We have analysed an archival *XMM-Newton* observation performed in 2001. The source coordinates, as computed on the *XMM-Newton* images, coincide with those of a bright source listed in optical and infrared catalogues. The X-ray spectrum is well described by an optically thin plasma model. No fast pulsations are seen, nor clear evidence of a supernova remnant associated to the source. Thus, we conclude that RX J0002+6246 is not an isolated neutron star, but the X-ray counterpart of the bright optical/infrared source, most likely a F7 spectral class star located at about 0.2 kpc.

6.1 Introduction

Most of the observed isolated neutron stars are identified as pulsars, whose emission derives either from rotational energy loss, or as magnetars, powered by magnetic field decay (e.g., Manchester 2004). The central compact objects (CCOs; see Pavlov et al. 2002) remain perhaps the least understood members of the isolated neutron stars family. These X-ray sources are located within supernova remnants (SNRs) and, despite intensive campaigns, have not been detected as radio or optical sources so far. CCOs are seemingly young ($\lesssim 10^4$ years) isolated neutron stars, with steady X-ray fluxes (with the notably exception of 1E 161348−5055 at the centre of the SNR RCW 103; De Luca et al. 2006), soft thermal spectra, and lack of surrounding pulsar wind nebulae. Two

CCOs out of seven are pulsating sources: 1E 1207.4−5209 in G 296.5+10.0, with period $P = 424$ ms (Zavlin et al. 2000), and PSR J1852+0040 in Kes 79, with $P = 105$ ms (Gotthelf et al. 2005). Both sources have small spin-down rates with period derivatives $\dot{P} < 2 \times 10^{-16}$ s s^{-1} (Gotthelf & Halpern 2007; Halpern et al. 2007).

The current sample of CCOs includes seven 'confirmed' sources and four 'candidates'. The confirmed CCOs are the central sources in RCW 103 (Tuohy & Garmire 1980), G 296.5+10.0 (Helfand & Becker 1984), Pup A (Petre et al. 1996), Vela Jr. (Aschenbach 1998), G 347.3−0.5 (Slane et al. 1999), Cas A (Tananbaum 1999), and Kes 79 (Seward et al. 2003). The candidates are those in G 349.7+0.2 (Lazendic et al. 2005), G 15.9+0.2 (Reynolds et al. 2006), G 330.2+1.0 (Park et al. 2006), and RX J0002+6246 in G 117.9+0.6 (Hailey & Craig 1995), which is the object of our research.

The X-ray point source RX J0002+6246 was discovered with the PSPC instrument on board *ROSAT* near the supernova remnant CTB 1, during a ∼9 ks long observation carried out on 1992 August 16–17. Hailey & Craig (1995) reported the position R.A. = $00^{\rm h}02^{\rm m}54.1^{\rm s}$, Decl. = $62°46'23''$ (epoch J2000). The observation showed a hint of a faint shell of soft X-ray emission (G 117.7+0.6), proposed as a SNR associated with RX J0002+6246 (Hailey & Craig 1995; Craig et al. 1997). The spectrum of the point source was fitted using a blackbody attenuated by interstellar absorption, with $k_BT \simeq 0.15$ keV. Assuming a distance of 3 kpc (Hailey & Craig 1995), this corresponds to a 0.5–2 keV luminosity of $\sim 2 \times 10^{32} d_3^2$ erg s^{-1} (where we indicate with $d_{\rm N}$ the distance in units of N kpc). Hailey & Craig (1995) also found some evidence for a possible periodicity in the X-ray emission of RX J0002+6246 with period $P = 242$ ms. Based on these results, Hailey & Craig (1995) proposed that RX J0002+6246 is an isolated neutron star in a SNR. Furthermore, the absence of counterparts at other wavelengths (Hailey & Craig 1995; Brazier & Johnston 1999) suggested that RX J0002+6246 could be a CCO.

In 2001 RX J0002+6246 has been observed for 33 ks with *XMM-Newton*. Pavlov et al. (2004) reported results of the analysis of those data. The spectrum was fitted by a two-component model: a soft blackbody with temperature $k_BT \simeq 0.1$ keV and a hard component, either a second blackbody with $k_BT \simeq 0.5$ keV or a power-law with photon index $\Gamma \simeq 2.6$. Any periodicity was excluded, as well as the presence of a SNR around the source. They concluded that RX J0002+6246 is most likely a middle-aged pulsar rather than a CCO.

Here we report on a re-analysis of the *XMM-Newton* observation of RX J0002+6246. This research presents evidence that, contrary to previous claims, the X-ray source RX J0002+6246 is neither a CCO nor a pulsar, but rather a non-degenerate star. We have also identified its likely stellar counterpart using near-infrared data.

6.2 Observation and analysis

The *XMM-Newton* X-ray observatory observed the field of RX J0002+6246 for 33 ks in 2001, from August 22 17:16 UT to August 23 02:30 UT (observation ID: 0016140101). The data were collected with the EPIC instrument, which consists of two MOS (Turner et al. 2001) and one pn (Strüder et al. 2001) cameras sensitive to photons with energies between 0.1 and 15 keV. The EPIC pn was operated in Small Window mode (time resolution 6 ms) while the EPIC MOS had the MOS 1 and MOS 2 units in Full Frame mode (time resolution 2.6 s). Both the pn and MOS mounted the medium thickness filter.

All the data reduction was performed using the Science Analysis Software (SAS) software package[1] version 7.1. The raw observation data files were processed using standard pipeline tasks (EPPROC for pn, EMPROC for MOS data).

We selected events with pattern 0–4 and pattern 0–12 for the pn and the MOS, respectively. To obtain the results presented in this work we filtered the data to reject intervals with soft-proton flares, reducing the net exposure time to 10.4 ks for the pn detector, 18.3 ks for the MOS 1, and 18.5 ks for the MOS 2.

6.2.1 Spatial analysis

For the imaging analysis we used the EPIC MOS data, since the pn camera in Small Window mode covers only a $4' \times 4'$ sky region, while MOS cameras were exposed in Full Frame mode, providing a $30'$ diameter field of view.

Absolute astrometry

The brightest point source in the 0.3–2 keV image (Figure 6.1) is detected near the centre of the field of view. The EMLDETECT routine reports a best-fit position of R.A. = $00^{\mathrm{h}}02^{\mathrm{m}}55.8^{\mathrm{s}}$, Decl. = $62°46'17.9''$ (epoch J2000), with an uncertainty of $0.2''$. This ($1\,\sigma$) uncertainty is statistical and does not include the systematic uncertainty in *XMM-Newton* pointing. Given the brightness of the source, the statistical error is smaller than the absolute astrometric accuracy of *XMM-Newton* ($1.5''$ root mean square; Kirsch et al. 2004).

We have detected about 40 point sources within the total field of view, most of them without an obvious counterpart at other wavelengths. We measured the position of the bright star TYC 4018–2777–1, visible in X-rays, to be $1.4''$ from its USNO-B1.0 catalog[2] (Monet et al. 2003) position, entirely consistent with the expected EPIC astrometric accuracy (the systematic uncertainty in connecting the USNO astrometry to the International Celestial Reference System is $0.2''$ in each coordinate). The lack of other X-ray sources with clear optical/infrared identification does not allow us to unambiguously register the X-ray image on the optical plates.

[1] See http://xmm.vilspa.esa.es/.

[2] See http://www.nofs.navy.mil/data/fchpix/.

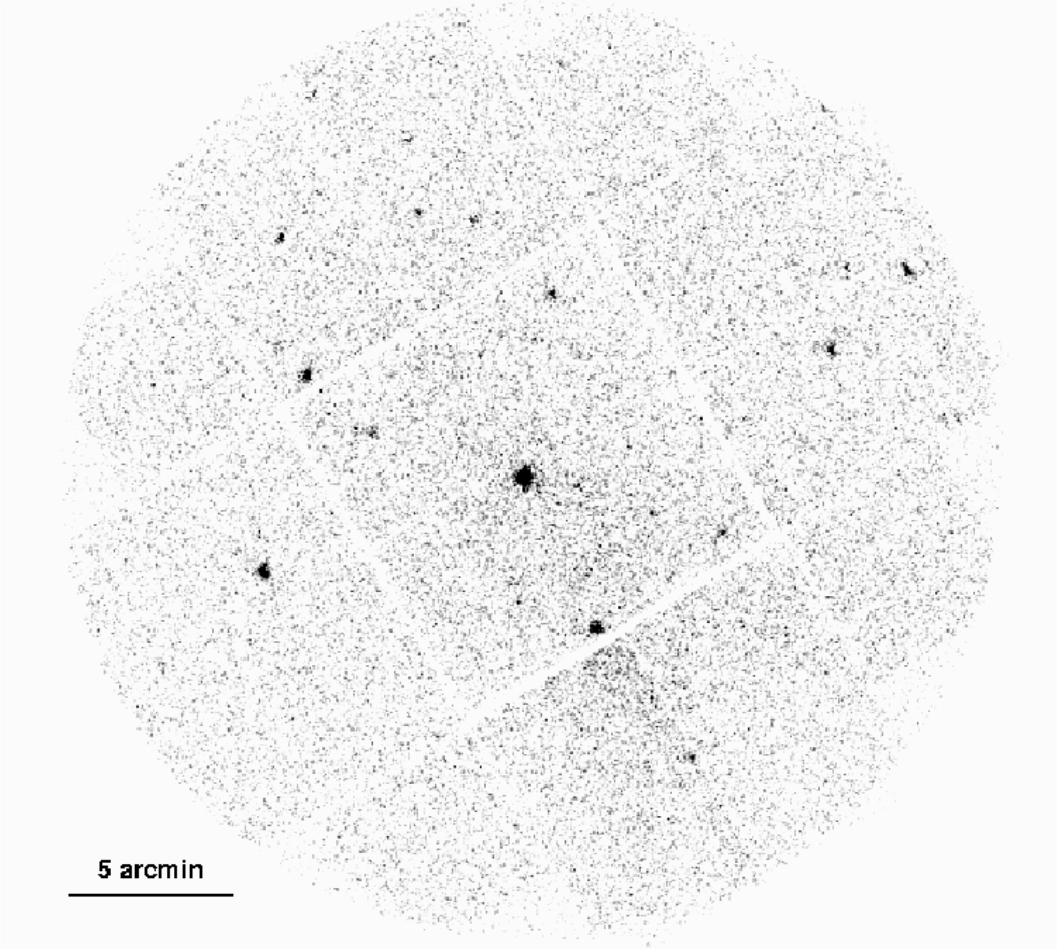

Figure 6.1 *XMM-Newton* EPIC MOS image of the field of RX J0002+6246 in the 0.3–2 keV energy range. North is to the top, east to the left. The imagine has been smoothed with a Gaussian function with kernel radius of three. The image shows the hint of faint diffuse emission (to the south-west) discussed in Section 6.2.1.

With respect to the nominal *ROSAT*/PSPC position of RX J0002+6246 reported by the WGACAT[3] Rev. 1 (White et al. 1994) and Hailey & Craig (1995), the positional offset of the *XMM-Newton* source is 12.6″. The astrometric accuracy of the WGACAT catalog is roughly 13″ (1σ error). The source positions are then well consistent within the uncertainties. Since no other X-ray source is consistent with the *ROSAT* position of RX J0002+6246, here and in the subsequent discussion we assume that the source detected in the EPIC cameras and RX J0002+6246 are the same X-ray source.

Identification of infrared counterparts

We searched for optical or infrared counterparts of RX J0002+6246 around our best-fit position in various catalogs, including the Two Micron All Sky Survey[4] (2MASS; Skrutskie et al. 2006). The 2MASS database covers the entire sky and its Point Source Catalog gives the positions and J (1.25 μm), H (1.65 μm), and K_s (2.17 μm) magnitudes of its sources. The astrometric accuracy of this catalog is better than 0.1″.

The only object from the 2MASS catalog with a position inside the *XMM-Newton* error circle is 2MASS 00025569+6246175. This source lies at R.A. = $00^h02^m55.70^s$, Decl. = 62°46′17.6″ (epoch J2000), only 0.6″ from the centroid of the X-ray source. Its magnitudes are 10.32 ± 0.02, 9.94 ± 0.03, and 9.81 ± 0.03 in the J, H, and K_s bands, respectively. The random chance probability of finding an object as bright in the near-infrared as 2MASS 00025569+6246175 (or brighter) inside the *XMM-Newton* error circle (at a 99% confidence level) is smaller than 2×10^{-5}, making the association with RX J0002+6246 very likely. The second closest infrared source to RX J0002+6246 lies at more than 10″ from its X-ray position.

Diffuse X-ray emission

The EPIC images hint the existence of a faint structure of diffuse emission located to the South-West of RX J0002+6246. Its surface brightness is of $(7 \pm 2) \times 10^{-4}$ counts s^{-1} $arcmin^{-2}$ in the 0.3–2 keV energy range. A detailed spectral analysis of such a faint feature is hampered by the low signal-to-noise ratio.

This diffuse structure, also detected in *ROSAT* images, as well as in radio maps (Craig et al. 1997, and references therein), corresponds to an apparent North-East extension of the nearby SNR CTB 1. Although the nature of such diffuse emission remains unclear (it could be related to CTB 1, or have a different origin – the region is complex and permeated by several diffuse features), it is most likely unrelated to RX J0002+6246.

[3]See http://wgacat.gsfc.nasa.gov/wgacat/wgacat.html .
[4]See http://www.ipac.caltech.edu/2mass/.

6.2.2 Timing analysis

We searched for pulsed X-ray emission from RX J0002+6246 using the high time resolution pn data (6 ms time resolution). Source photons were selected in the 0.3–2 keV energy range from a circular region centred on RX J0002+6246 with radius of 30″. Photon arrival times were converted to the solar system barycentre using the SAS task BARYCEN. For the barycentric correction, we used the position inferred from the MOS image fitting (see Section 6.2.1).

We searched the data for pulsations using the Z_n^2 test (Buccheri et al. 1983), with the number of harmonics n being varied from 1 to 4. We searched for a pulsed signal over a wide period range centred on the value suggested by Hailey & Craig (1995) (0.24181 ± 0.00001 s). No statistically significant signal was detected. We found a 99% confidence upper limit on the pulsed fraction of 15 percent (assuming a sinusoidal modulation). Indeed, also the detection of the modulation reported by Hailey & Craig (1995) was marginal. We then searched the data for pulsations to a minimum period of 12 ms, but we again did not detect any significant signal.

6.2.3 Spectral analysis

The source spectra were accumulated from circular regions (30″ radius) centred on RX J0002+6246. The background spectra were extracted from source-free regions of the same chip as the source: annular regions with radii of 80″ and 125″ for the MOSs, and a rectangular region with area of $\sim 2.8 \times 10^3$ arcsec^2 located on the side of the source for the pn. We carefully checked that the choice of different background extraction regions did not affect the spectral results. During the observation, between 0.3 and 2 keV a total of 905 ± 32 counts above the background were collected from RX J0002+6246 by the pn detector, 400 ± 21 by the MOS 1 detector, and 422 ± 22 by the MOS 2 detector.

Spectral redistribution matrices and ancillary response files were generated using the SAS scripts RMFGEN and ARFGEN, and spectra grouped with a minimum of 30 counts per energy bin were fed into the spectral fitting package XSPEC[5] version 12.3 (Arnaud 1996). Spectral channels having energies below 0.3 keV and above 2.0 keV were ignored, owing to the very low counts from RX J0002+6246.

We jointly fit the spectra by MOS 1, MOS 2, and pn to a number of different models including a blackbody, power-law, blackbody plus power-law, two blackbodies, bremsstrahlung, Raymond-Smith plasma (Raymond & Smith 1977), MEKAL (Mewe et al. 1985, 1986; Liedahl et al. 1995), and APEC (Smith et al. 2001), all corrected for interstellar absorption. The abundances used are those of Anders & Grevesse (1989) and photoelectric absorption cross-sections from Balucinska-Church & McCammon (1992). The data are well described by the Raymond-Smith, MEKAL, and APEC models, with plasma temperatures of $\sim$0.7 keV (see Table 6.1 for the best-fit model parameters), whereas all the

[5]See http://heasarc.gsfc.nasa.gov/docs/xanadu/xspec/.

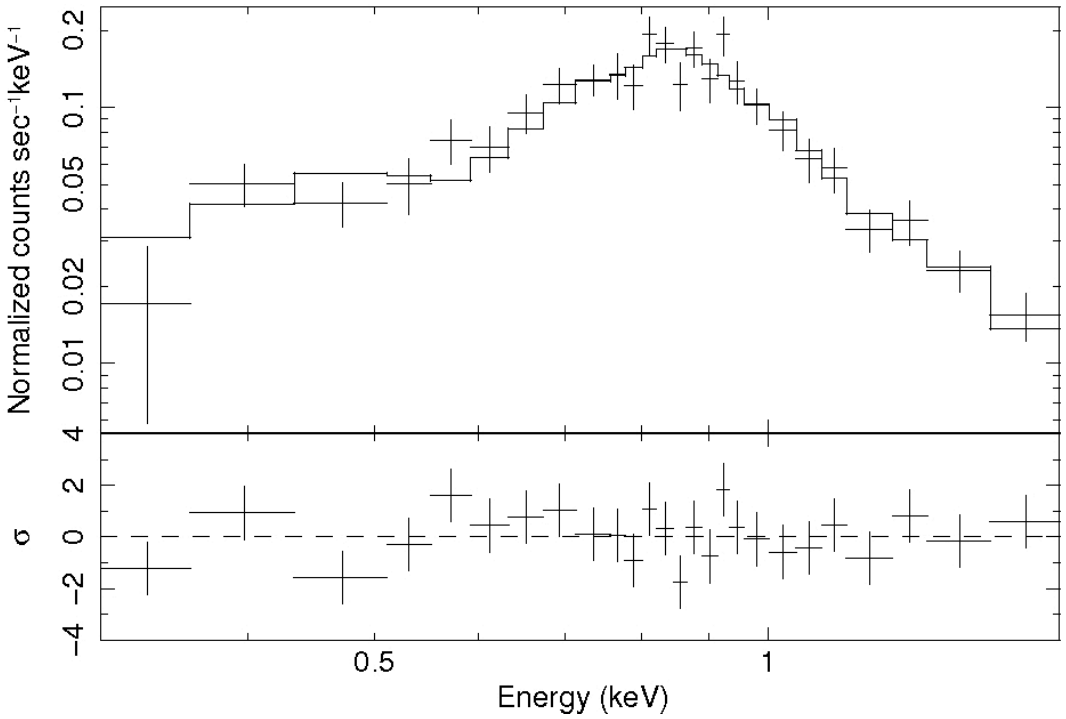

Figure 6.2 EPIC pn spectrum of RX J0002+6246. Upper panel: data and best-fit MEKAL model for the parameters given in Table 6.1. Lower panel: residuals in units of sigma.

other models yield statistically unacceptable fits (with $\chi^2_r > 1.5$). In Figure 6.2 the spectrum of RX J0002+6246 fitted with the MEKAL model is shown.

6.3 Discussion and conclusions

The X-ray source RX J0002+6246 is clearly detected in the *XMM-Newton* images and its position is consistent with a rather bright star (2MASS 00025569+6246175). Hailey & Craig (1995) ruled out this star as a possible counterpart of RX J0002+6246 mainly for the angular separation of 12″ from their X-ray position. However, they relied upon a positional uncertainty of 10″, a value that in subsequent releases of the WGACAT was conservatively increased to 13″ (1 σ). Moreover, the source coordinates in the WGACAT are affected by a systematic error[6]. The recent (2001) Second ROSAT Source Catalog of Pointed Observations with the Position Sensitive Proportional Counter[7] (ROSPSPCCAT/2RXP) using the same observation of Hailey & Craig (1995) provides more reliable coordinates: R.A. = $00^{\rm h}02^{\rm m}55.4^{\rm s}$,

[6]See Haberl F., Pietsch W., and Voges W., 'Differences in the two ROSAT catalogs of pointed PSPC observations' (1994), and comments by White N. E., Angelini L., and Giommi P.. The document is available at
ftp://ftp.xray.mpe.mpg.de/rosat/catalogues/sourcecat/wga_rosatsrc.html .

[7]See http://www.mpe.mpg.de/xray/wave/rosat/rra/.

Table 6.1 Spectral results in the 0.3–2 keV energy range. Errors are quoted at the 90% confidence level for a single interesting parameter.

Model[a]	$N_{\rm H}$ (10^{21} cm^{-2})	k_BT (keV)	Metal abundances[b]	Absorbed flux[c] (erg cm^{-2} s^{-1})	Unabsorbed flux[c] (erg cm^{-2} s^{-1})	χ^2_r (d.o.f.)
RS	1.1 ± 0.3	0.75 ± 0.05	$0.09^{+0.05}_{-0.03}$	1.3×10^{-13}	2.4×10^{-13}	1.18 (49)
APEC	$1.4^{+0.3}_{-0.4}$	$0.66^{+0.07}_{-0.04}$	$0.10^{+0.03}_{-0.02}$	1.3×10^{-13}	2.6×10^{-13}	1.00 (49)
MEKAL	1.5 ± 0.3	0.64 ± 0.04	0.09 ± 0.02	1.3×10^{-13}	2.8×10^{-13}	0.93 (49)

[a] Models applied in XSPEC notation: RS=PHABS*RAYMOND, APEC=PHABS*APEC, and MEKAL=PHABS*MEKAL.

[b] With the abundance ratios of Anders & Grevesse (1989).

[c] Flux in the 0.3–2 keV energy range.

Decl. = 62°46′21.0″ (epoch J2000). Adopting this position, the offset between the *XMM-Newton* and *ROSAT* positions decreases to 4.0″, and that from 2MASS 00025569+6246175 to 4.0″.

With the J, H, and K_s magnitudes of 2MASS 00025569+6246175 (RX J0002+6246) at hand (see Section 6.2.1), we used the relation between the N_H of the X-ray best-fits (Table 6.1) and the interstellar extinction A_V of Predehl & Schmitt (1995), as well as the relations between the extinctions at different wavelengths of Cardelli et al. (1989) to derive the intrinsic colours of the source $(J–H)_\circ \simeq 0.30$ and $(H–K)_\circ \simeq 0.06$. In a similar way, taking optical photometric data from the Tycho-2 Catalogue[8] (Høg et al. 2000), we derived also the colour $(B–V)_\circ \simeq 0.50$. These values are consistent with a F or G type star in the case of a main-sequence star, or with a G type in the case of a supergiant (e.g., Cox 2000). In particular, the intrinsic colours point to a F7-type main-sequence star.

In the reasonable frame of a F7-type main-sequence star, the expected absolute optical magnitudes is $M_V \simeq 3.4$ (e.g., Cox 2000; Zombeck 2007), implying a distance of ∼230 pc. Such a relatively small distance is well consistent with the measure of the photoabsorption derived from the best-fitting models of the X-ray spectrum ($N_H \simeq 1.5 \times 10^{21}$ cm^{-2}, see Table 6.1). This value is in fact significantly smaller than the measurements of the interstellar hydrogen in this direction by Dickey & Lockman (1990) and Kalberla et al. (2005), that give N_H values of $\sim(6–7) \times 10^{21}$ cm^{-2}. The X-ray-to-optical flux ratio is $\log(f_X/f_V) \simeq -3.3$, in good agreement with the value of $\langle \log(f_X/f_V) \rangle = -3.7 \pm 0.7$ obtained by Krautter et al. (1999) averaging *ROSAT*/PSPC and optical data on a sample of 53 F-type stars. This scenario is further confirmed by the X-ray spectrum of RX J0002+6246 measured by *XMM-Newton* that is well fit by either the APEC or MEKAL codes, with temperatures typical of non-degenerate stellar atmospheres.

Based on the accurately identified counterpart (thanks to *XMM-Newton* imaging capabilities) as well as on the spectral properties of RX J0002+6246, together with the lack of an associated SNR and the absence of X-ray pulsations, we conclude that the source is not a neutron star (in any of its manifestations, including a CCO) and its properties are clearly consistent with a non-degenerate star.

[8] See http://www.astro.ku.dk/∼erik/Tycho-2/.

Bibliography

Adler, S. L., Bahcall, J. N., Callan, C. G., & Rosenbluth, M. N. 1970, Physical Review Letters, 25, 1061

Alfvén, H. & Herlofson, N. 1950, Physical Review, 78, 616

Alpar, M. A. 2001, ApJ, 554, 1245

Anders, E. & Grevesse, N. 1989, Geochim. Cosmochim. Acta, 53, 197

Aptekar, R. L., Frederiks, D. D., Golenetskii, S. V., et al. 2001, ApJS, 137, 227

Arnaud, K. A. 1996, in ASP Conf. Ser., San Francisco CA, Vol. 101, Jacoby, G. H. and Barnes, J., eds., Astronomical Data Analysis Software and Systems V., 17

Aschenbach, B. 1998, Nature, 396, 141

Atteia, J.-L., Boer, M., Hurley, K., et al. 1987, ApJ, 320, L105

Baade, W. 1942, ApJ, 96, 188

Baade, W. & Zwicky, F. 1934, Proceedings of the National Academy of Science, 20, 259

Balucinska-Church, M. & McCammon, D. 1992, ApJ, 400, 699

Bamba, A., Koyama, K., Hiraga, J. S., et al. 2007, PASJ, 59, 209

Baring, M. G. & Harding, A. K. 2007, Ap&SS, 308, 109

Barthelmy, S. D., Barbier, L. M., Cummings, J. R., et al. 2005, Space Science Reviews, 120, 143

Baykal, A., İnam, S. Ç., & Beklen, E. 2006, MNRAS, 369, 1760

Becker, W. & Pavlov, G. G. 2001, in The century of space science (edited by Johan A. M. Bleeker, Johannes Geiss, Martin C. E. Huber; history consultant, Arturo Russo. Dordrecht; Boston: Kluwer Academic.), 721–758

Becker, W. & Truemper, J. 1997, A&A, 326, 682

Beloborodov, A. M. & Thompson, C. 2007, ApJ, 657, 967

Boella, G., Chiappetti, L., Conti, G., et al. 1997, A&AS, 122, 327

Bolton, J. G., Stanley, G. J., & Slee, O. B. 1949, Nature, 164, 101

Bowyer, S., Byram, E. T., Chubb, T. A., & Friedman, H. 1964a, AJ, 69, 135

Bowyer, S., Byram, E. T., Chubb, T. A., & Friedman, H. 1964b, Nature, 201, 1307

Brazier, K. T. S. & Johnston, S. 1999, MNRAS, 305, 671

Buccheri, R., Bennett, K., Bignami, G. F., et al. 1983, A&A, 128, 245

Burrows, D. N., Hill, J. E., Nousek, J. A., et al. 2005, Space Science Reviews, 120, 165

Cameron, P. B., Chandra, P., Ray, A., et al. 2005, Nature, 434, 1112

Camilo, F., Kaspi, V. M., Lyne, A. G., et al. 2000, ApJ, 541, 367

Camilo, F., Manchester, R. N., Lyne, A. G., et al. 2004, ApJ, 611, L25

Cardelli, J. A., Clayton, G. C., & Mathis, J. S. 1989, ApJ, 345, 245

Cavallo, G. & Rees, M. J. 1978, MNRAS, 183, 359

Chadwick, J. 1932, Proc. Roy. Soc., A, 136, 692

Chandrasekhar, S. 1931, ApJ, 74, 81

Chatterjee, P., Hernquist, L., & Narayan, R. 2000, ApJ, 534, 373

Cheng, A. F. 1983, ApJ, 275, 790

Cheng, K. S., Ho, C., & Ruderman, M. 1986a, ApJ, 300, 500

Cheng, K. S., Ho, C., & Ruderman, M. 1986b, ApJ, 300, 522

Chiang, J. & Romani, R. W. 1994, ApJ, 436, 754

Chiu, H.-Y. 1964, AJ, 69, 537

Chiu, H.-Y. & Salpeter, E. E. 1964, Physical Review Letters, 12, 413

Corbel, S., Chapuis, C., Dame, T. M., & Durouchoux, P. 1999, ApJ, 526, L29

Corbel, S., Wallyn, P., Dame, T. M., et al. 1997, ApJ, 478, 624

Cox, A. N. 2000, Allen's astrophysical quantities (4th ed. Publisher: New York: AIP Press; Springer, 2000. Editedy by Arthur N. Cox. ISBN: 0387987460)

Craig, W. W., Hailey, C. J., & Pisarski, R. L. 1997, ApJ, 488, 307

De Luca, A. 2008, in AIP Conf. Proc., Melville NY, Vol. 983, Bassa C., Wang Z., Cumming A., Kaspi V. M., eds., 40 years of pulsars: Millisecond Pulsars, Magnetars and More., 311

De Luca, A., Caraveo, P. A., Mereghetti, S., Tiengo, A., & Bignami, G. F. 2006, Science, 313, 814

den Hartog, P. R. 2008, Ph. D. Thesis, University of Amsterdam

den Hartog, P. R., Hermsen, W., Kuiper, L., et al. 2006, A&A, 451, 587

Dickey, J. M. & Lockman, F. J. 1990, ARA&A, 28, 215

Dombrovsky, V. A. 1954, Dokl. Akad. Nauk. SSSR, 94, 1021

Duncan, A. R., Stewart, R. T., Haynes, R. F., & Jones, K. L. 1997, MNRAS, 287, 722

Duncan, R. C. 2000, in American Institute of Physics Conference Series, Vol. 526, Gamma-ray Bursts, 5th Huntsville Symposium, ed. R. M. Kippen, R. S. Mallozzi, & G. J. Fishman, 830–841

Duncan, R. C. & Thompson, C. 1992, ApJ, 392, L9

Eddington, A. S. 1926, The Internal Constitution of the Stars (Cambridge: Cambridge University Press)

Eichler, D., Lyubarsky, Y., Kouveliotou, C., & Wilson, C. A. 2006, eprint (astro-ph/0611747)

Eikenberry, S. S., Garske, M. A., Hu, D., et al. 2001, ApJ, 563, L133

Esposito, P., De Luca, A., Tiengo, A., et al. 2008a, MNRAS, 384, 225

Esposito, P., Israel, G. L., Zane, S., et al. 2008b, MNRAS, L84

Esposito, P., Mereghetti, S., Tiengo, A., et al. 2007a, A&A, 461, 605

Esposito, P., Mereghetti, S., Tiengo, A., et al. 2007b, A&A, 476, 321

Esposito, P., Tiengo, A., De Luca, A., & Mattana, F. 2007c, A&A, 467, L45

Fahlman, G. G. & Gregory, P. C. 1981, Nature, 293, 202

Faucher-Giguère, C.-A. & Kaspi, V. M. 2006, ApJ, 643, 332

Fenimore, E. E., Laros, J. G., & Ulmer, A. 1994, ApJ, 432, 742

Fernández, R. & Thompson, C. 2007, ApJ, 660, 615

Feroci, M., Caliandro, G. A., Massaro, E., Mereghetti, S., & Woods, P. M. 2004, ApJ, 612, 408

Feroci, M., Costa, E., Amati, L., et al. 1998, IAU Circ., 6945, 3

Feroci, M., Hurley, K., Duncan, R. C., & Thompson, C. 2001, ApJ, 549, 1021

Feroci, M., Mereghetti, S., Costa, E., et al. 2002, in ASP Conf. Ser. 271: Neutron Stars in Supernova Remnants, ed. P. O. Slane & B. M. Gaensler

Feroci, M., Mereghetti, S., Woods, P., et al. 2003, ApJ, 596, 470

Ferrario, L. & Wickramasinghe, D. 2006, MNRAS, 367, 1323

Figer, D. F., Najarro, F., Geballe, T. R., Blum, R. D., & Kudritzki, R. P. 2005, ApJ, 622, L49

Forman, W., Jones, C., Cominsky, L., et al. 1978, ApJS, 38, 357

Frail, D. A., Kulkarni, S. R., & Bloom, J. S. 1999, Nature, 398, 127

Frederiks, D. D., Golenetskii, S. V., Palshin, V. D., et al. 2007, Astronomy Letters, 33, 1

Friedman, H. 1981, in Space Science Comes of Age: Perspectives in the History of the Space Sciences, ed. P. A. Hanle & V. D. Chamberlain, 31–44

Frontera, F., Costa, E., dal Fiume, D., et al. 1997, A&AS, 122, 357

Gaensler, B. M., Kouveliotou, C., Gelfand, J. D., et al. 2005, Nature, 434, 1104

Gaensler, B. M. & Slane, P. O. 2006, ARA&A, 44, 17

Gamow, G. & Schoenberg, M. 1941, Physical Review, 59, 539

Gavriil, F. P., Gonzalez, M. E., Gotthelf, E. V., et al. 2008, Science, 319, 1802

Gavriil, F. P. & Kaspi, V. M. 2004, ApJ, 609, L67

Gavriil, F. P., Kaspi, V. M., & Woods, P. M. 2002, Nature, 419, 142

Gehrels, N. 1986, ApJ, 303, 336

Gehrels, N., Chincarini, G., Giommi, P., et al. 2004, ApJ, 611, 1005

Ghosh, P. & Lamb, F. K. 1979, ApJ, 234, 296

Giacconi, R. 1974, in Astrophysics and Space Science Library, Vol. 43, X-Ray Astronomy, ed. Giacconi, R. and Gursky, H.

Giacconi, R., Gursky, H., Kellogg, E., Schreier, E., & Tananbaum, H. 1971a, ApJ, 167, L67

Giacconi, R., Gursky, H., Paolini, F. R., & Rossi, B. B. 1962, Physical Review Letters, 9, 439

Giacconi, R., Kellogg, E., Gorenstein, P., Gursky, H., & Tananbaum, H. 1971b, ApJ, 165, L27

Giacconi, R., Murray, S., Gursky, H., et al. 1972, ApJ, 178, 281

Gold, T. 1968, Nature, 218, 731

Gold, T. 1969, Nature, 221, 25

Goldreich, P. & Julian, W. H. 1969, ApJ, 157, 869

Goldreich, P. & Reisenegger, A. 1992, ApJ, 395, 250

Golenetskii, S., Aptekar, R., Mazets, E., et al. 2006, GRB Circular Network, 4936

Golenetskii, S., Aptekar, R., Mazets, E., et al. 2007, GCN Circ. 6684

Golenetskii, S., Aptekar, R., Mazets, E., et al. 2008, GCN Circ., 7778

Golenetskii, S. V., Aptekar, R. L., Guryan, Y. A., Ilinskii, V. N., & Mazets, E. P. 1987, Soviet Astronomy Letters, 13, 166

Gonzalez, M. E., Kaspi, V. M., Camilo, F., Gaensler, B. M., & Pivovaroff, M. J. 2005, ApJ, 630, 489

Gotthelf, E. V. 2003, ApJ, 591, 361

Gotthelf, E. V. & Halpern, J. P. 2007, ApJ, 664, L35

Gotthelf, E. V., Halpern, J. P., & Dodson, R. 2002, ApJ, 567, L125

Gotthelf, E. V., Halpern, J. P., & Seward, F. D. 2005, ApJ, 627, 390

Götz, D., Mereghetti, S., Hurley, K., et al. 2008, in AIP Conf. Proc., Melville NY, Vol. 983, Bassa C., Wang Z., Cumming A., Kaspi V. M., eds., 40 years of pulsars: Millisecond Pulsars, Magnetars and More., 289

Götz, D., Mereghetti, S., Tiengo, A., & Esposito, P. 2006, A&A, 449, L31

Göğüş, E., Kouveliotou, C., Woods, P. M., Finger, M. H., & van der Klis, M. 2002, ApJ, 577, 929

Göğüş, E., Kouveliotou, C., Woods, P. M., et al. 2001, ApJ, 558, 228

Gruber, D. E., Matteson, J. L., Peterson, L. E., & Jung, G. V. 1999, ApJ, 520, 124

Guidorzi, C., Montanari, E., Frontera, F., et al. 2001, GCN Circ. 1041

Gunn, J. E. & Ostriker, J. P. 1969, Nature, 221, 454

Haberl, F. 2007, Ap&SS, 308, 181

Hailey, C. J. & Craig, W. W. 1995, ApJ, 455, L151

Halpern, J. P., Gotthelf, E. V., Camilo, F., & Seward, F. D. 2007, ApJ, 665, 1304

Hartman, R. C., Bertsch, D. L., Bloom, S. D., et al. 1999, ApJS, 123, 79

Heger, A., Fryer, C. L., Woosley, S. E., Langer, N., & Hartmann, D. H. 2003, ApJ, 591, 288

Helfand, D. J. & Becker, R. H. 1984, Nature, 307, 215

Helfand, D. J. & Becker, R. H. 1987, ApJ, 314, 203

Hewish, A., Bell, S., Pilkington, J., Scott, P., & Collins, R. 1968, Nature, 217, 709

Heyl, J. S. & Hernquist, L. 1997, ApJ, 489, L67

Heyl, J. S. & Kulkarni, S. R. 1998, ApJ, 506, L61

Høg, E., Fabricius, C., Makarov, V. V., et al. 2000, A&A, 355, L27

Hoyle, F., Narlikar, J. V., & Wheeler, J. A. 1964, Nature, 203, 914

Hurley, K., Boggs, S. E., Smith, D. M., et al. 2005, Nature, 434, 1098

Hurley, K., Cline, T., Mazets, E., et al. 1999a, Nature, 397, 41

Hurley, K., Kouveliotou, C., Woods, P., et al. 1999b, ApJ, 510, L107

Hurley, K., Kouveliotou, C., Woods, P., et al. 1999c, ApJ, 519, L143

Hurley, K., Li, P., Kouveliotou, C., et al. 1999d, ApJ, 510, L111

Hurley, K., Mazets, E., Golenetskii, S., & Cline, T. 2002, GCN Circ. 1715

Ibrahim, A. I., Strohmayer, T. E., Woods, P. M., et al. 2001, ApJ, 558, 237

in't Zand, J. J. M., Miller, J. M., Oosterbroek, T., & Parmar, A. N. 2002, A&A, 394, 553

Israel, G., Covino, S., Mignani, R., et al. 2005a, A&A, 438, L1

Israel, G. L., Belloni, T., Stella, L., et al. 2005b, ApJ, 628, L53

Israel, G. L., Campana, S., Dall'Osso, S., et al. 2007, ApJ, 664, 448

Israel, G. L., Mereghetti, S., & Stella, L. 1994, ApJ, 433, L25

Israel, G. L., Romano, P., Mangano, V., et al. 2008, ApJ, in press, 805

Jansen, F., Lumb, D., Altieri, B., et al. 2001, A&A, 365, L1

Kalberla, P. M. W., Burton, W. B., Hartmann, D., et al. 2005, A&A, 440, 775

Kaspi, V. M., Gavriil, F. P., Woods, P. M., et al. 2003, ApJ, 588, L93

Kaspi, V. M. & McLaughlin, M. A. 2005, ApJ, 618, L41

Kaspi, V. M., Roberts, M. S. E., & Harding, A. K. 2006, in Compact stellar X-ray sources, ed. W. H. G. Levin and M. van der Klis (Cambridge: Cambridge University Press), 279

Kim, Y., Rieke, G. H., Krause, O., et al. 2008, ApJ, 678, 287

Kirsch, M. G., Briel, U. G., Burrows, D., et al. 2005, in UV, X-Ray, and Gamma-Ray Space Instrumentation for Astronomy XIV. Edited by Siegmund, Oswald H. W. Proceedings of the SPIE, Volume 5898, 22–33

Kirsch, M. G. F., Altieri, B., Chen, B., et al. 2004, in UV and Gamma-Ray Space Telescope Systems. Proceedings of the SPIE. SPIE, Bellingham WA, ed. G. Hasinger & M. J. L. Turner, Vol. 5488, 103

Klebesadel, R. W., Strong, I. B., & Olson, R. A. 1973, ApJ, 182, L85

Klose, S., Henden, A. A., Geppert, U., et al. 2004, ApJ, 609, L13

Kokubun, M., Makishima, K., Takahashi, T., et al. 2007, PASJ, 59, 53

Kosugi, G., Ogasawara, R., & Terada, H. 2005, ApJ, 623, L125

Kouveliotou, C., Dieters, S., Strohmayer, T., et al. 1998a, Nature, 393, 235

Kouveliotou, C., Eichler, D., Woods, P. M., et al. 2003, ApJ, 596, L79

Kouveliotou, C., Fishman, G. J., Meegan, C. A., et al. 1993, Nature, 362, 728

Kouveliotou, C., Kippen, M., Woods, P., et al. 1998b, IAU Circ., 6944, 2

Kouveliotou, C., Strohmayer, T., Hurley, K., et al. 1999, ApJ, 510, L115

Kouveliotou, C., Tennant, A., Woods, P. M., et al. 2001, ApJ, 558, L47

Koyama, K., Hoshi, R., & Nagase, F. 1987, PASJ, 39, 801

Koyama, K., Tsunemi, H., Dotani, T., et al. 2007, PASJ, 59, 23

Krause, O., Rieke, G. H., Birkmann, S. M., et al. 2005, Science, 308, 1604

Krautter, J., Zickgraf, F.-J., Appenzeller, I., et al. 1999, A&A, 350, 743

Kuiper, L., Hermsen, W., den Hartog, P. R., & Collmar, W. 2006, ApJ, 645, 556

Kuiper, L., Hermsen, W., & Mendez, M. 2004, ApJ, 613, 1173

Kulkarni, S. R., Kaplan, D. L., Marshall, H. L., et al. 2003, ApJ, 585, 948

Lai, D. 2001, Reviews of Modern Physics, 73, 629

Landau, L. D. 1932, Physik. Z. Sowjetunion, 1, 285

Laros, J. G., Fenimore, E. E., Fikani, M. M., Klebesadel, R. W., & Barat, C. 1986, Nature, 322, 152

Laros, J. G., Fenimore, E. E., Klebesadel, R. W., et al. 1987, ApJ, 320, L111

Lattimer, J. M. & Prakash, M. 2007, Phys. Rep., 442, 109

Lazendic, J. S., Slane, P. O., Hughes, J. P., Chen, Y., & Dame, T. M. 2005, ApJ, 618, 733

Lebrun, F., Leray, J. P., Lavocat, P., et al. 2003, A&A, 411, L141

Lebrun, F., Terrier, R., Bazzano, A., et al. 2004, Nature, 428, 293

Lenters, G. T., Woods, P. M., Goupell, J. E., et al. 2003, ApJ, 587, 761

Liedahl, D. A., Osterheld, A. L., & Goldstein, W. H. 1995, ApJ, 438, L115

Liu, Q. Z., van Paradijs, J., & van den Heuvel, E. P. J. 2000, A&AS, 147, 25

Livingstone, M. A., Kaspi, V. M., Gavriil, F. P., et al. 2007, Ap&SS, 308, 317

Lorimer, D. R., Faulkner, A. J., Lyne, A. G., et al. 2006, MNRAS, 372, 777

Lund, N., Budtz-Jørgensen, C., Westergaard, N. J., et al. 2003, A&A, 411, L231

Lyubarsky, Y. E. 2002, MNRAS, 332, 199

Lyutikov, M. 2002, ApJ, 580, L65

Lyutikov, M. 2003, MNRAS, 346, 540

Lyutikov, M. & Gavriil, F. P. 2006, MNRAS, 368, 690

Manchester, R. N. 2004, Science, 304, 542

Manchester, R. N., Hobbs, G. B., Teoh, A., & Hobbs, M. 2005, AJ, 129, 1993

Marsden, D., Gruber, D. E., Heindl, W. A., Pelling, M. R., & Rothschild, R. E. 1998, ApJ, 502, L129

Marsden, D., Lingenfelter, R. E., Rothschild, R. E., & Higdon, J. C. 2001, ApJ, 550, 397

Marsden, D. & White, N. E. 2001, ApJ, 551, L155

Mazets, E. P., Aptekar, R. L., Butterworth, P. S., et al. 1999a, ApJ, 519, L151

Mazets, E. P., Cline, T. L., Aptekar', R. L., et al. 1999b, Astronomy Letters, 25, 635

Mazets, E. P., Golenetskii, S. V., Gurian, I. A., & Ilinskii, V. N. 1982, Ap&SS, 84, 173

Mazets, E. P., Golentskii, S. V., Ilinskii, V. N., Aptekar, R. L., & Guryan, I. A. 1979, Nature, 282, 587

McClure-Griffiths, N. M. & Gaensler, B. M. 2005, ApJ, 630, L161

McLaughlin, M. A., Lyne, A. G., Lorimer, D. R., et al. 2006, Nature, 439, 817

McLaughlin, M. A., Rea, N., Gaensler, B. M., et al. 2007, ApJ, 670, 1307

Mereghetti, S. 2008, A&A Rev., 15, 225

Mereghetti, S., Bandiera, R., Bocchino, F., & Israel, G. L. 2002a, ApJ, 574, 873

Mereghetti, S., Chiarlone, L., Israel, G. L., & Stella, L. 2002b, in Neutron Stars, Pulsars, and Supernova Remnants, ed. W. Becker, H. Lesch & J. Trümper. MPE Report, Vol. 278, 29–43

Mereghetti, S., Esposito, P., & Tiengo, A. 2007, Ap&SS, 308, 13

Mereghetti, S., Esposito, P., Tiengo, A., et al. 2006, A&A, 450, 759

Mereghetti, S., Götz, D., Mirabel, I. F., & Hurley, K. 2005a, A&A, 433, L9

Mereghetti, S., Götz, D., von Kienlin, A., et al. 2005b, ApJ, 624, L105

Mereghetti, S., Israel, G. L., & Stella, L. 1998, MNRAS, 296, 689

Mereghetti, S. & Stella, L. 1995, ApJ, 442, L17

Mereghetti, S., Tiengo, A., Esposito, P., et al. 2005c, ApJ, 628, 938

Mewe, R., Gronenschild, E. H. B. M., & van den Oord, G. H. J. 1985, A&AS, 62, 197

Mewe, R., Lemen, J. R., & van den Oord, G. H. J. 1986, A&AS, 65, 511

Minkowski, R. 1942, ApJ, 96, 199

Mitsuda, K., Bautz, M., Inoue, H., et al. 2007, PASJ, 59, 1

Molkov, S., Hurley, K., Sunyaev, R., et al. 2005, A&A, 433, L13

Molkov, S. V., Cherepashchuk, A. M., Lutovinov, A. A., et al. 2004, Astronomy Letters, 30, 534

Monet, D. G., Levine, S. E., Canzian, B., et al. 2003, AJ, 125, 984

Morrison, P. 1967, ARA&A, 5, 325

Morrison, P., Olbert, S., & Rossi, B. 1954, Physical Review, 94, 440

Murakami, T., Tanaka, Y., Kulkarni, S. R., et al. 1994, Nature, 368, 127

Murray, S. S., Austin, G. K., Chappell, J. H., et al. 2000, in Proc. SPIE Vol. 4012, X-Ray Optics, Instruments, and Missions III, ed. J. E. Truemper & B. Aschenbach, 68

Nakagawa, Y. E., Yoshida, A., Hurley, K., et al. 2007, PASJ, 59, 653

Nobili, L., Turolla, R., & Zane, S. 2008a, MNRAS, 386, 1527

Nobili, L., Turolla, R., & Zane, S. 2008b, MNRAS, 389, 989

Olive, J.-F., Hurley, K., Sakamoto, T., et al. 2004, ApJ, 616, 1148

Oort, J. H. & Walraven, T. 1956, Bull. Astron. Inst. Netherlands, 12, 285

Oppenheimer, J. R. & Volkoff, G. M. 1939, Physical Review, 55, 374

Pacini, F. 1967, Nature, 216, 567

Pacini, F. 1968, Nature, 219, 145

Pacini, F. & Salvati, M. 1973, ApJ, 186, 249

Paczynski, B. 1992, Acta Astronomica, 42, 145

Palmer, D., Esposito, P., Barthelmy, S., et al. 2008, GCN Circ., 7777

Palmer, D., Sakamoto, T., Barthelmy, S., et al. 2006, Astron. Tel. 789

Park, S., Mori, K., Kargaltsev, O., et al. 2006, ApJ, 653, L37

Parmar, A. N., Martin, D. D. E., Bavdaz, M., et al. 1997, A&AS, 122, 309

Pavlov, G. G., Sanwal, D., Garmire, G. P., & Zavlin, V. E. 2002, in Astronomical Society of the Pacific Conference Series,, 247

Pavlov, G. G., Sanwal, D., & Teter, M. A. 2004, in IAU Symposium, Vol. 218, Young Neutron Stars and Their Environments, ed. F. Camilo & B. M. Gaensler, 239

Pavlov, G. G., Zavlin, V. E., Sanwal, D., Burwitz, V., & Garmire, G. P. 2001, ApJ, 552, L129

Perotti, F., Giuliani, A., Mereghetti, S., et al. 2007, GCN Circ. 6688

Petre, R., Becker, C. M., & Winkler, P. F. 1996, ApJ, 465, L43

Pivovaroff, M. J., Kaspi, V. M., & Camilo, F. 2000, ApJ, 535, 379

Possenti, A., Cerutti, R., Colpi, M., & Mereghetti, S. 2002, A&A, 387, 993

Possenti, A., Colpi, M., D'Amico, N., & Burderi, L. 1998, ApJ, 497, L97+

Predehl, P. & Schmitt, J. H. M. M. 1995, A&A, 293, 889

Raymond, J. C. & Smith, B. W. 1977, ApJS, 35, 419

Rea, N., Israel, G., Covino, S., et al. 2005a, Astron. Tel. 645

Rea, N., Tiengo, A., Mereghetti, S., et al. 2005b, ApJ, 627, L133

Rea, N., Zane, S., Lyutikov, M., & Turolla, R. 2007, Ap&SS, 308, 61

Revnivtsev, M. G., Sunyaev, R. A., Varshalovich, D. A., et al. 2004, Astronomy Letters, 30, 382

Reynolds, S. P., Borkowski, K. J., Hwang, U., et al. 2006, ApJ, 652, L45

Richards, D. W. & Comella, J. M. 1969, Nature, 222, 551

Romani, R. W. & Yadigaroglu, I.-A. 1995, ApJ, 438, 314

Roming, P. W. A., Kennedy, T. E., Mason, K. O., et al. 2005, Space Science Reviews, 120, 95

Rothschild, R. E., Kulkarni, S. R., & Lingenfelter, R. E. 1994, Nature, 368, 432

Rothschild, R. E., Lingenfelter, R. E., & Marsden, D. 2002a, in ASP Conf. Ser. 271: Neutron Stars in Supernova Remnants, 257

Rothschild, R. E., Marsden, D., & Lingenfelter, E. 2002b, Memorie della Societa Astronomica Italiana, 73, 508

Ruderman, M. A. & Sutherland, P. G. 1975, ApJ, 196, 51

Serlemitsos, P. J., Soong, Y., Chan, K.-W., et al. 2007, PASJ, 59, 9

Seward, F. D., Slane, P. O., Smith, R. K., & Sun, M. 2003, ApJ, 584, 414

Seward, F. D. & Wang, Z.-R. 1988, ApJ, 332, 199

Shklovsky, I. S. 1967, ApJ, 148, L1

Shklovsky, J. S. 1954, Memoires of the Societe Royale des Sciences de Liege, 1, 515

Shull, Jr., P. 1983, ApJ, 275, 611

Skrutskie, M. F., Cutri, R. M., Stiening, R., et al. 2006, AJ, 131, 1163

Slane, P., Gaensler, B. M., Dame, T. M., et al. 1999, ApJ, 525, 357

Smith, D. A., Bradt, H. V., & Levine, A. M. 1999, ApJ, 519, L147

Smith, R. K., Brickhouse, N. S., Liedahl, D. A., & Raymond, J. C. 2001, ApJ, 556, L91

Staelin, D. H. & Reifenstein, E. C. 1968, Science, 162, 1481

Stephenson, F. R. & Green, D. A. 2002, Historical supernovae and their remnants. International series in astronomy and astrophysics, vol. 5. (Oxford: Clarendon Press, 2002, ISBN 0198507666.)

Strüder, L., Briel, U., Dennerl, K., et al. 2001, A&A, 365, L18

Sturrock, P. A. 1971, ApJ, 164, 529

Sugizaki, M., Mitsuda, K., Kaneda, H., et al. 2001, ApJS, 134, 77

Takahashi, T., Abe, K., Endo, M., et al. 2007, PASJ, 59, 35

Tananbaum, H. 1999, IAU Circ., 7246, 1

Taylor, G. B., Gelfand, J. D., Gaensler, B. M., et al. 2005, ApJ, 634, L93

Taylor, J. H., Manchester, R. N., & Lyne, A. G. 1993, ApJS, 88, 529

Terasawa, T., Tanaka, Y. T., Takei, Y., et al. 2005, Nature, 434, 1110

Thompson, C. 2002, Memorie della Societa Astronomica Italiana, 73, 572

Thompson, C. & Beloborodov, A. M. 2005, ApJ, 634, 565

Thompson, C. & Duncan, R. C. 1993, ApJ, 408, 194

Thompson, C. & Duncan, R. C. 1995, MNRAS, 275, 255

Thompson, C. & Duncan, R. C. 1996, ApJ, 473, 322

Thompson, C. & Duncan, R. C. 2001, ApJ, 561, 980

Thompson, C., Lyutikov, M., & Kulkarni, S. R. 2002, ApJ, 574, 332

Tiengo, A., Esposito, P., Mereghetti, S., et al. 2005, A&A, 440, L63

Tiengo, A., Rea, N., Klein-Wolt, M., et al. 2008, Astron. Tel., 1559

Tuohy, I. & Garmire, G. 1980, ApJ, 239, L107

Turner, M. J. L., Abbey, A., Arnaud, M., et al. 2001, A&A, 365, L27

Ubertini, P., Lebrun, F., Di Cocco, G., et al. 2003, A&A, 411, L131

Valinia, A. & Marshall, F. E. 1998, ApJ, 505, 134

van Paradijs, J., Taam, R. E., & van den Heuvel, E. P. J. 1995, A&A, 299, L41

Vancura, O., Blair, W. P., Long, K. S., & Raymond, J. C. 1992, ApJ, 394, 158

Vasisht, G., Kulkarni, S. R., Frail, D. A., & Greiner, J. 1994, ApJ, 431, L35

Vietri, M., Stella, L., & Israel, G. L. 2007, ApJ, 661, 1089

Vrba, F. J., Henden, A. A., Luginbuhl, C. B., et al. 2000, ApJ, 533, L17

Wachter, S., Patel, S. K., Kouveliotou, C., et al. 2004, ApJ, 615, 887

Weber, F., Negreiros, R., Rosenfield, P., & Torres I Cuadrat, A. 2007, in American Institute of Physics Conference Series, Vol. 892, Quark Confinement and the Hadron Spectrum VII, ed. J. E. F. T. Ribeiro, N. Brambilla, A. Vairo, K. Maung, & G. M. Prosperi, 515–517

White, N. E., Giommi, P., & Angelini, L. 1994, IAU Circ., 6100, 1

Wilson, C. A., Finger, M. H., Göğüş, E., Woods, P. M., & Kouveliotou, C. 2002, ApJ, 565, 1150

Woltjer, L. 1964, ApJ, 140, 1309

Woods, P. M., Kaspi, V. M., Thompson, C., et al. 2004, ApJ, 605, 378

Woods, P. M., Kouveliotou, C., Finger, M. H., et al. 2002, IAU Circ., 7856, 1

Woods, P. M., Kouveliotou, C., Finger, M. H., et al. 2007, ApJ, 654, 470

Woods, P. M., Kouveliotou, C., Göğüş, E., et al. 2003, ApJ, 596, 464

Woods, P. M., Kouveliotou, C., Göğüş, E., et al. 2001, ApJ, 552, 748

Woods, P. M., Kouveliotou, C., Gavriil, F. P., et al. 2005, ApJ, 629, 985

Woods, P. M., Kouveliotou, C., Göğüş, E., & Hurley, K. 2008a, Astron. Tel., 1549

Woods, P. M., Kouveliotou, C., Göğüş, E., Hurley, K., & Tomsick, J. 2008b, Astron. Tel., 1564

Woods, P. M., Kouveliotou, C., van Paradijs, J., Finger, M. H., & Thompson, C. 1999a, ApJ, 518, L103

Woods, P. M., Kouveliotou, C., van Paradijs, J., et al. 1999b, ApJ, 524, L55

Woods, P. M., Kouveliotou, C., van Paradijs, J., et al. 1999c, ApJ, 519, L139

Woods, P. M. & Thompson, C. 2006, in Compact stellar X-ray sources, ed. W. H. G. Levin and M. van der Klis (Cambridge University Press), 547

Zavlin, V. E. 2007, in The 363-rd Heraeus Seminar on Neutron Stars and Pulsars, Springer Lecture Notes, in press, preprint (astro-ph/0702426)

Zavlin, V. E. & Pavlov, G. G. 2002, in Neutron Stars, Pulsars, and Supernova Remnants, ed. W. Becker, H. Lesch, & J. Trümper, 263

Zavlin, V. E., Pavlov, G. G., Sanwal, D., & Trümper, J. 2000, ApJ, 540, L25

Zeldovich, Y. B. & Guseynov, O. H. 1966, ApJ, 144, 840

Zombeck, M. 2007, Handbook of Space Astronomy and Astrophysics: Third Edition (Published by Cambridge University Press, Cambridge, UK, 2007.)

List of publications

Papers in refereed journals

1. S. Mereghetti, A. Tiengo, **P. Esposito**, D. Götz, L. Stella, G. L. Israel, N. Rea, M. Feroci, R. Turolla, & S. Zane
An XMM-Newton View of the Soft Gamma Repeater SGR 1806–20: Long-Term Variability in the Pre-Giant Flare Epoch
The Astrophysical Journal, Volume 628, Issue 2, pp. 938–945 (2005)

2. A. Tiengo, **P. Esposito**, S. Mereghetti, N. Rea, L. Stella, G. L. Israel, R. Turolla, & S. Zane
The calm after the storm: XMM-Newton observation of SGR 1806–20 two months after the Giant Flare of 2004 December 27
Astronomy and Astrophysics, Volume 440, Issue 3, September IV 2005, pp. L63–L66

3. D. Götz, S. Mereghetti, A. Tiengo, & **P. Esposito**
Magnetars as persistent hard X-ray sources: INTEGRAL discovery of a hard tail in SGR 1900+14
Astronomy and Astrophysics, Volume 449, Issue 2, April II 2006, pp. L31–L34

4. S. Mereghetti, **P. Esposito**, A. Tiengo, R. Turolla, S. Zane, L. Stella, G. L. Israel, M. Feroci, & A. Treves
XMM-Newton observations of the Soft Gamma Ray Repeater SGR 1627–41 in a low luminosity state
Astronomy and Astrophysics, Volume 450, Issue 2, May I 2006, pp. 759–762

5. S. Mereghetti, **P. Esposito**, A. Tiengo, S. Zane, R. Turolla, L. Stella, G. L. Israel, D. Götz, & M. Feroci
The first XMM-Newton observations of the Soft Gamma-ray Repeater SGR 1900+14
The Astrophysical Journal, Volume 653, Issue 2, pp. 1423–1428 (2006)

6. F. Mattana, D. Götz, M. Falanga, F. Senziani, A. De Luca, **P. Esposito**, & P. A. Caraveo
A new symbiotic low mass X-ray binary system: 4U 1954+319
Astronomy and Astrophysics, Volume 460, Issue 2, December III 2006, pp. L1–L4

7. **P. Esposito**, S. Mereghetti, A. Tiengo, L. Sidoli, M. Feroci, & P. Woods
Five years of SGR 1900+14 observations with BeppoSAX
Astronomy and Astrophysics, Volume 461, Issue 2, January II 2007, pp. 605–612

8. S. Mereghetti, **P. Esposito**, & A. Tiengo
XMM-Newton observations of Soft Gamma-ray Repeaters
Astrophysics and Space Science, Volume 308, Issue 1-4, 2007, pp. 13–23

9. A. Tiengo, **P. Esposito**, S. Mereghetti, L. Sidoli, D. Götz, M. Feroci, R. Turolla, S. Zane, G. L. Israel, L. Stella, & P. Woods
Long term spectral variability in the Soft Gamma-ray Repeater SGR 1900+14
Astrophysics and Space Science, Volume 308, Issue 1-4, 2007, pp. 33–37

10. **P. Esposito**, A. Tiengo, A. De Luca, & F. Mattana
Discovery of X-ray emission from the young radio pulsar PSR J1357–6429
Astronomy and Astrophysics, Volume 467, Issue 2, May IV 2007, pp. L45–L48

11. **P. Esposito**, P. A. Caraveo, A. Pellizzoni, A. De Luca, N. Gehrels, & M. A. Marelli
Swift/XRT monitoring of five orbital cycles of LS I +61° 303
Astronomy and Astrophysics, Volume 474, Issue 2, November I 2007, pp. 575–578

12. D. Götz, N. Rea, G. L. Israel, S. Zane, **P. Esposito**, E. V. Gotthelf, S. Mereghetti, A. Tiengo, & R. Turolla
Long Term Hard X-Ray Variability of the Anomalous X-ray Pulsar 1RXS J170849.0–400910 discovered with INTEGRAL
Astronomy and Astrophysics, Volume 475, Issue 1, November III 2007, pp. 317–321

13. **P. Esposito**, S. Mereghetti, A. Tiengo, S. Zane, R. Turolla, D. Götz, N. Rea, N. Kawai, M. Ueno, G. L. Israel, L. Stella, & M. Feroci
SGR 1806–20 about two years after the giant flare: Suzaku, XMM-Newton and INTEGRAL observations
Astronomy and Astrophysics, Volume 476, Issue 1, December II 2007, pp. 321–330

14. **P. Esposito**, A. De Luca, A. Tiengo, A. Paizis, S. Mereghetti, & P. A. Caraveo
Unveiling the nature of RX J0002+6246 with XMM-Newton
Monthly Notices of the Royal Astronomical Society, Volume 384, Issue 1, pp. 225–229 (2008)

15. S. Mereghetti, A. Tiengo, & **P. Esposito**
The XMM-Newton view of magnetars
Astronomische Nachrichten, Volume 329, Issue 2, pp. 194–197 (2008)

16. A. Pellizzoni, A. Tiengo, A. De Luca, **P. Esposito**, & S. Mereghetti
PSR J0737–3039: Interacting Pulsars in X-rays[1]
The Astrophysical Journal, Volume 679, Issue 1, pp. 664–674 (2008)

17. A. Tiengo, **P. Esposito**, & S. Mereghetti
XMM-Newton observation of CXOU J010043.1–721134: the first deep look at the soft X-ray emission of a magnetar
The Astrophysical Journal Letters, Volume 680, Issue 2, pp. L133–L136 (2008)

18. **P. Esposito**, G. L. Israel, S. Zane, F. Senziani, R. L. C. Starling, N. Rea, D. M. Palmer, N. Gehrels, A. Tiengo, A. De Luca, D. Götz, S. Mereghetti, P. Romano, T. Sakamoto, S. D. Barthelmy, L. Stella, R. Turolla, M. Feroci, & V. Mangano
The 2008 May burst activation of SGR 1627–41
Monthly Notices of the Royal Astronomical Society: Letters, Volume 390, Issue 1, pp. L34–L38 (2008)

19. A. Giuliani, S. Mereghetti, F. Fornari, E. Del Monte, M. Feroci, M. Marisaldi, **P. Esposito**, F. Perotti, A. Argan, G. Barbiellini, F. Boffelli, A. Bulgarelli, P. Caraveo, P. W. Cattaneo, A. W. Chen, E. Costa, F. D'Ammando, G. Di Cocco, I. Donnarumma, Y. Evangelista, M. Fiorini, F. Fuschino, M. Galli, F. Gianotti, C. Labanti, I. Lapshov, F. Lazzarotto, P. Lipari, F. Longo, A. Morselli, L. Pacciani, A. Pellizzoni, P. Picozza, M. Prest, G. Pucella, A. Rappoldi, L. Salotti, P. Soffitta, M. Tavani, M. Trifoglio, A. Trois, E. Vallazza, S. Vercellone, D. Zanello, S. Cutini, C. Pittori, B. Preger, P. Santolamazza, F. Verrecchia, N. Gehrels, K. L. Page, D. Burrows, A. Rossi, K. Hurley, I. Mitrofanov, & W. Boynton
AGILE discovery of long duration MeV emission from GRB 080514B[2]
Astronomy & Astrophysics, in press

[1]Press releases: Italian National Institute for Astrophysics (INAF) - *La pulsar "pigra" brilla nei raggi X grazie alla compagna* (2008-05-20); European Space Agency (ESA) - *XMM-Newton watches lazy pulsar being jazzed up by companion* (2008-06-23).

[2]Press release: INAF/National Institute of Nuclear Physics/Italian Space Agency - *Due importanti "prime" per la missione AGILE* (2008-10-13).

20. A. Pellizzoni, M. Pilia, A. Possenti, F. Fornari, P. Caraveo, E. Del Monte, S. Mereghetti, M. Tavani, A. Argan, A. Trois, M. Burgay, A. Chen, I. Cognard, E. Costa, N. D'Amico, **P. Esposito**, Y. Evangelista, M. Feroci, F. Fuschino, A. Giuliani, G. Hobbs, A. Hotan, S. Johnston, M. Kramer, F. Longo, R. N. Manchester, M. Marisaldi, J. Palfreyman, P. Weltevrede, G. Barbiellini, F. Boffelli, A. Bulgarelli, P. W. Cattaneo, V. Cocco, F. D'Ammando, G. De Paris, G. Di Cocco, I. Donnarumma, M. Fiorini, T. Froysland, M. Galli, F. Gianotti, J. Halpern, A. Harding, C. Labanti, I. Lapshov, F. Lazzarotto, P. Lipari, F. Mauri, A. Morselli, L. Pacciani, F. Perotti, P. Picozza, M. Prest, G. Pucella, M. Rapisarda, A. Rappoldi, P. Soffitta, M. Trifoglio, E. Vallazza, S. Vercellone, V. Vittorini, A. Zambra, D. Zanello, C. Pittori, F. Verrecchia, B. Preger, P. Santolamazza, P. Giommi, & L. Salotti
High-Resolution Timing Observations of Spin-Powered Pulsars with the AGILE Gamma-Ray Telescope
The Astrophysical Journal, in press

21. A. De Luca, P. A. Caraveo, **P. Esposito**, & K. Hurley
Chandra astrometry sets a tight upper limit to the proper motion of SGR 1900+14
The Astrophysical Journal, in press

22. F. Mattana, M. Falanga, D. Götz, R. Terrier, **P. Esposito**, A. Pellizzoni, A. De Luca, V. Marandon, A. Goldwurm, & P. A. Caraveo
On the evolution of the gamma- and X-ray luminosities of pulsar wind nebulae
The Astrophysical Journal, in press

Conference proceedings

23. Proceedings of the 2005 EPIC XMM-Newton Consortium Meeting - 5 years of Science with XMM-Newton, Max-Planck-Institut für extraterrestrische Physik, Schloss Ringberg, Germany, April 11–13 2005

    S. Mereghetti, A. Tiengo, D. Götz, **P. Esposito**, N. Rea, L. Stella, G. L. Israel, R. Turolla, S. Zane, & M. Feroci
    EPIC observations of two magnetars: 1E 1048.1-5937 and SGR 1806–20
    MPE Report 288, pp. 45–48 (2005)

24. Proceedings of The 363rd Heraeus Seminar on: Neutron Stars and Pulsars, Physikzentrum Bad Honnef, Germany, May 14–19 2006

    P. Esposito, S. Mereghetti, A. Tiengo, D. Götz, L. Sidoli, & M. Feroci
    Long term spectral variability in the Soft Gamma-ray Repeater SGR 1900+14
    MPE Report 291, pp. 201–204 (2006)

25. Proceedings of the 6th INTEGRAL Workshop - The Obscured Universe, Moscow, July 2006

    D. Götz, S. Mereghetti, K. Hurley, I. F. Mirabel, **P. Esposito**, A. Tiengo, G. Weidenspointner, & A. von Kienlin
    INTEGRAL and magnetars
    ESA Special Publications 622 (2006)

26. Proceedings of the conference 40 Years of Pulsars: Millisecond Pulsars, Magnetars and More - Montréal, Canada, August 12–17

    P. Esposito, A. Tiengo, S. Zane, R. Turolla, D. Götz, S. Mereghetti, G. L. Israel, & N. Rea
    The first Suzaku observation of SGR 1806–20
    AIP Conf. Proc. – February 27, 2008, Volume 983, pp. 286–288

27. Proceedings of the conference 40 Years of Pulsars: Millisecond Pulsars, Magnetars and More - Montréal, Canada, August 12–17

    D. Götz, S. Mereghetti, K. Hurley, **P. Esposito**, E. V. Gotthelf, G. L. Israel, N. Rea, A. Tiengo, R. Turolla, & S. Zane
    Hard X-ray variability of Magnetar's Tails observed with INTEGRAL
    AIP Conf. Proc. – February 27, 2008, Volume 983, pp. 289–291

Gamma ray bursts Coordinates Network Circulars and Reports

28. A. De Luca, P. A. Caraveo, **P. Esposito**, S. Mereghetti, & A. Tiengo
    GRB 050925: analysis of the XMM-Newton observation
    GCN Circular 4274 (2005)

29. **P. Esposito**, A. De Luca, A. Tiengo, G. Vianello, & K. L. Page
    GRB 080514B: second epoch Swift XRT data confirms the X-ray afterglow
    GCN Circular 7750 (2008)

30. S. T. Holland, **P. Esposito**, & K. L. Page
    Swift observation of GRB 080514B
    GCN Report 135 (2008)

31. D. M. Palmer, **P. Esposito**, S. Barthelmy, J. R. Cummings, N. Gehrels, G. L. Israel, H. Krimm, T. Sakamoto, R. Starling
    Reactivation of SGR 1627–41
    GCN Circular 7777 (2008)

32. N. Rea, G. L. Israel, S. Mereghetti, A. Tiengo, **P. Esposito**, D. Götz
SGR 0501+4516: XMM-Newton monitoring schedule
GCN Circular 8152 (2008)

33. N. Rea, S. Mereghetti, G. L. Israel, **P. Esposito**, A. Tiengo, & S. Zane
SGR 0501+4516: preliminary results of the first XMM-Newton observation
GCN Circular 8165 (2008)

34. Y. E. Nakagawa, K. Yamaoka, A. Yoshida, T. Enoto, K. Nakazawa, K. Makishima, N. Rea, **P. Esposito**, T. Sakamoto, & K. Hurley
SGR 0501+4516: preliminary results of the Suzaku ToO observation
GCN Circular 8265 (2008)

35. N. Rea, **P. Esposito**, H. A. Krimm, D. M. Palmer, S. Mereghetti, A. Tiengo, & G. L. Israel
SGR 1550-5418 = AXP 1E 1547.0-5408 (Trigger 330353)
GCN Circular 8313 (2008)

Astronomer's Telegrams

36. N. Rea, G. L. Israel, S. Covino, A. Tiengo, E. Nichelli, R. Turolla, S. Zane, S. Mereghetti, **P. Esposito**, & L. Stella
SGR 1806-20: X-ray and IR post-Giant Flare monitoring
The Astronomer's Telegram, #645 (2005)

37. A. Tiengo, S. Mereghetti, **P. Esposito**, A. De Luca, & D. Götz
Analysis of archival XMM-Newton observation of the field of the short soft burst GRB 071017
The Astronomer's Telegram, #1243 (2007)

38. G. L. Israel, H. A. Krimm, N. Rea, D. Perez, D. N. Burrows, A. P. Beardmore, S. Campana, S. Covino, J. Cummings, A. De Luca, **P. Esposito**, P. A. Evans, D. Götz, J. E. Hill, S. T. Holland, J. A. Kennea, C. B. Markwardt, G. Novara, P. T. O'Brien, J. P. Osborne, K. L. Page, P. Roming, T. Sakamoto, G. K. Skinner, and A. Tiengo
Swift detects an X-ray and optical outburst from a Galactic source probably associated with 1RXH J173523.7–354013
The Astronomer's Telegram, #1528 (2008)

39. D. M. Palmer, **P. Esposito**, S. Barthelmy, J. R. Cummings, N. Gehrels, G. L. Israel, H. Krimm, T. Sakamoto, R. Starling
Reactivation of Soft Gamma Repeater 1627–41
The Astronomer's Telegram, #1548 (2008)

40. **P. Esposito**, G. L. Israel, R. Starling, D. Palmer, N. Gehrels, S. Barthelmy, S. Zane, A. Tiengo, N. Rea, A. De Luca, D. Götz, & S. Mereghetti
Swift/XRT observations of SGR 1627–41's flux decay
The Astronomer's Telegram, #1555 (2008)

41. A. Tiengo, N. Rea, M. Klein-Wolt, R. Wijnands, G. L. Israel, **P. Esposito**, S. Zane, R. Starling, S. Mereghetti, A. De Luca, & D. Götz
A Chandra observation ∼20 hrs before the renewed bursting activity of SGR 1627–41
The Astronomer's Telegram, #1559 (2008)

42. N. Rea, S. Mereghetti, G. L. Israel, **P. Esposito**, A. Tiengo, & S. Zane
SGR 0501+4516: preliminary results of the first XMM-Newton observation
The Astronomer's Telegram, #1688 (2008)

43. G. L. Israel, N. Rea, V. Mangano, P. Esposito, A. Tiengo, S. Mereghetti, D. Gotz, S. Zane, J. Kennea, M. Perri, G. Cusumano, D. N. Burrows, N. Gehrels, D. Palmer, & S. Barthelmy
Swift/XMM-Newton refined timing solution for SGR 0501+4516
The Astronomer's Telegram, #1692 (2008)

44. Y. E. Nakagawa, K. Yamaoka, A. Yoshida, T. Enoto, K. Nakazawa, K. Makishima, N. Rea, **P. Esposito**, T. Sakamoto, & K. Hurley
SGR 0501+4516: preliminary results of the Suzaku ToO observation
The Astronomer's Telegram, #1722 (2008)

45. N. Rea, **P. Esposito**, H. A. Krimm, D. M. Palmer, S. Mereghetti, A. Tiengo, & G. L. Israel
The new SGR 1550-5418 is the old AXP 1E 1547.0-5408
The Astronomer's Telegram, #1756 (2008)

46. R. P. Mignani, N. Rea, G.L. Israel, V. Testa, & **P. Esposito**
Possible NIR counterpart to the AXP 1E 1547.0-5408
The Astronomer's Telegram, #1758 (2008)

47. **P. Esposito**, G.L. Israel, N. Rea, H. A. Krimm, D. M. Palmer, N. Gehrels, S. D. Bart helmy, S. Mereghetti, A. Tiengo, & D. Götz **Swift XRT follow-up of the transient AXP 1E 1547.0–5408 in outburst**
The Astronomer's Telegram, #1763 (2008)

48. G.L. Israel, **P. Esposito**, N. Rea, H. A. Krimm, D. M. Palmer, N. Gehrels, S. Mereghetti, A. Tiengo, F. Senziani, D. Götz, & S. Zane
Swift phase-coherent P-Pdot solution for the 1E 1547.0–5408 outburst
The Astronomer's Telegram, #1770 (2008)

Ackowledgements

Most of the work presented in this thesis was carried out at INAF - Istituto di Astrofisica Spaziale e Fisica Cosmica Milano, and it was partially supported there through ASI, MIUR, and INAF contracts. Chapters 2 through 6 have been published in scientific papers. The reader is referred to the following papers for the specific acknowledgment on each project developed in this thesis. Most importantly, I would like to thank all the co-authors for their help and contribution:

- Chapter 2 (Esposito et al. 2007c): A. Tiengo, A. De Luca, & F. Mattana
- Chapter 3 (Esposito et al. 2007a): S. Mereghetti, A. Tiengo, L. Sidoli, M. Feroci, & P. Woods
- Chapter 4 (Esposito et al. 2007b): S. Mereghetti, A. Tiengo, S. Zane, R. Turolla, D. Götz, N. Rea, N. Kawai, M. Ueno, G. L. Israel, L. Stella, & M. Feroci
- Chapter 5 (Esposito et al. 2008b): G. L. Israel, S. Zane, F. Senziani, R. L. C. Starling, N. Rea, D. Palmer, N. Gehrels, A. Tiengo, A. De Luca, D. Götz, S. Mereghetti, P. Romano, T. Sakamoto, S. D. Barthelmy, L. Stella, R. Turolla, M. Feroci, & V. Mangano
- Chapter 6 (Esposito et al. 2008a): A. De Luca, A. Tiengo, A. Paizis, S. Mereghetti, & P. A. Caraveo

Ringrazio i miei supervisori, Marco Roncadelli e Sandro Mereghetti, per la libertà assoluta di cui ho potuto godere durante il dottorato ed il supporto che mi hanno dato. Ringrazio Lucio Claudio Andreani, Sergio Peppino Ratti e Dario Maccagni per avermi accolto nelle loro scuole e strutture e per la loro grande disponibilità.

Un sentito ringraziamento va ad Andrea Tiengo ed Andrea De Luca, per avermi insegnato la maggior parte di quello che so di astronomia X. Ringrazio gli altri colleghi, che ho la fortuna di poter anche chiamare amici, con cui ho lavorato in questi anni: Andrea Giuliani, Diego Götz, Gian Luca Israel,

Fabio Mattana, Ada Paizis, Alberto Pellizzoni, Nanda Rea, Pat Romano, Lara Sidoli, Roberto Turolla (che anche letto con grande attenzione questa tesi), Stefano Vercellone e Silvia Zane. Ringrazio Constantinos Paizis, Silvano Molendi e Patrizia Caraveo - tra le altre cose - per avermi sempre incoraggiato. Sperando di non scordare nessuno, vorrei ringraziare tutti gli altri colleghi e amici tra Milano, Pavia, Cagliari e Trieste: Paolo Baesso, Andrea Belfiore, Giovanni Bignami, Fabrizio Boffelli, Silva Bortolussi, Marta Burgay, Mauro Fiorini, Andrea Fontana, Fabio Gastaldello, Gabriella Gaudio, Simona Ghizzardi, Alessandro Grelli, Nicola La Palombara, Alberto Leccardi, Enrico Mattaini, Roberto Mignani, Monica Maria Necchi, Giovanni Novara, Maura Pilia, Manuel Pincetti, Fabio Pizzolato, Pierre Pizzochero, Mariachiara Rossetti, Fabio Senziani, Simona Soldi, Federica Sozzi, Michela Uslenghi, Giacomo Vianello e Gabriele Villa. Infine ringrazio il personale amministrativo del Dipartimento di Fisica Nucleare e Teorica dell'Università di Pavia (e Anna Rita Mangia in particolare), dell'INFN-Pavia e dello IASF-Milano per essersi presi carico di me e delle mie pratiche con cura ed efficienza.